SANDIA REPORT

SAND2006-0533
Unlimited Release
Printed February 2006

Blast Mitigation Capabilities of Aqueous Foam

William F. Hartman, Bruce A. Boughton, Marvin E. Larsen

Prepared by
Sandia National Laboratories
Albuquerque, NM 87185 and Livermore, California 94550

Sandia is a multiprogram laboratory operated by Sandia Corporation, a
Lockheed Martin Company, for the United States Department of Energy's
National Nuclear Security Administration under Contract DE-AC04-94AL85000.

Issued by Sandia National Laboratories, operated for the United States Department of Energy by Sandia Corporation.

Available to DOE and DOE contractors from
U.S. Department of Energy
Office of Scientific and Technical Information
P.O. Box 62
Oak Ridge, TN 37831

Telephone: (865)576-8401
Facsimile: (865)576-5728
E-Mail: reports@adonis.osti.gov
Online ordering: http://www.osti.gov/bridge

Available to the public from
U.S. Department of Commerce
National Technical Information Service
5285 Port Royal Rd
Springfield, VA 22161

Telephone: (800)553-6847
Facsimile: (703)605-6900
E-Mail: orders@ntis.fedworld.gov
Online order: http://www.ntis.gov/help/ordermethods.asp?loc=7-4-0#online

SAND2006-0533
Unlimited Release
Printed February 2006

Blast Mitigation Capabilities of Aqueous Foam

William F. Hartman (Retired Sandian)

Tucson, Arizona

Bruce A. Boughton, Marvin E. Larsen

Sandia National Laboratories
PO BOX 5800
Albuquerque, NM 87185

Abstract

A series of tests involving detonation of high explosive blanketed by aqueous foam (conducted from 1982 to 1984) are described in primarily terms of recorded peak pressure, positive phase specific impulse, and time of arrival. The investigation showed that optimal blast mitigation occurs for foams with an expansion ratio of about 60:1. Simple analyses representing the foam as a shocked single phase mixture are presented and shown inadequate. The experimental data demonstrate that foam slows down and broadens the propagated pressure disturbance relative to a shock in air. Shaped charges and flyer plates were evaluated for operation in foam and appreciable degradation was observed for the flyer plates due to drag created by the foam.

Acknowledgements

A large number of people need to be acknowledged for their roles in gathering this body of data. Foremost among them were Lew Fjelseth who was the primary experimenter for most of the series, Kermit Goettsche who had the responsibility of overseeing the tests, Howard Tessler and Paul Johnson who developed the exceptional instrumentation system which would function in the foam environment and who also set up and conducted all of the experiments, Maurice Gilmer and Steve Winter of the SNL Underground Testing Organization who provided the data recording support, our indomitable photographer Irv Lenz, and, finally, our boss and chief counselor at the time, Milt Madsen. (WFH)

We had organized the opportunity to publish this work and, under contract, Bill Hartman wrote the bulk of the report which describes the experimental test series. For a time the completion of this report could be counted among the incidental losses arising from the events of September 11, 2001. We were pleased when the opportunity arose to finally complete the writing. The testing reported predated our membership in Bill's organization and we were fortunate to have worked with Bill and many of the others he mentions in the previous paragraph. (BAB and MEL)

Table of Contents

Acknowledgements 4
Table of Contents 5
List of Figures 7
List of Tables 9
Nomenclature 10
1 Introduction 11
1.1 Report Organization 11
1.2 Motivation 11
1.3 Background and Historical Basis 11
2 Description of Experimental Setup and Instrumentation 12
3 Blast Wave Measurements 15
3.1 Overview 15
3.2 Air Only Baseline Experiment 17
3.3 1000:1 Foam Experiment 20
3.4 400:1 (375:1) Foam Experiment 22
3.5 200:1 Foam Experiment 23
3.6 100:1 Foam Experiments 25
3.7 60:1 Foam Experiments 32
3.8 20:1 Foam Experiment 42
3.9 10:1 Foam Experiment 43
4 Discussion and Implications of Experimental Data 45
4.1 Consistency of Results 45
4.2 Pressure Decrease for Different Foam Densities 49
4.3 Impulse Reduction as a Function of Foam Density 51
4.4 Time of Arrival Data 53
4.5 Reflected Pressures 56
4.6 Pressure Decrease Across an Interface 63
4.7 Effects of Foam on Shaped Charges and Flyer Plates 65
5 Analyses 67
5.1 Introduction 67
5.2 Summary of the Conservation Equations 67

5.3 Equations of State 68
5.4 Computed Hugoniots Comparison 68
5.5 Comparison of Computed Hugoniot with Experimental Data 69
5.6 Impedance Mismatch Calculations 70
6 Conclusions 71
7 References 72
Appendix A: Transient signals from the 6/18/83 Test 73
Appendix B: Curve fits for pressure and time of arrival 83
Appendix C: B.A. Boughton Memo of 3/3/88 87

List of Figures

Figure 1: A typical setup with pressure gauges arranged around an explosive charge inside a plywood foam containment system. 13

Figure 2: The forward end of a pencil gauge arrangement for measuring side-on overpressure. 14

Figure 3: Transient side-on pressure record measured at 2 feet from charge center, June 16, 1983, 100:1 foam. 16

Figure 4: Transient side-on pressure record at 10 feet, June 16, 1983, 100:1 foam. 16

Figure 5: Plot of overpressure, impulse, and time of arrival data for baseline shot, 11/23/82. 19

Figure 6: Plot of overpressure, impulse, and time of arrival data for 1000:1 foam, 9/6/83. 21

Figure 7: Plot of overpressure, impulse, and time of arrival data for 375:1 foam, 3/28/83. 23

Figure 8: Plot of overpressure, impulse, and time of arrival data for 200:1 foam, 4/13/83. 25

Figure 9: Plot of overpressure, impulse, and time of arrival data for 100:1 foam, 11/15/82. 27

Figure 10: Plot of overpressure, impulse, and time of arrival data for 100:1 foam, 7/6/83. 29

Figure 11: Plot of overpressure, impulse, and time of arrival data for 100:1 foam, 8/9/83. 31

Figure 12: Plot of overpressure, impulse, and time of arrival data for 54:1 foam, 11/23/82. 33

Figure 13: Plot of overpressure, impulse, and time of arrival data for 60:1 foam, 4/28/83 (50-lb charge). 35

Figure 14: Test of overpressure versus scaled distance. 36

Figure 15: Test of scaled specific impulse of arrival (i"/$W^{1/3}$) versus scaled distance. 37

Figure 16: Test of scaled time of arrival (TOA/$W^{1/3}$) versus scaled distance. 38

Figure 17: Plot of overpressure, impulse, and time of arrival data for 100:1 foam, 8/2/83. 40

Figure 18: Plot of overpressure, impulse, and time of arrival data for 60:1 foam, 3/8/84. 41

Figure 19: Plot of overpressure, impulse, and time of arrival data for 20:1 foam, 6/17/82. 43

Figure 20: Plot of overpressure, impulse, and time of arrival data for 10:1 foam, 9/29/82. 44

Figure 21: Plot of pressures for tests with 60:1 and 100:1 foams. 46
Figure 22: Plot of scaled impulse for tests with 60:1 and 100:1 foams. 47
Figure 23: Plot of scaled TOA for tests with 60:1 and 100:1 foams. 48
Figure 24: Screened pressure data and empirical fits for all expansion ratios. 50
Figure 25: Scaled specific impulse data for all expansion ratios. 52
Figure 26: Time of arrival data and empirical fits for all expansion ratios. 54
Figure 27: Shock speed versus range for various ER as derived from TOA fit. 55
Figure 28: Face-on and side-on data comparisons. 59
Figure 29: Ratio of observed face-on peak overpressure to predicted (Eq. 4) peak side-on pressure vs. predicted side-on pressure at the range of the observation. 60
Figure 30: Peak face-on measurements (symbols) and side-on pressure estimates for various foam densities. 61
Figure 31: Face-on and side-on specific impulse measurement comparisons. 63
Figure 32: Shock wave system. 67
Figure 33: Predicted Hugoniots for two equations of state. 69
Figure 34: P-U "Hugoniots" as measured and calculated from simple model. 70
Figure 35: Impedance mismatch calculation for conditions of Table 24. 71
Figure 36: Transient pressure and specific impulse at 2 feet, 100:1 foam, 6/16/83. 74
Figure 37: Transient pressure and specific impulse at 2.5 feet, 100:1 foam, 6/16/83. 75
Figure 38: Transient pressure and specific impulse at 3 feet, 100:1 foam, 6/16/83. 76
Figure 39: Transient pressure and specific impulse at 4 feet, 100:1 foam, 6/16/83. 77
Figure 40: Transient pressure and specific impulse at 4 feet, 100:1 foam, 6/16/83 (amplified gauge). 78
Figure 41: Transient pressure and specific impulse at 5 feet, 100:1 foam, 6/16/83. 79
Figure 42: Transient pressure and specific impulse at 7 feet, 100:1 foam, 6/16/83. 80
Figure 43: Transient pressure and specific impulse at 7 feet, 100:1 foam, 6/16/83 (amplified gauge). 81
Figure 44: Transient pressure and specific impulse at 10 feet, 100:1 foam, 6/16/83 (amplified gauge). 82

List of Tables

Table 1: Summary of experiments described 17
Table 2: Results of air baseline experiment 18
Table 3: Results of 1000:1 foam experiment 20
Table 4: Results of 400:1 (375:1) foam experiment 22
Table 5: Results of 200:1 foam experiment 24
Table 6: Results of First (Nov. 82) 100:1 foam experiment 26
Table 7: Results of June 18, 83 100:1 foam experiment 28
Table 8: Results of experiment with high viscosity 100:1 foam 30
Table 9: Results of experiment with 60:1 (54:1) foam 32
Table 10: Results of 50-lb, 60:1 scaling experiment 34
Table 11: Results of extended range experiment with 60:1 (100:1) foam 39
Table 12: Results of extended range 60:1 foam test 41
Table 13: Results of 20:1 foam experiment 42
Table 14: Results of 10:1 foam experiment 44
Table 15: Results of redundant measurements in foam attenuation experiments 49
Table 16: Distance from a 1-lb C-4 surface burst for the pressure to decrease to 10 psi 51
Table 17: Velocity of leading edge of wave at low pressures 56
Table 18: Side-on measurements in 130:1 ratio test 57
Table 19: Face-on data for 130:1 ratio test 57
Table 20: Side-on data for 60:1 foam experiment 58
Table 21: Data from face-on gauges in 60:1 ratio test 58
Table 22: Ratio of reflected to incident pressures and impulses in aqueous foams 62
Table 23: Experimental results from measurements to determine interface decrease 64
Table 24: Interface pressures and reduction across foam/air interface 64
Table 25: Effects of foam on shaped charge penetration 65
Table 26: Results of test to assess effects of foam on flyer plate performance 66
Table 27: Summary of data used in fits of Equations 4 and 5. 84

Nomenclature

a_0	Speed of sound	m/s
C4	Composition C-4 high explosive	
e	Internal energy	J/kg
E	Emissive power	W/m^2
ER	Foam expansion ratio, the number of cubic feet of foam containing one cubic foot of liquid phase	
f	Capture fraction	
h	Specific enthalpy	J/kg
i''	Specific impulse associated with a blast	psi-ms
P	Peak overpressure associated with a blast	psi or MPa
R	Foam containment thickness	ft
u	Particle velocity	m/s
U	Shock velocity	m/s
W	Equivalent weight of C4	lb
x	Distance from charge	ft
x_{air}	Mass fraction of air in foam	
ρ	Foam density	lb/ft^3

1 Introduction

1.1 Report Organization

This introduction is followed by five major report sections ending with conclusions. The next section describes the experimental system that applies for most of the testing reported. The third and largest section documents a substantial experimental effort to measure pressure conditions for HE detonations mitigated by aqueous foam. All the experiments used C-4 explosive and results, including comparisons to TNT standards, are reported in C-4 equivalent. Section 4 discusses the implications of the blast mitigation tests and adds related tests directed at understanding behaviors other than simple foam mitigation. Section 5 documents analyses that were performed to estimate peak pressure near the charge and to compare simple classical shock analyses to the observed data. The final section closes with conclusions.

1.2 Motivation

This report documents a rather long-term effort at Sandia to characterize the response of aqueous foams to the pressure loading produced by the detonation of high explosives. While several facets of blast wave behavior in the foam environment are discussed, the major impetus for the effort was to determine the pressure attenuation capabilities of these foams. The experimental work on these foams was conducted in the 1982 to 1984 time frame. The included theoretical effort is also somewhat dated. However, the experimental results and analyses should be of general interest to new or ongoing efforts to characterize shock behavior in aqueous foam.

When undertaking the shock transmission characterization of a material like aqueous foam, a whole series of questions presents itself. Does the material support a pressure discontinuity, how do the pressure and impulse attenuation vary with foam density, what is the relationship between the free-field and reflected pressures, how much does the pressure drop across a foam-air interface, are the explosive scaling laws which were developed for air shocks equally applicable in foam, and does the actual foam chemistry play a role in all of these behaviors? Experiments were conducted which provided engineering answers to most of these questions and each of these topics will be discussed in this report.

1.3 Background and Historical Basis

Our interest in the behavior of aqueous foams stemmed from the desire to find methods of reducing the consequences of high explosive detonations, assuming that sufficient time was available to take protective action. Of the two major consequences which were of our concern, the blast wave attenuation was of lesser importance than was the capture of the fine particulate that could result from the detonation. While research endeavors into both aspects of the problem were begun at nearly the same time, the longer lead times required to develop a satisfactory particle capture experimental facility led to the blast wave measurements being conducted first.

The value of aqueous foams for both of these purposes had been established in a qualitative fashion at least two decades earlier. References exist of its use in blasting operations in mines, both for dust suppression and for the reduction of the distances which the miners had to retreat to escape possible overpressure effects. Work on measuring pressure attenuation in foams had been done several years previously in both Canada [1] and Australia [2] and people in the UK, trying to solve a similar problem to the one with which we were faced, had also started pressure attenuation experiments. John Maw in the UK and Stew Griffith at Sandia both had looked at the shock transmission problem theoretically and the understanding derived from their analyses provided the guidance for much of the early experimental effort.

2 Description of Experimental Setup and Instrumentation

The intent of this paper is to discuss the experimental results and not to delve extensively into the measurement techniques and procedures. This is fortuitous as it would be nearly impossible to recreate many of the experimental details from the written records still in existence.

A major concern in any experimental program is in the determination of methods to assess the validity of the data which is being collected. To provide confidence that the measurements which were being made represented reality, experiments were conducted in air to compare data with the established data published in TM 5-1300 [3]. Also, the results of the attenuation experiments were compared to the previously mentioned tests conducted in aqueous foam in the UK. In addition, several experiments were repeated to assure that the results could be duplicated and, in many experiments, redundant measurements were made to check on reproducibility. The results of these experiments gave confidence that the data was credible.

A typical experiment would involve a surface detonation of a one-pound hemisphere of explosive in an 8 ft. by 8 ft. by 6 ft. high enclosure filled with aqueous foam of the prescribed density**.** Figure 1 shows a charge and gauges in a plywood containment structure. While many different measurements systems and gauges were used over the evolution of the test series, the workhorse was the Kulite HKM-375 piezoresistive device. To measure the side-on (also referred to in this paper as free-field or incident) pressure, the gauge was mounted flush with, and a few inches behind, the leading edge of a heavy blade-shaped stand with the axis of the gauge perpendicular to the direction of travel of the wave front. “Pencil style” gauges (Figure 2) were also used for side-on measurements. The same type of gauge was also mounted rigidly with it’s axis aligned toward the pressure wave to measure the face-on (reflected) pressures; the mounting structure for these face-on gauges was designed to be massive enough to minimize the motion of the gauge and to preclude pressure relief from the edges of the structure during the positive phase of the pressure pulse. Other gauges used during the course of the investigation included the Entran EPF-200 piezoresistive gauge and the air-foil shaped Celesco LC-33 and the Susquehanna ST-4 piezoelectric devices; charge amplifiers frequently were required for use with the piezoelectric gauges. All of the gauge types were evaluated in a shock tube before their use and were recalibrated for each experiment.

Of the different gauge types considered, the Kulites proved to be the most reliable, produced the highest quality data, and provided most of the data which appears in this report. In the following report section interpreted recording results are reported for each transducer of each test. Unless specifically designated, all of the data reported were from the unamplified Kulite gauges; an A in the distance column indicates an amplifier was required, a C indicates a Celesco gauge reading, FO is for gauges mounted face on to the incoming pressure (gauges which measure a reflected rather than the free field pulse), and S signifies that the signal was recorded on an oscilloscope. When more than one measurement is shown at the same distance from the charge, the gauges were frequently mounted on the same stand with care being exercised to minimize any interference of the flow field between gauges.

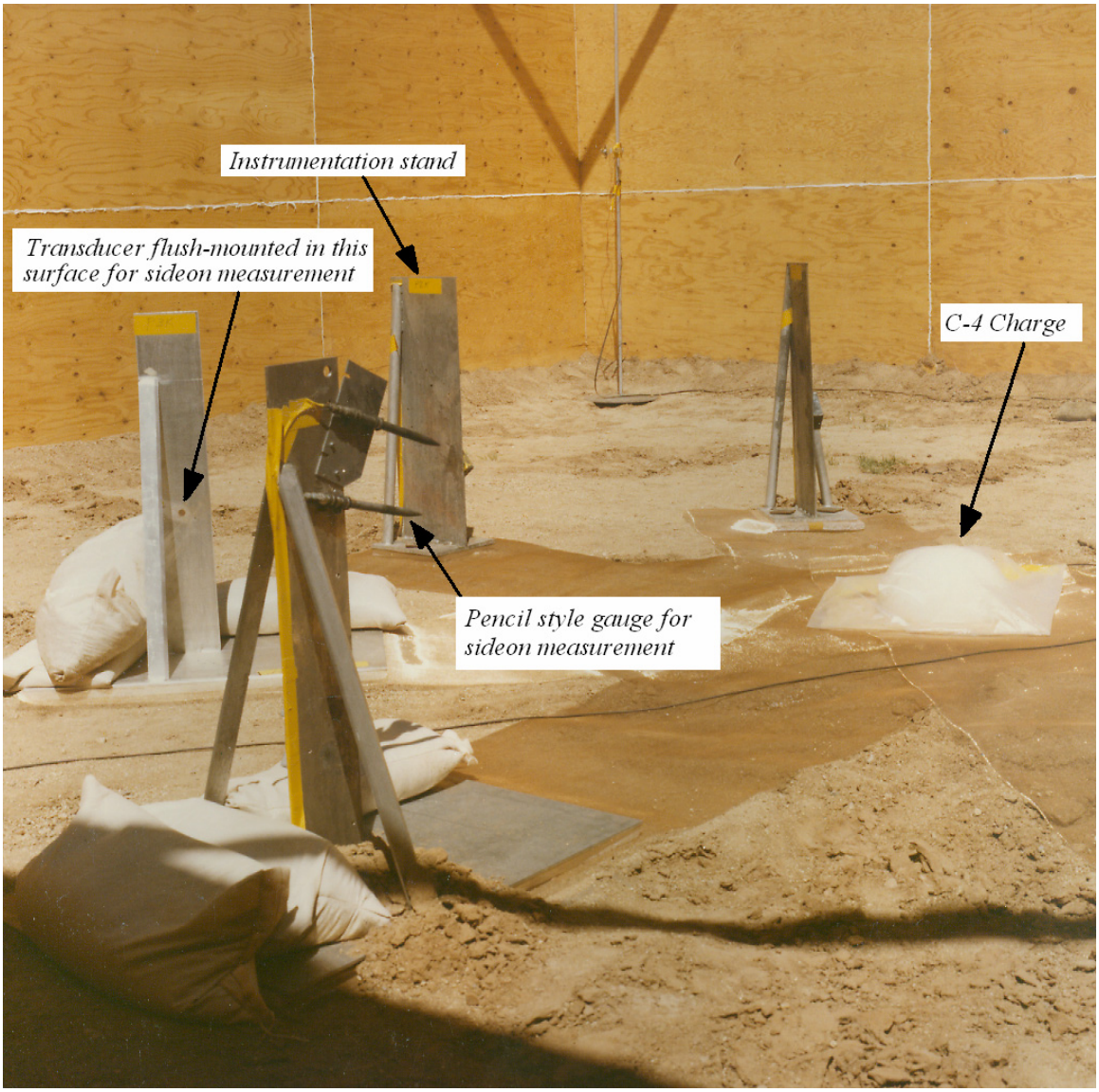

Figure 1: A typical setup with pressure gauges arranged around an explosive charge inside a plywood foam containment system.

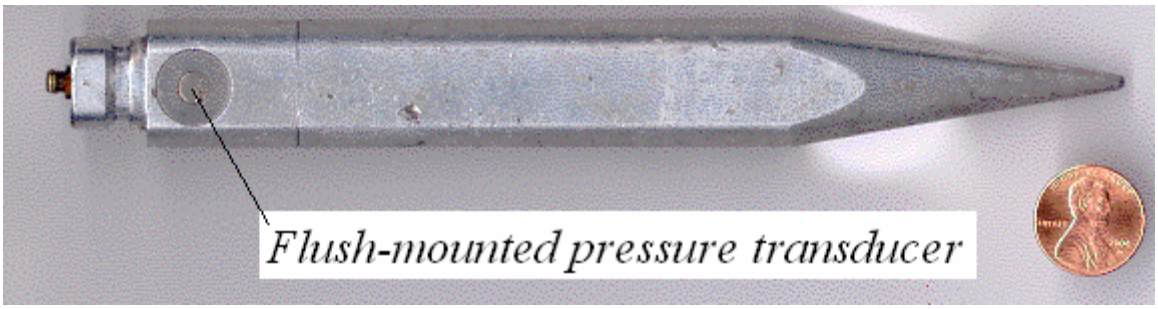

Figure 2: The forward end of a pencil gauge arrangement for measuring side-on overpressure.

In the cases where the recovered data was obviously in error - no signal, baseline shifts, improper signature, etc. - the data has not been included in this report. Extreme care was taken in this culling process to ensure that real, but unexpected, information was not being discarded. This is particularly true of the piezoelectric gauges recorded by the wide-band FM system. The reduction of this data required precise determination of the input capacitance of the recording system and, in the case of that data recorded in the instrumentation trailer, the effort to make an accurate dynamic assessment of this impedance was never completely successful. This same Celesco data was also measured on the recording oscilloscope and, in these cases, the data usually was very consistent with the Kulite measurements.

The test arrangement and instrumentation were modified frequently during the course of the experiments to enhance signal quality. The gauge bodies and connections were coated to isolate them from the slightly-conducting foam. The faces of the gauges were coated with a very thin film of non-conducting grease for the same purpose. The blade type gauge stands were made extremely rigid and massive, the stands were mounted on one-inch thick pads of rigid foam to reduce ground shock effects, the gauges were mounted in insulating bushings and their housings were connected to a single, common earth ground, and the entire area under the explosive charge and out to the gauge stands was covered with conducting mesh to minimize spurious signals from the HE detonation. Because of these evolutionary modifications, the quality of the information showed a continuous improvement over the course of the experiments.

One of the difficulties in making these measurements is to minimize the influence of pressure waves reflected from the ground or other surfaces or interfaces which may be present. For the close-in gauges, where the pressure front is steep and the pulse is of short duration, this was usually possible. At greater distances, reflections were inevitable and, while the peak pressure reading probably was not strongly affected, the trailing edge of the wave front undoubtedly included reflected contributions in some instances. As the impulse was determined by time integration of the pressure pulse, any reflections which were present would alter the impulse determination.

Many of the details of the recording system have been lost. The initial system employed was a wide band FM magnetic tape system formerly used at the Nevada Test Site (NTS); while the frequency response capability is not known, most of the data was reduced

through a 20 KHz low pass filter. Later in the test series, the analog recording system was replaced by a digital system (known as DAASY) which also had been built for use at NTS and by the use of digitizing oscilloscopes.

In all of the experiments, the foam density was calculated from flow meter-time measurements and also from a calibrated parallel plate resistance meter developed by K. C. Goettsche.

Repeated attempts were made to measure pressures close in (within 5 to 10 times the explosive radius) without much success. Outside of this distance, the system produced (usually) exceptionally clean records and reproducible results.

3 Blast Wave Measurements

3.1 Overview

This section of the report deals with those experiments which were designed primarily to measure the attenuation of HE-induced pressures passing through aqueous foams of different densities. Aqueous foams, unlike air, do not support sharp pressure discontinuities. Figure 3[1] and Figure 4 show the transient pressures recorded 2 feet and at 10 feet for the test of June 16, 1983. Notice the increase in TOA, rise time, and positive phase duration associated with the greater distance. At ten feet (Figure 4) the rise time of about 8 ms is about half of the positive phase duration and very much longer than the sharp rise that would be witnessed in air.

There are thirteen experiments reported here whose basic purpose was to measure attenuation. The experiments are summarized in and will be discussed in order of increasing foam density (decreasing expansion ratio).

[1] Figures 3 and 4 were carefully hand-digitized from printed analog records. Consequently, some high frequency oscillations will have been filtered.

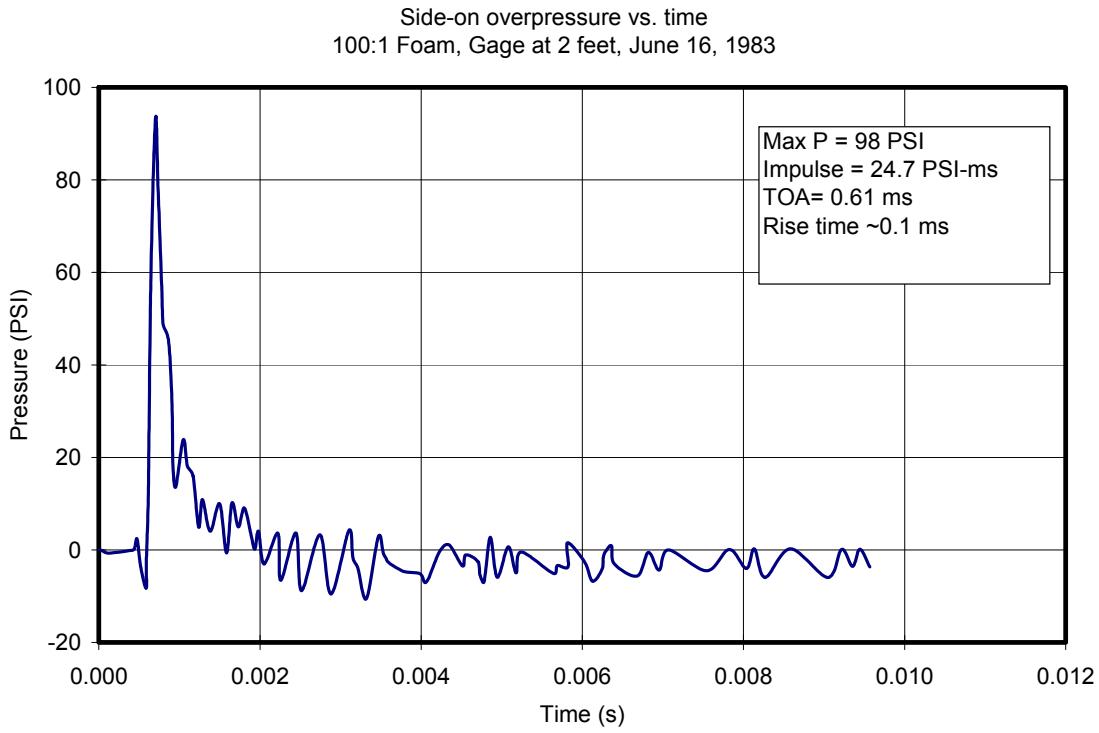

Figure 3: Transient side-on pressure record measured at 2 feet from charge center, June 16, 1983, 100:1 foam.

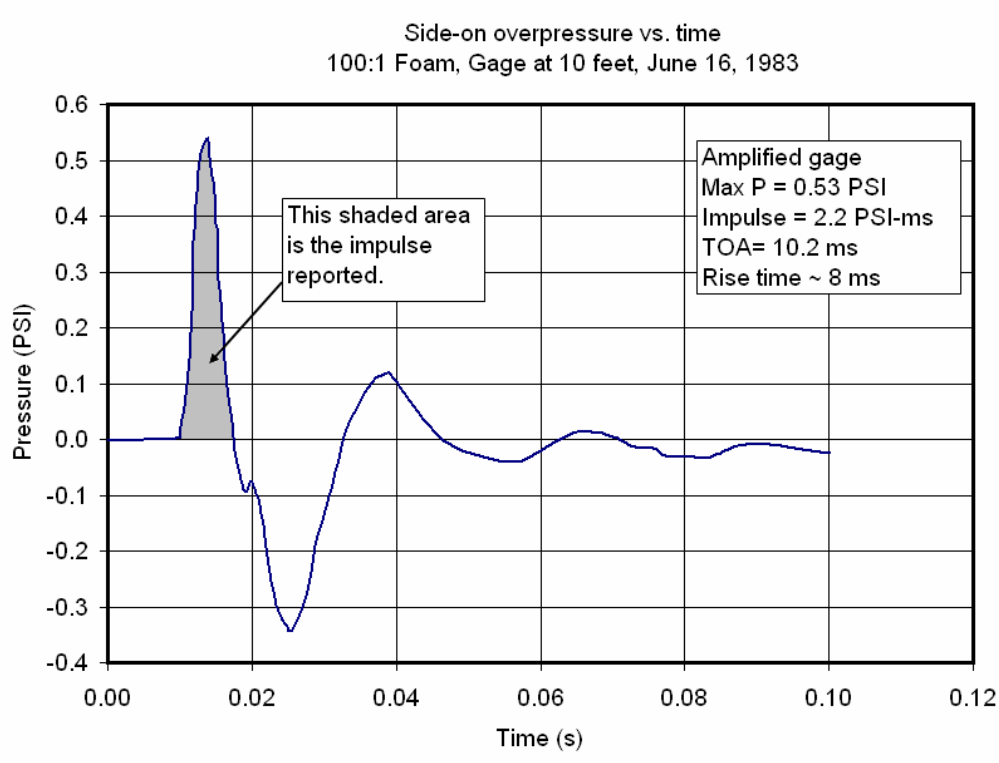

Figure 4: Transient side-on pressure record at 10 feet, June 16, 1983, 100:1 foam.

Table 1: Summary of experiments described.

Intended ER	Actual ER	Test Date	Explosive mass (lbs)	Comments
None (air)	None (air)	11/23/82	0.15	Baseline test
1000:1	1000:1	9/6/83	1	Good face-on measurements
400:1	375:1	3/28/83	1	
200:1	200:1	4/13/83	1	
100:1	100:1	11/18/82	1	Includes foam/air interface meas.
100:1	100:1	6/6/83	1	
100:1	100:1	8/9/83	1	High viscosity foam
60:1	54:1	10/28/82	1	Includes foam/air interface meas.
60:1	60:1	4/28/83	50	Scaling test
60:1	100:1	8/2/83	1	Extended instrument distances
60:1	60:1	3/1/9/84	1	Extended instrument distances
20:1	27:1	7/29/82	1	
10:1	10:1	9/1/82	1	

3.2 Air Only Baseline Experiment [2]

The purpose of this experiment was to verify the experimental capability by comparison of the measured data with the standard air shock data of TM 5-1300. To keep the blast pressures within the range of the gauges which were used for the foam experiments, a 0.15 pound explosive charge was used rather than the standard one-pound hemisphere.

As the experiments reported in this series were conducted in Albuquerque, barometric pressure was lower than standard. Sachs scaling [4, 5] for pressure, impulse, and time are as follows:

$$\frac{p}{p_0} = f_1\left(\frac{R\,p_0^{1/3}}{E^{1/3}}\right) \tag{1}$$

$$\frac{i''a_0}{E^{1/3}p_0^{2/3}} = f_2\left(\frac{R\,p_0^{1/3}}{E^{1/3}}\right) \tag{2}$$

[2] Memo. L. A. Fjelseth to Distribution, "Pressure Instrumentation for Baseline Test in Air", SNL, Nov. 23, 1982 (a report analyzing the results of this test was not located although the reduced data is available)

$$\frac{ta_0\, p_0^{1/3}}{E^{1/3}} = f_3\left(\frac{R\, p_0^{1/3}}{E^{1/3}}\right) \qquad (3)$$

The predicted values for overpressure, specific impulse, and time of arrival in Table 2 and Figure 5 are based on the curves documented in TM 5-1300 for TNT surface bursts. They are adjusted according to Sachs scaling assuming an absolute pressure of 12.05 psia and a detonation energy density such that one pound of C-4 is equivalent to 1.08 lbs of TNT. An additional element of uncertainty is associated with the "contact surface multiplier." That is, the extent of energy lost to work on the charge-supporting surface is not characterized.

Table 2: Results of air baseline experiment

Distance (ft)	Measured Pressure (psi)	Predicted Pressure (psi)	Measured Impulse (psi-ms)	Predicted Impulse (psi-ms)	Measured TOA (ms)	Predicted TOA (ms)
1.5 C	155 (101%)	154	13.1 (131%)	10.0	0.22 (105%)	0.21
2	64 (78%)	82	11.1 (118%)	9.4	0.31 (89%)	0.35
2.5	No Data					
4	16.8 (99%)	17	4.6 (71%)	6.5	1.35 (105%)	1.28

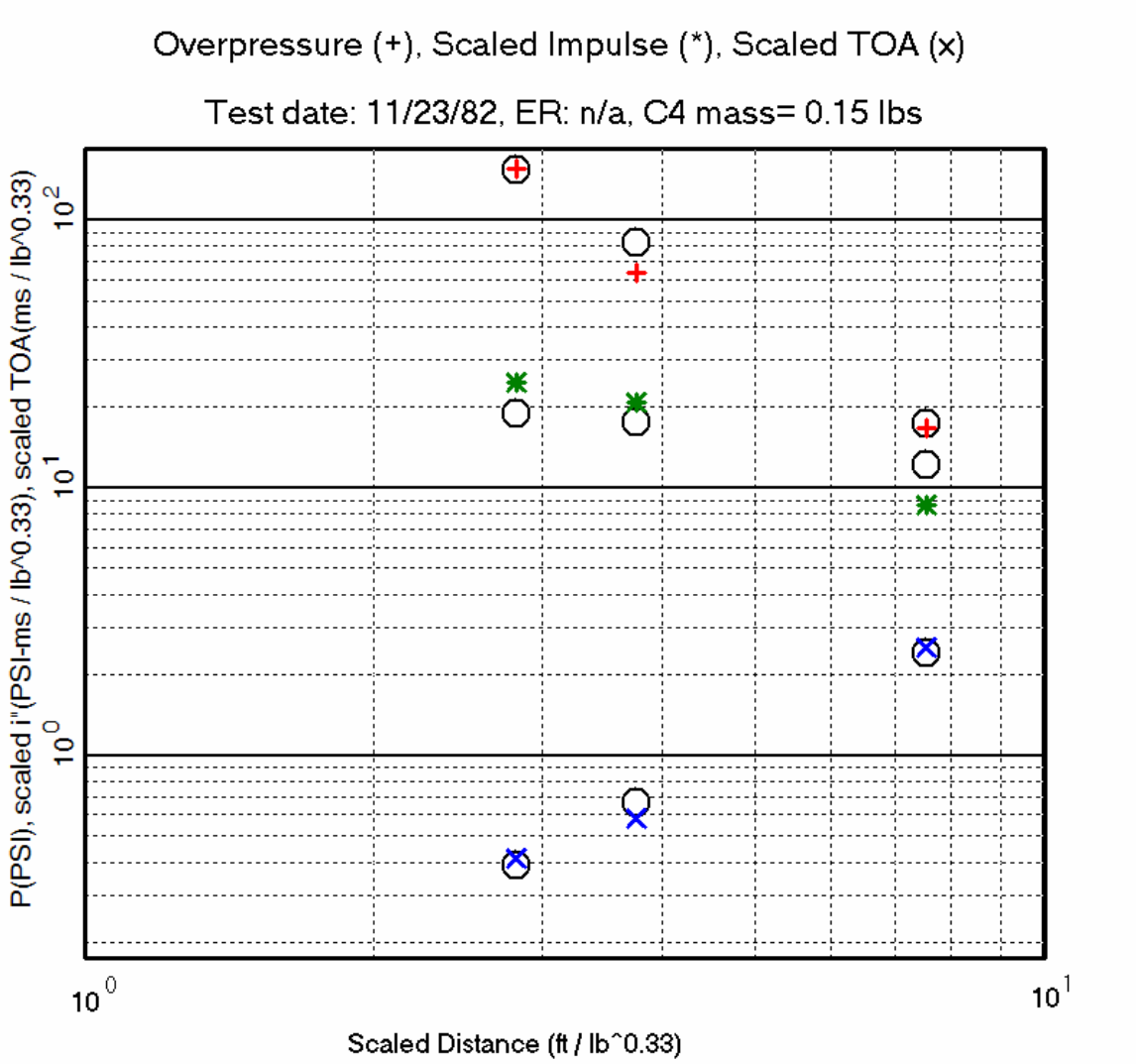

Note: Predicted overpressure, Impulse, and TOA are circles.

Figure 5: Plot of overpressure, impulse, and time of arrival data for baseline shot, 11/23/82.

The comparison was good enough that it gave us confidence that our measurements were valid. As can be seen in Table 2 and will also be apparent in other experiments, the impulse - determined by integration of the pressure pulse from the time it broke away from the baseline until it crossed back over at the start of the negative phase of the pulse - is probably less reliable than either the peak pressure or the time of arrival measurement. This results from both the baseline drift in the recording system and the integration of any noise bursts or reflections that appear on the trace.

3.3 1000:1 Foam Experiment [3]

This test produced good data (Table 3 and Figure 6) not only for blast wave attenuation but also for the comparison of the free field to reflected pressures and impulses.

Table 3: Results of 1000:1 foam experiment

Distance (ft)	Pressure (psi)	Impulse (psi-ms)	Time of Arrival (ms)
3	45.1	7.4	0.66
3.5	37.8	8.8	0.87
4	21.2	9.1	1.26
4.0 (FO)	59.3	38.5	1.37
4.0 (FO)	55.8	37.5	1.37
5.5	5.6	7.6	2.43
5.5(5)	5.4	5.6	2.95
8	2.34	7	4.61
10	1.92	6.6	6.43
10(5)	2.04	5.82	7.05

[3] Memo, Lewis J. Fjelseth, "Results of 1000:1 Aqueous Foam Test" SNL, Sept. 6, 1983

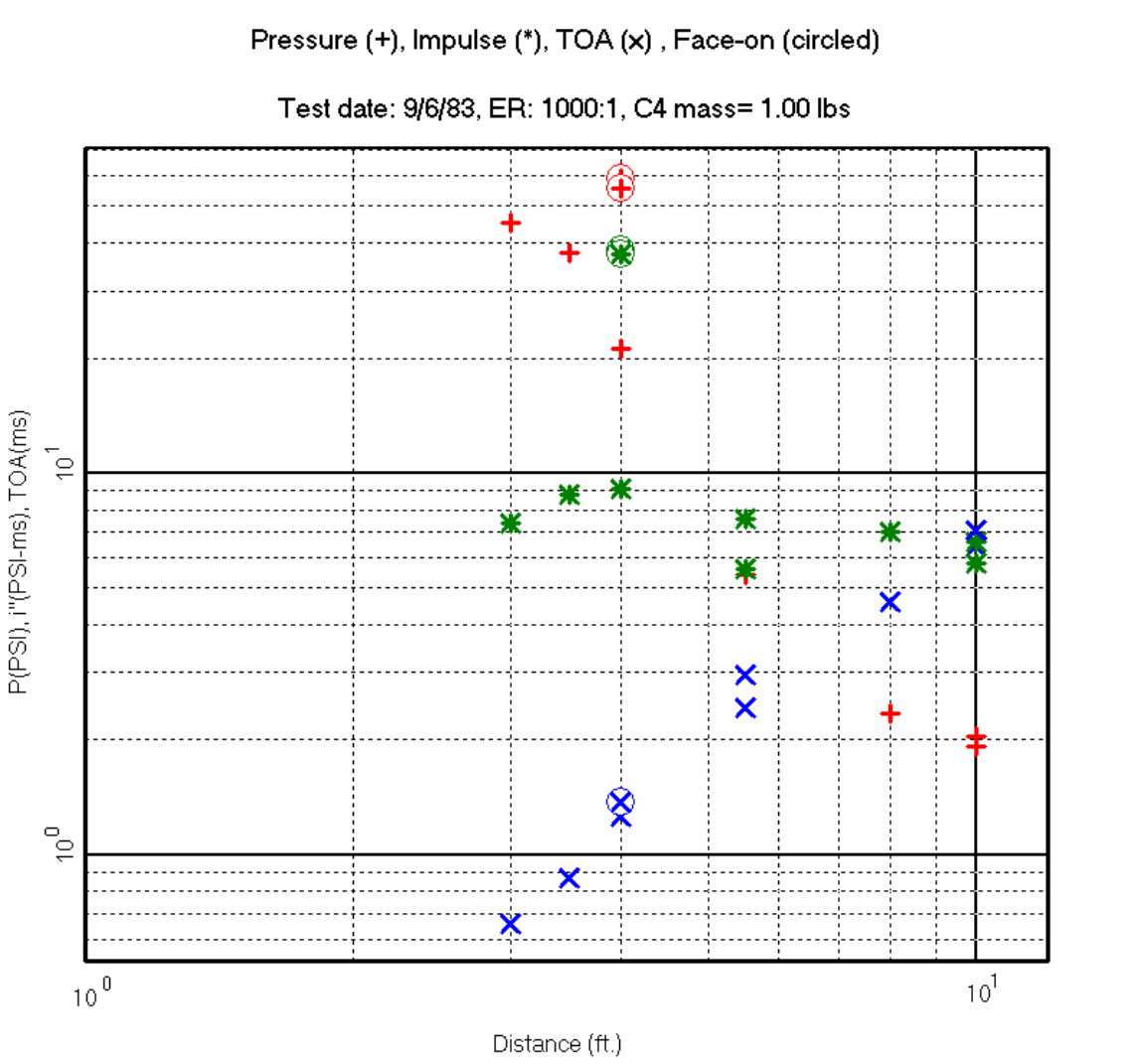

Figure 6: Plot of overpressure, impulse, and time of arrival data for 1000:1 foam, 9/6/83.

The data in this experiment looks reasonable, the pressures falling monotonically and the times of arrival increasing with distance. From distances of 3 foot out, there appears to be little significant decrease in impulse for the free field measurements. Note the consistency of the pressure measurements for the redundant gauges at 5.5 and 10 feet. As expected the reflected peak pressure and impulse for the face-on measurements at 4 feet are greater than side-on quantities at the same distance. Notice that the side-on pressure measurements in at a scaled distance around 10 ft/lb$^{1/3}$ are reduced about a factor of two.

3.4 400:1 (375:1) Foam Experiment [4] [5]

The intent for this test was to use 400:1 foam, but the measured expansion ratio at gauge height at shot time was about 375:1. Results are summarized in Table 4 and Figure 7.

Several of the gauges in this experiment produced suspicious results. In particular, the face on gauge data at 40 inches is obviously erroneous. As shown, two other gauges yielded no useful data. The gauge at 3.3 feet was one of the initial attempts to measure the pressure pulse in air after it had left the foamed enclosure, having passed through 2.2 feet of foam, a one-quarter inch plywood wall of the enclosure and 1.1 feet of air. The pressure and impulse are lower for this station. As expected the reflected peak pressure and impulse for the face-on measurements at 4 feet are greater than side-on quantities at the same distance.

Several other tests which will be discussed later also employed a gauge similarly positioned outside of the foam to determine the pressure drop across such interfaces.

Table 4: Results of 400:1 (375:1) foam experiment

Distance (ft)	Pressure (psi)	Impulse (psi-ms)	Time of Arrival (ms)
2.5	77.6	16.8	0.52
3	21	7.5	0.97
4	10	7	1.73
4.0 A	9.8	6.9	1.75
4.0 C, A	No Data		
4.0 C, S	7.8	No Data	No Data
5	4.5	7.8	2.59
7	3.3	7.8	4.3
10	1.4	4.2	7.11
10.0S	No Data		
3.3 (foam/air)	3.8	3.6	1.36
4.0 (FO)	45	23.7	1.47
11.8 A	2.3	7.5	8.9

[4] Memo, L. A. Fjelseth, "400:1 Aqueous Foam Test", SNL, March 28, 1983. This is the instrumentation plan but the data traces are available.

[5] Memo, L. A. Fjelseth, "Summary of Aqueous Foam Test Results," July 21, 1983.

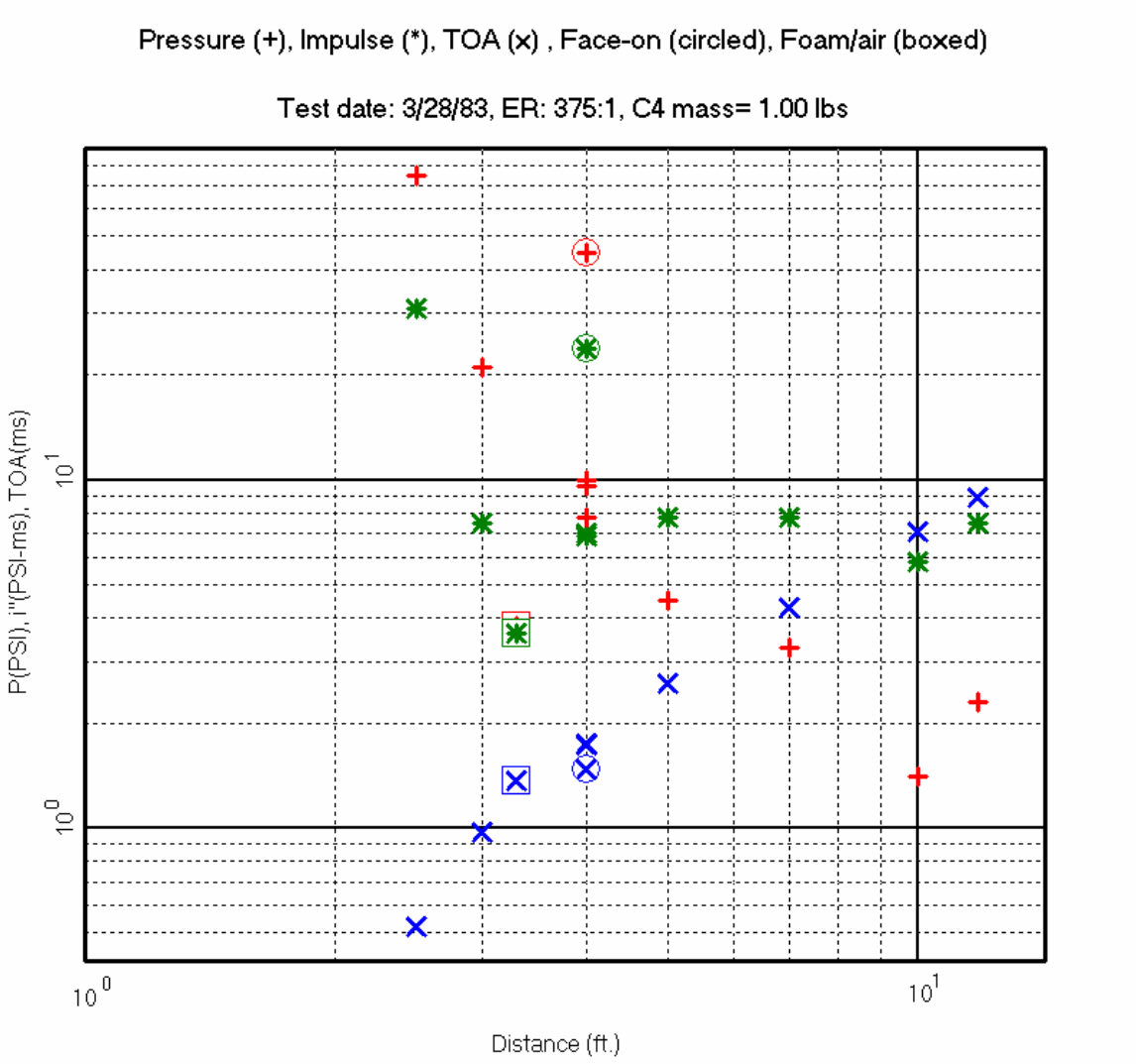

Figure 7: Plot of overpressure, impulse, and time of arrival data for 375:1 foam, 3/28/83.

3.5 200:1 Foam Experiment [6]

The experimental setup in this test was similar to those previously discussed again with a face-on gauge at 4 feet. The pressure data recorded on the amplified gauge at 4.0 feet was judged to be erroneous and was discarded. This experiment again included a gauge placed exterior to the foam enclosure to record the pressure in air after it had traversed 2.2 feet of foam and 1.1 feet of air. Results are summarized in Table 5 and Figure 8.

[6] Memo, L. A. Fjelseth, "Experimental Plan Data for 200:1 Aqueous Foam Test", April 13, 1983. The report and/or resume of this test was not located although the final data is available.

Table 5: Results of 200:1 foam experiment

Distance (ft)	Pressure (psi)	Impulse (psi-ms)	Time of Arrival (ms)
2	181	25	0.49
2.5	26	11.5	0.93
3	13.9	8.8	1.35
4	3.6	8.7	2.36
4.0 A	1.1		2.36
4.0 A, C	5.1		2.09
5	2.1	7	3.07
7	1.48	4.6	5.47
10	No Data		
3.3 (foam-air)	1.96		1.93
4.0 FO	7		2.09

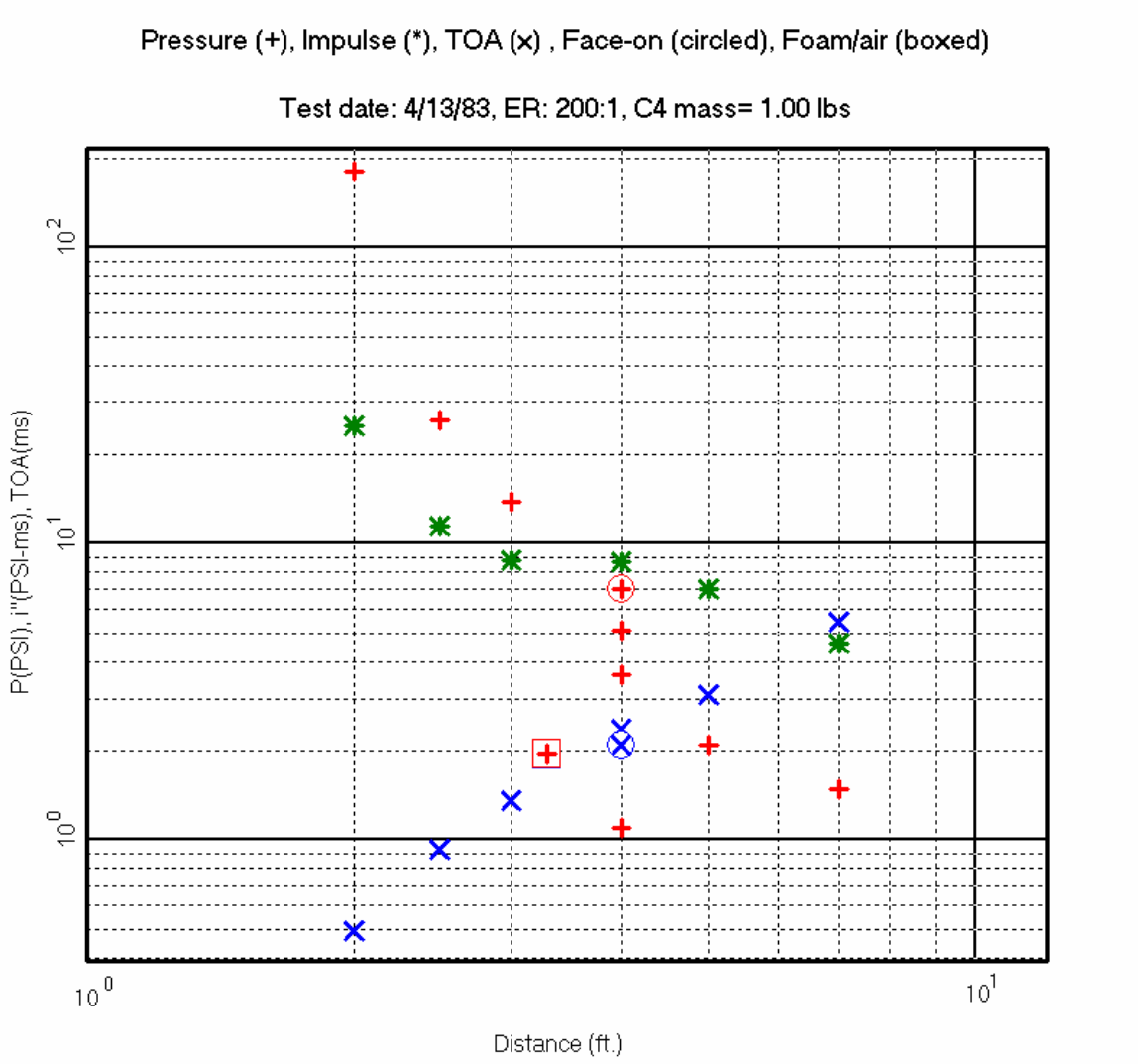

Figure 8: Plot of overpressure, impulse, and time of arrival data for 200:1 foam, 4/13/83.

3.6 100:1 Foam Experiments

During the period of time that this test series was being conducted, it became apparent that the optimum foam for the purposes of our program was going to be in the range of 60:1 to 100:1. Foams in this moderate density range exhibited strong mitigation and retain the advantages of moderate resource consumption and moderate load requirements in retaining structures. Because of this, three experiments were conducted with 100:1 foam; the first two were to evaluate the pressure and impulse attenuation, the third was to examine the change in these capabilities with an alteration - an increase in viscosity - in the foam concentrate.

The first 100:1 test (November 82 [7]) used both the Kulite piezoresistive and the Celesco piezoelectric gauges; none of the later gauges yielded acceptable data in this experiment. The results are summarized in Table 6 and Figure 9. The last gauge in the table again looked at the pressure drop across the foam-air interface.

Table 6: Results of First (Nov. 82) 100:1 foam experiment

Distance (ft)	Pressure (psi)	Impulse (psi-ms)	Time of Arrival (ms)
1.5	154	23.2	0.33
2	115	not useable	0.59
2.5	63	8.1	1.2
4	2.8	3.3	2.39
3.3 (foam/air)	2.6	reflections	1.75

[7] Memo, L. A. Fjelseth, "Pressure Instrumentation for 100:1 Aqueous Foam Test" Nov. 15. 1982. The final data is available although no test report could be found.

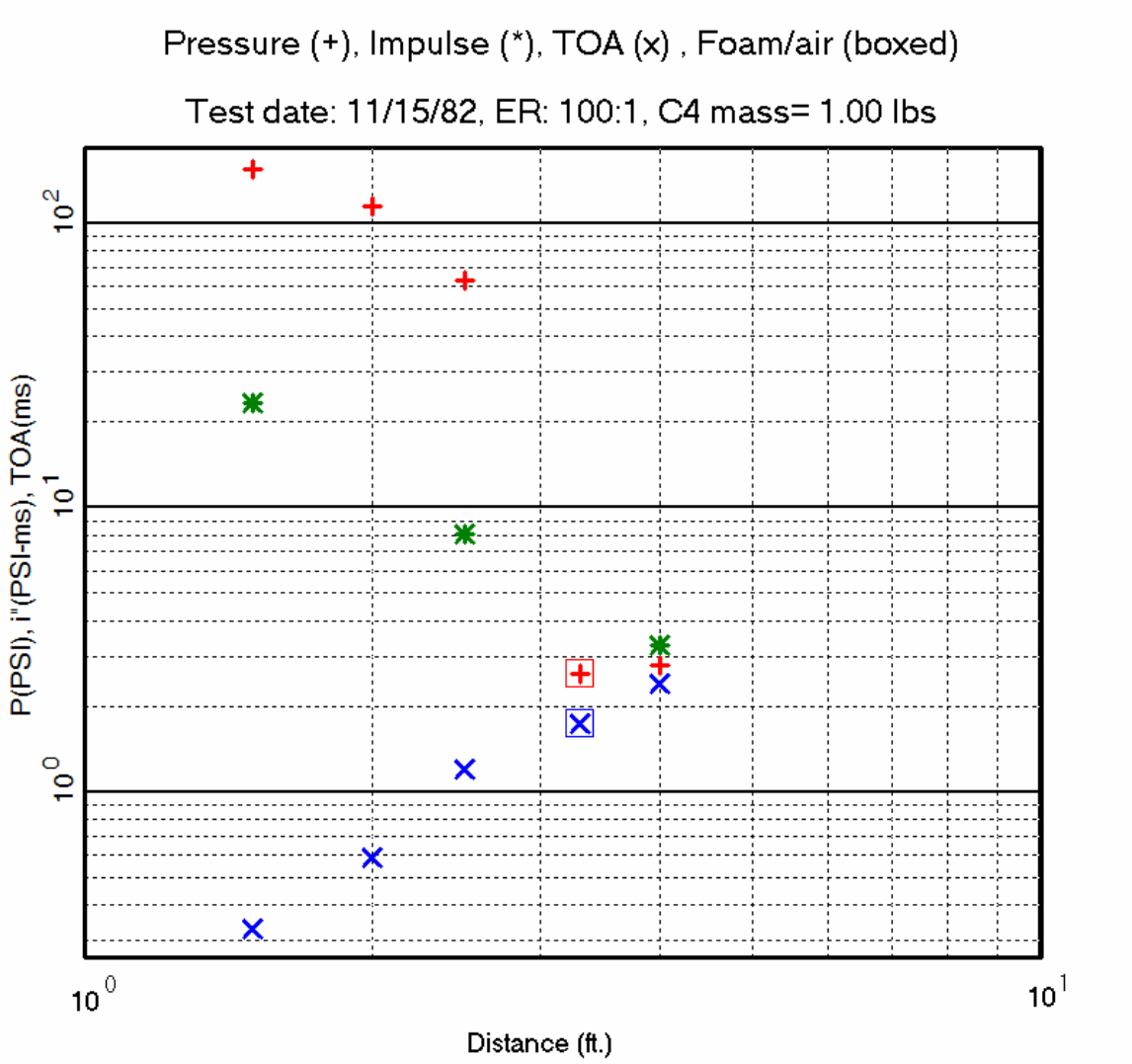

Figure 9: Plot of overpressure, impulse, and time of arrival data for 100:1 foam, 11/15/82.

The second test (June 83 [8]) provided what might have been the best set of data recovered in the entire series of foam tests. The data is summarized in Table 7 and Figure 10. The complete set of pressure pulses from this experiment appears in Appendix A . Not only are the records clean but the redundant measurements (those for which duplicate measurements were made at a specific distance), which used both different gauges and different recording systems, gave nearly identical results.

[8] Memo. L. A. Fjelseth, "Results of 100:1B Foam Test", SNL, July 6, 1983

Table 7: Results of June 18, 83 100:1 foam experiment

Distance (ft)	Pressure (psi)	Impulse (psi-ms)	Time of Arrival (ms)
2	98	24.7	0.61
2.5	21	11.7	1.01
3	9	9.6	1.61
4	3.1	10.1	2.01
4 A	3.1	9.8	2.07
5	2.2	7.8	3.9
5 A,S	2.65	8.4	
7	0.82	3.8	6.4
7 A	0.9	4.2	6.5
10	0.53	2.2	10.2
10A.S	0.46	1.7	

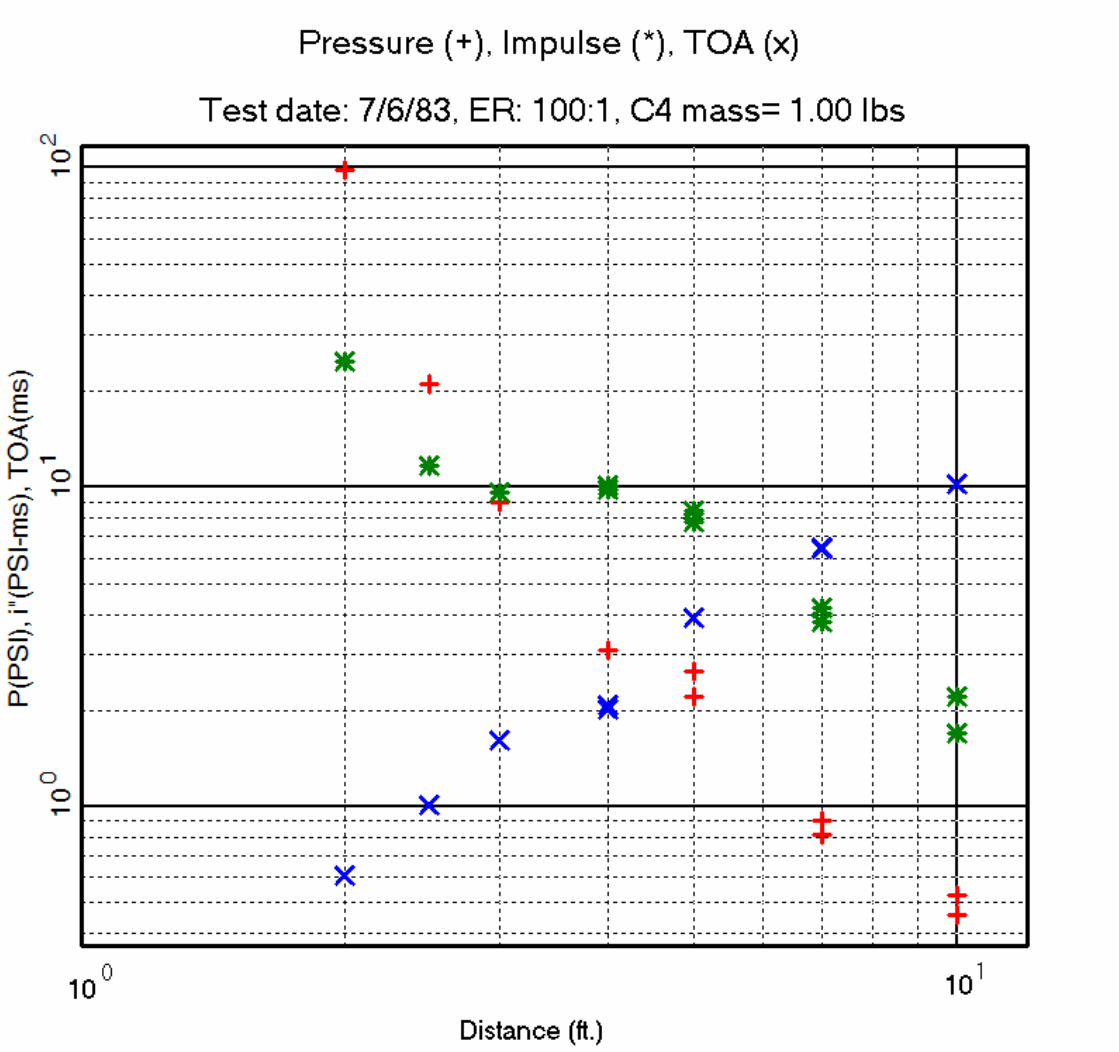

Figure 10: Plot of overpressure, impulse, and time of arrival data for 100:1 foam, 7/6/83.

The absence of time of arrival data from the scope records resulted from the use of the pressure pulse itself as the scope trigger mechanism.

A High Viscosity Foam Concentrate Test [9] was conducted to determine if changes in foam concentrate, particularly to a concentrate which is more viscoelastic, would change the blast mitigation properties of the foam. The results of the test are summarized in Table 8 and Figure 11. The conjecture was that mechanical breakup of the individual bubbles plays a significant role in the mitigation process and the effect of the increased viscoelasticity might be discernible, particularly at the lower pressures. Because of

[9] Memo, L. A. Fjelseth, "Results of 100:1 High Viscosity Foam Test", SNL, Aug. 9,1983

limitations on foamability and availability, the concentrate used for this experiment possessed a viscosity that was only 15% higher than the standard concentrate used for the remainder of the experiments.

Table 8: Results of experiment with high viscosity 100:1 foam

Distance (ft)	Pressure (psi)	Impulse (psi-ms)	Time of Arrival (ms)
2	74.5	18.5	0.61
2.5	23.2	13.8	0.9
3	10.2	11.6	1.44
4	2.9	8.8	2.36
4 A	3.7	11.1	2.24
5	1.4	6.1	3.24
7	0.98	3.2	6.7
7 A	1.01	3.8	6.05

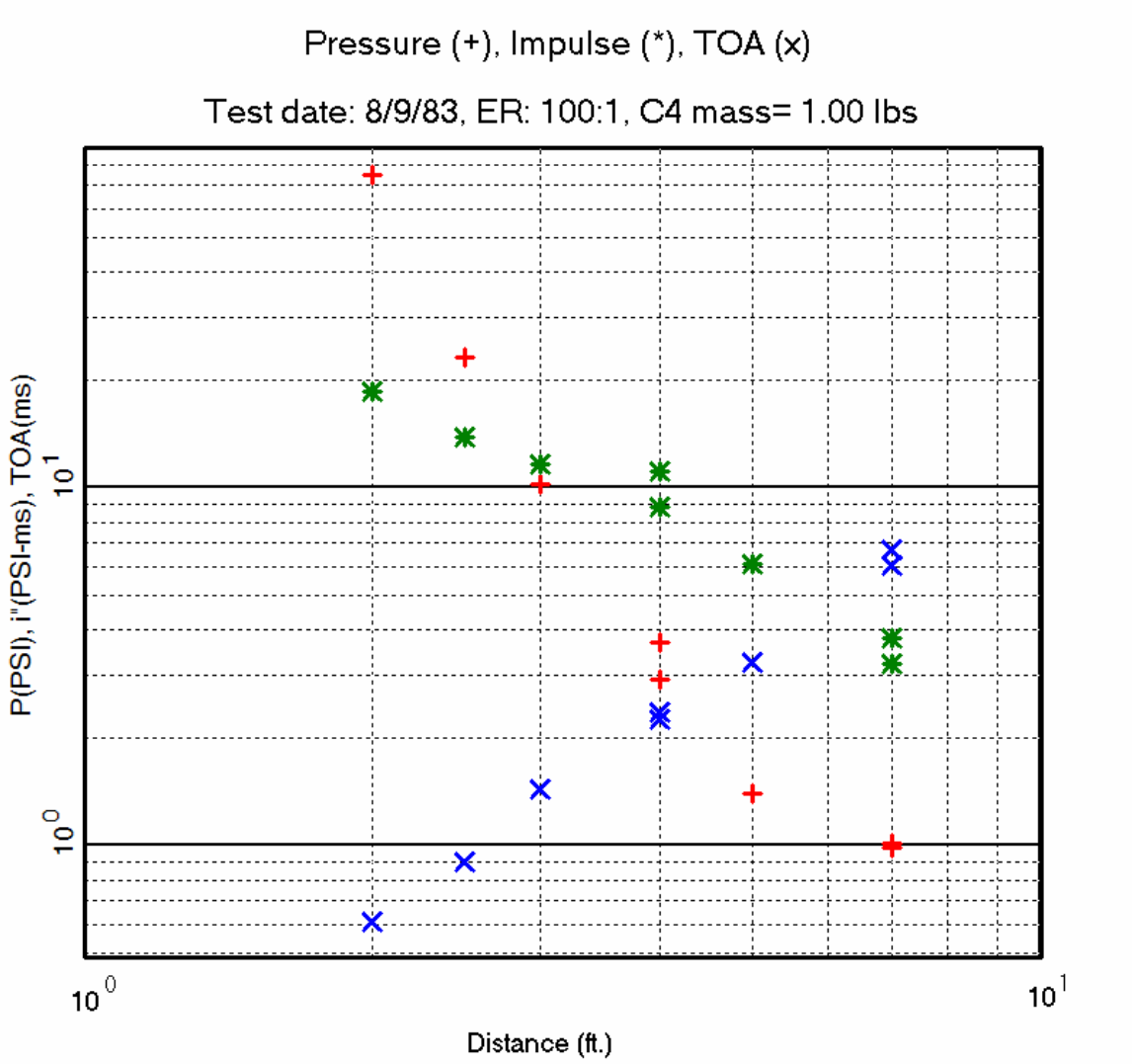

Figure 11: Plot of overpressure, impulse, and time of arrival data for 100:1 foam, 8/9/83.

The impulse data in this particular experiment is somewhat suspect as several of the recordings did not return to zero, making interpretation of the duration of the positive pressure phase uncertain.

Comparison of these results with June 83 100:1 (Figure 10) experiment indicates little effect. The differences between the two experiments are consistent with the differences between the redundant readings on a single experiment. In retrospect, this probably is not surprising as present estimates of the pressures required to break individual foam bubbles are in the region of 10 psi and the slope of the attenuation curve is so steep (it changes 2-3 psi per each inch of error in gauge placement at 10 psi) at these pressures that it would be difficult to observe experimentally.

3.7 60:1 Foam Experiments

Four tests were conducted with foams which were intended to have a 60:1 expansion ratio. The first of these was conducted in October 1982 and had a measured expansion ratio of 54:1. The second test, in May 1983, used a fifty pound HE charge and was designed to ascertain if the $W^{1/3}$-scaling laws developed for air detonations were equally applicable for detonations in foam - there was no real reason to suspect that they weren't but it was deemed advisable to conduct such an experiment to provide verification. The third 60:1 experiment (August 83) was for the purpose of securing additional data at distances where the pressure had decreased to less than one psi; while the data in this test was good, the foam in this experiment drained very rapidly and was less than 100:1 by the time the shot was fired. The last test in the series of four, in March 1984, was a repeat of the August 83 experiment and this time the desired 60:1 foam density was present at detonation time.

The initial 60:1 experiment (October 82 Test [10]) was a part of the set of screening experiments aimed at determining if, as predicted by the analytical models, the pressure mitigation began to decrease as the foam became more dense. This experiment was conducted, in fact, after the 10:1 and 20:1 experiments which will be discussed later. As previously mentioned, the actual expansion ratio of the foam at the time of detonation was measured to be 54:1. The results are summarized in Table 9 and Figure 12.

Table 9: Results of experiment with 60:1 (54:1) foam

Distance (ft)	Pressure (psi)	Impulse (psi-ms)	Time of Arrival (ms)
1.5	107	22.5	0.5
2	44	18.3	0.7
2.5	38	19.3	1
4	2.3	10.5	2.9
4 C,S	2.1		
3.3 (foam/air)	1.7	2.8	2.2

[10] Memos, L. A. Fjelseth, "Preliminary Data From 60:1 Foam Test" Nov. 2, 1982 and "Digitized Data For 60:1 (54:1 Actual) Foam Test", Nov.23, 1982, SNL

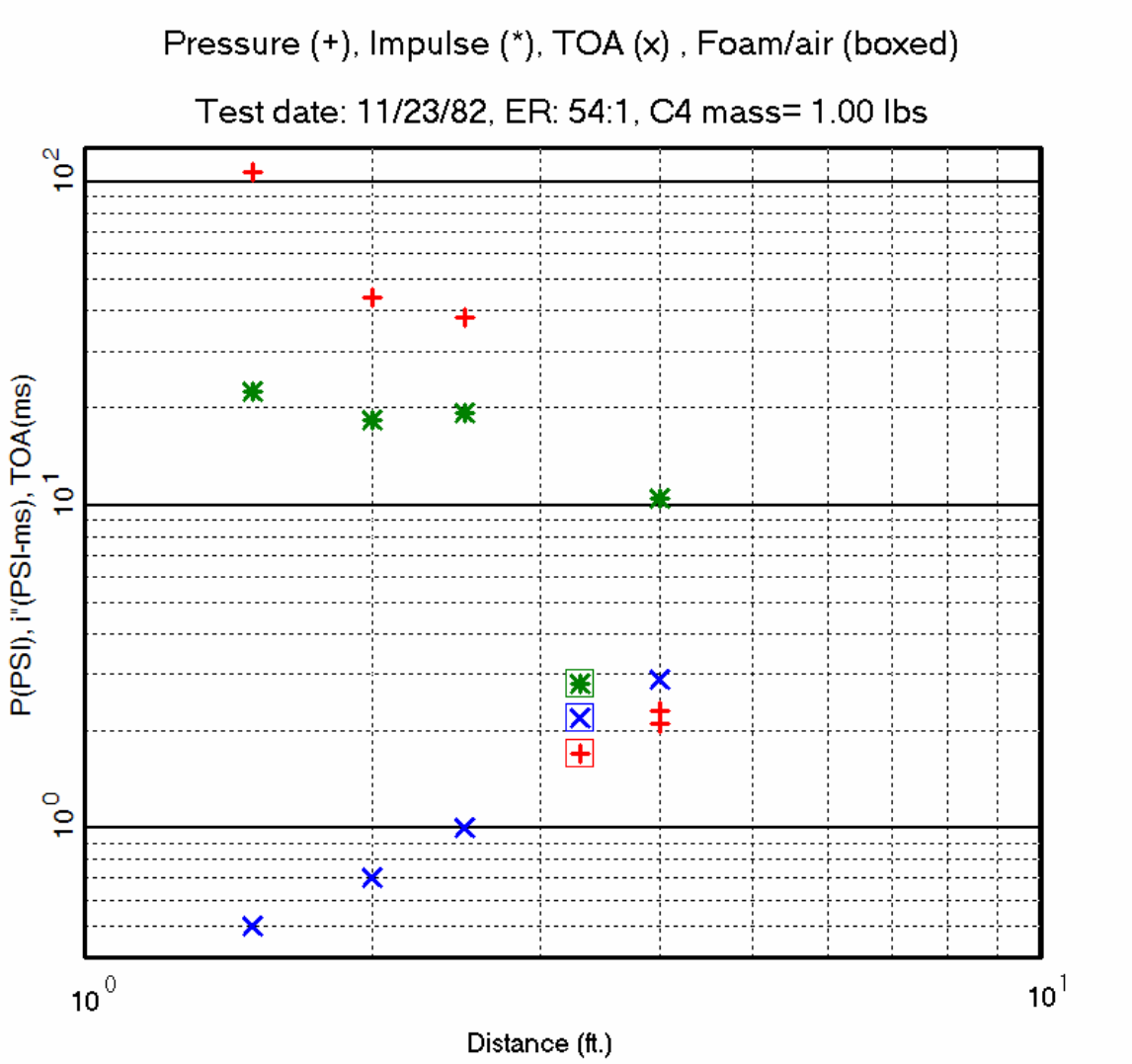

Figure 12: Plot of overpressure, impulse, and time of arrival data for 54:1 foam, 11/23/82.

A larger charge was used (May 83 Test [11]) to ascertain the assumed scaling relationships. A 32 foot square by 16 foot deep foam enclosure was used with the 50 lb. explosive charge offset from the center of the enclosure to permit readings to be made out to an 18 foot distance. The results are summarized in Table 10 and Figure 13. As had been the case for other foam experiments, gauges closer in than a scaled distance of about 2 feet yielded erratic wave shapes, presumably because of close in fireball and ionization effects.

[11] Memo. L. A. Fjelseth, "Results of 50 lb/60:1 Test", June 7, 1983.

Table 10: Results of 50-lb, 60:1 scaling experiment

Actual Distance (ft)	Scaled Distance ($ft/1b^{1/3}$)	Pressure (psi)	Impulse (psi-ms)	Time of Arrival (ms)
7	1.9	66	55.5	2.8
8	2.17	18.8	45.8	4.1
8 A	2.17	19	44.3	4
9.5	2.58	11.4	57.5	5.9
11.5	3.13	7.2	56.5	8.9
18	4.89	2.3	38.4	18.9
18 (16 foam/2 air)	4.89	0.38	8.9	18
18 A (16 foam/2 air)	4.89	0.48	8.7	19

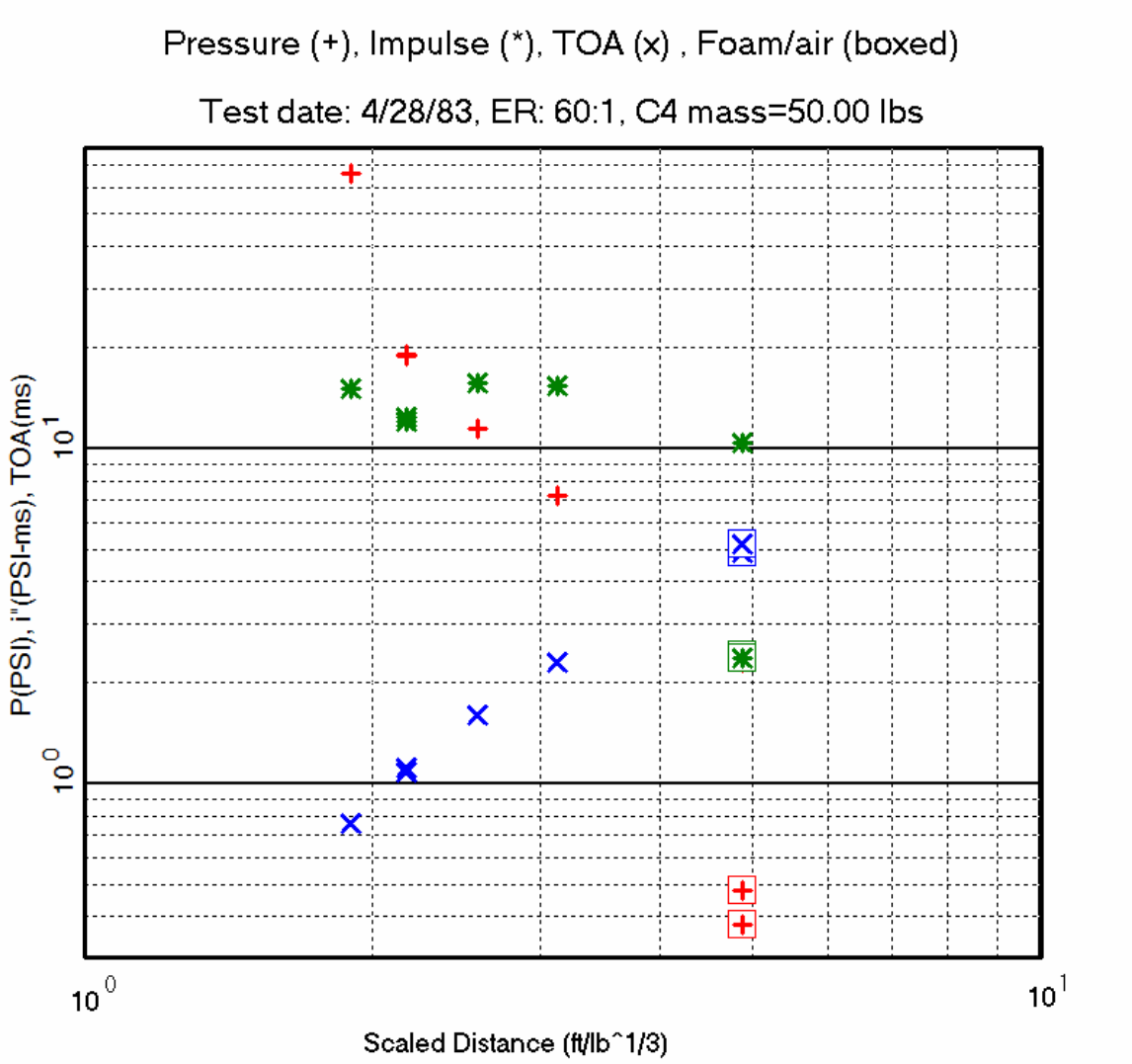

Figure 13: Plot of overpressure, impulse, and time of arrival data for 60:1 foam, 4/28/83 (50-lb charge).

Figure 14 shows peak overpressure versus scaled distance for the test data of Table 9, Table 10, and Table 12. The figure shows pressure data plotted versus scaled distance are consistent, within experimental accuracy, with the other 60:1 measurements. The results of the test with 54:1 are also include and generally lie a bit below the other two tests. This agreement led to the conclusion that the $W^{1/3}$-scaling laws were applicable within the foam environment for pressure. Figure 15 shows scaled specific impulse versus scaled distance for the test data of Table 9, Table 10, and Table 12. The scaling is marginally successful. Neither of the experiments with one pound charges has as steep a decline with increased scaled distance at moderate ranges as that for the 50 pound charge.

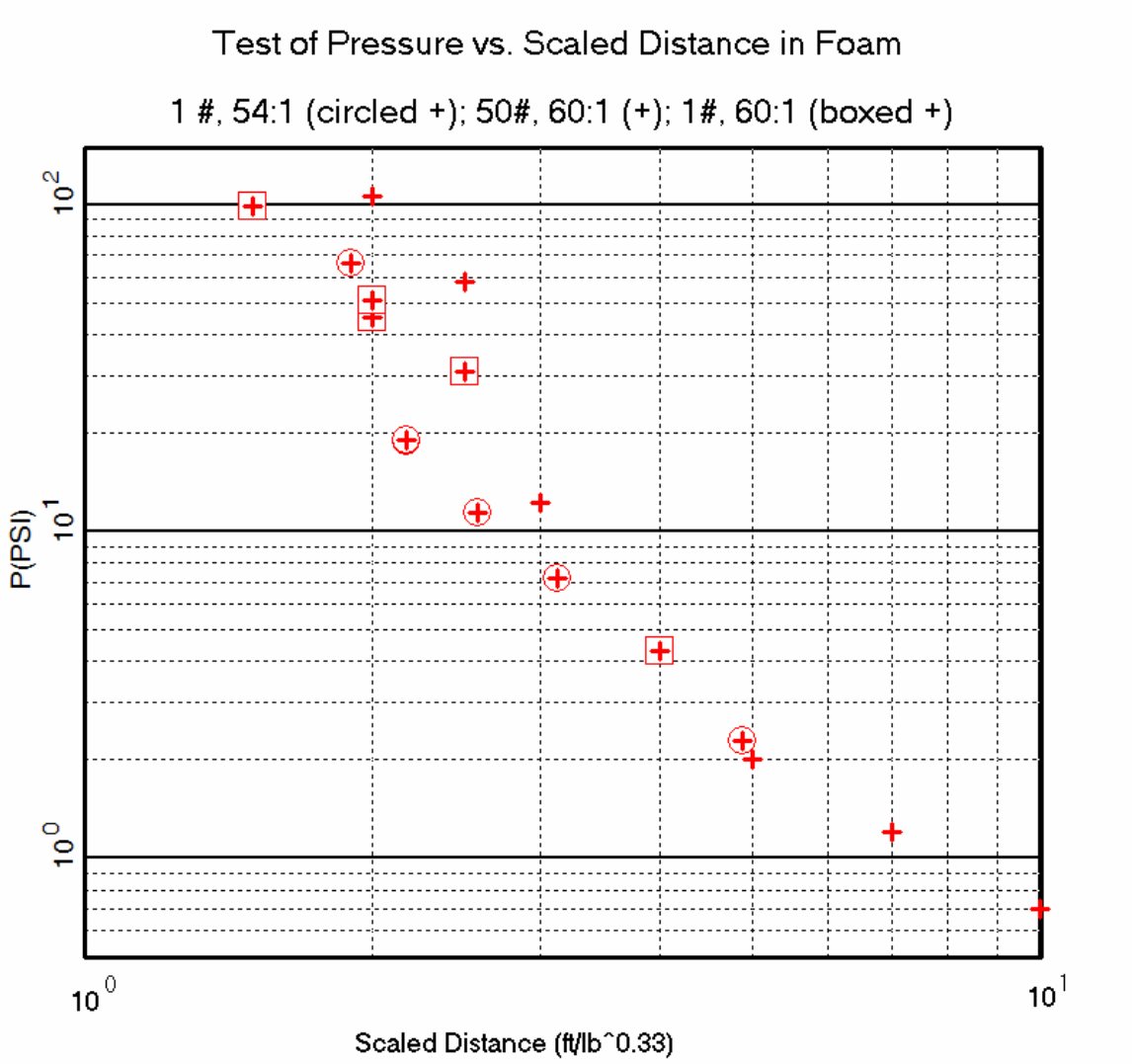

Figure 14: Test of overpressure versus scaled distance.

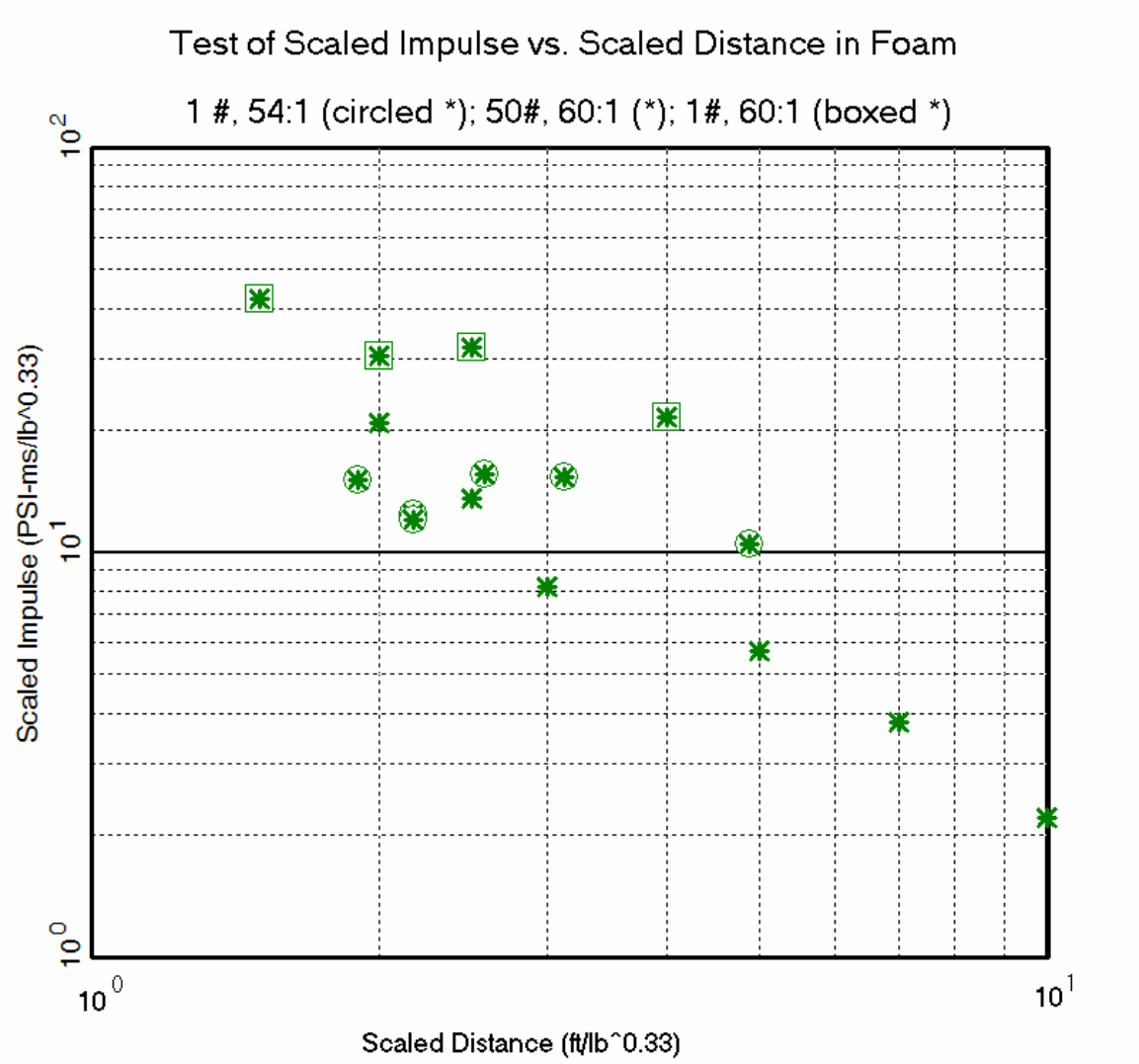

Figure 15: Test of scaled specific impulse of arrival (i"/W$^{1/3}$) versus scaled distance.

Figure 16 shows scaled time of arrival versus scaled distance for the test data of Table 9, Table 10, and Table 12. Each of the three tests follows its own clear (and nearly straight line) course and are significantly separate from each other. Based on the two tests with 60:1 foam, the W$^{1/3}$-scaling appears to fail. On the other hand comparing the two 1 lb shots in 60:1 and in 54:1 foams significant sensitivity to the foam density is implied. The apparent failure to scale as anticipated may be significantly due to poor knowledge of the foam density.

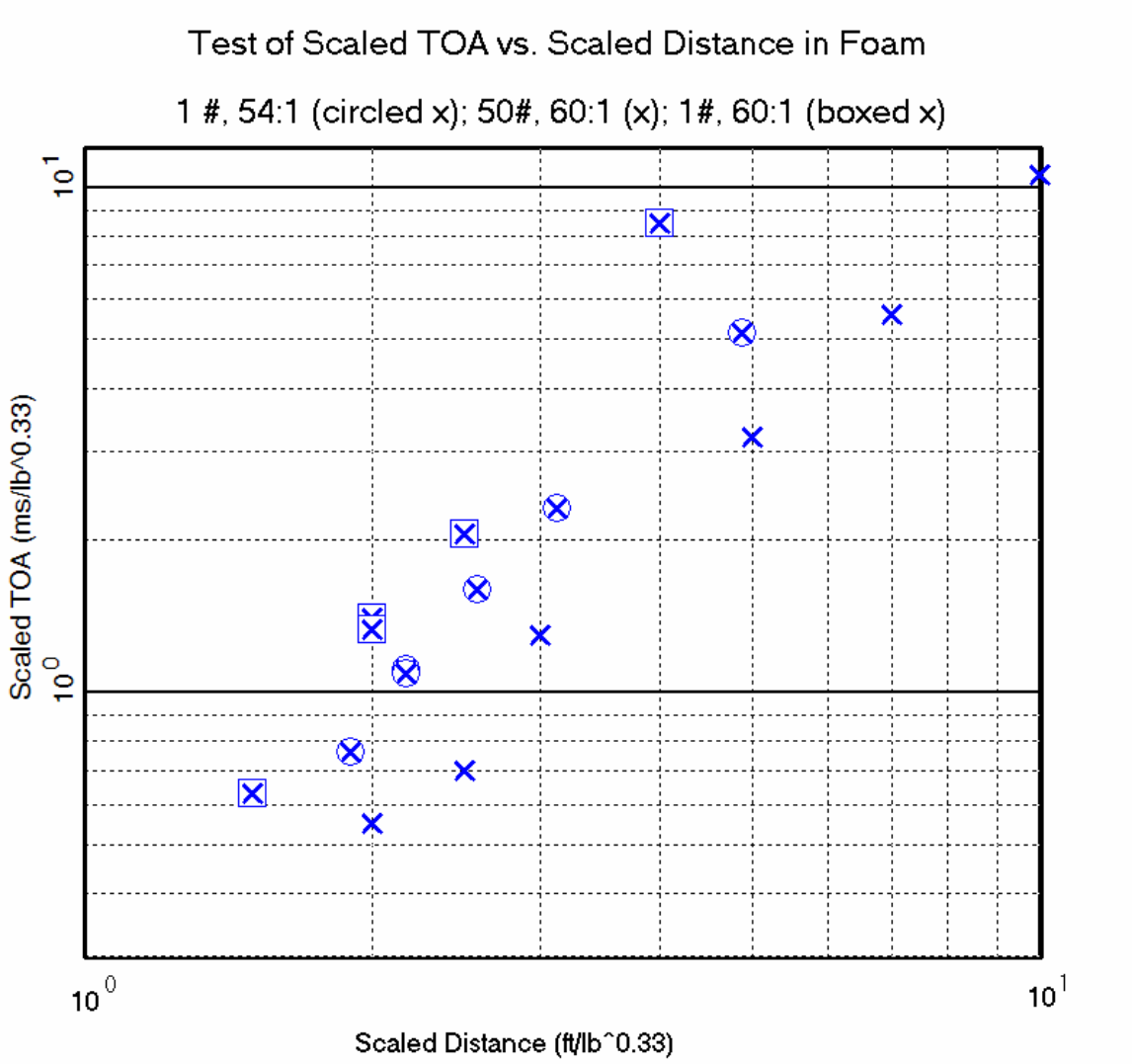

Figure 16: Test of scaled time of arrival (TOA/W$^{1/3}$) versus scaled distance.

The remaining two tests designed to use 60:1 foam shared the objective of making measurements at greater ranges than the tests discussed thus far. It was desired to obtain measurements at distances corresponding to peak overpressures less than 1 psi.
In the first extended range experiment (August 83 Test [12]) the foam had drained to 100:1 by the time the test was conducted. The results are summarized in Table 1, Table 11, and Figure 17.

[12] Memo. L. A. Fjelseth, "60:1 Extended Distance Test", August 24, 1983.

Table 11: Results of extended range experiment with 60:1 (100:1) foam

Distance (ft)	Pressure (psi)	Impulse (psi-ms)	Time of Arrival (ms)
2	106	20.8	0.55
2.5	58	13.5	0.7
3	12.3	8.2	1.3
4 A FO	35.5	42.1	2
5	2	5.7	3.2
7	1.2	3.8	5.6
10	0.7	2.2	10.6

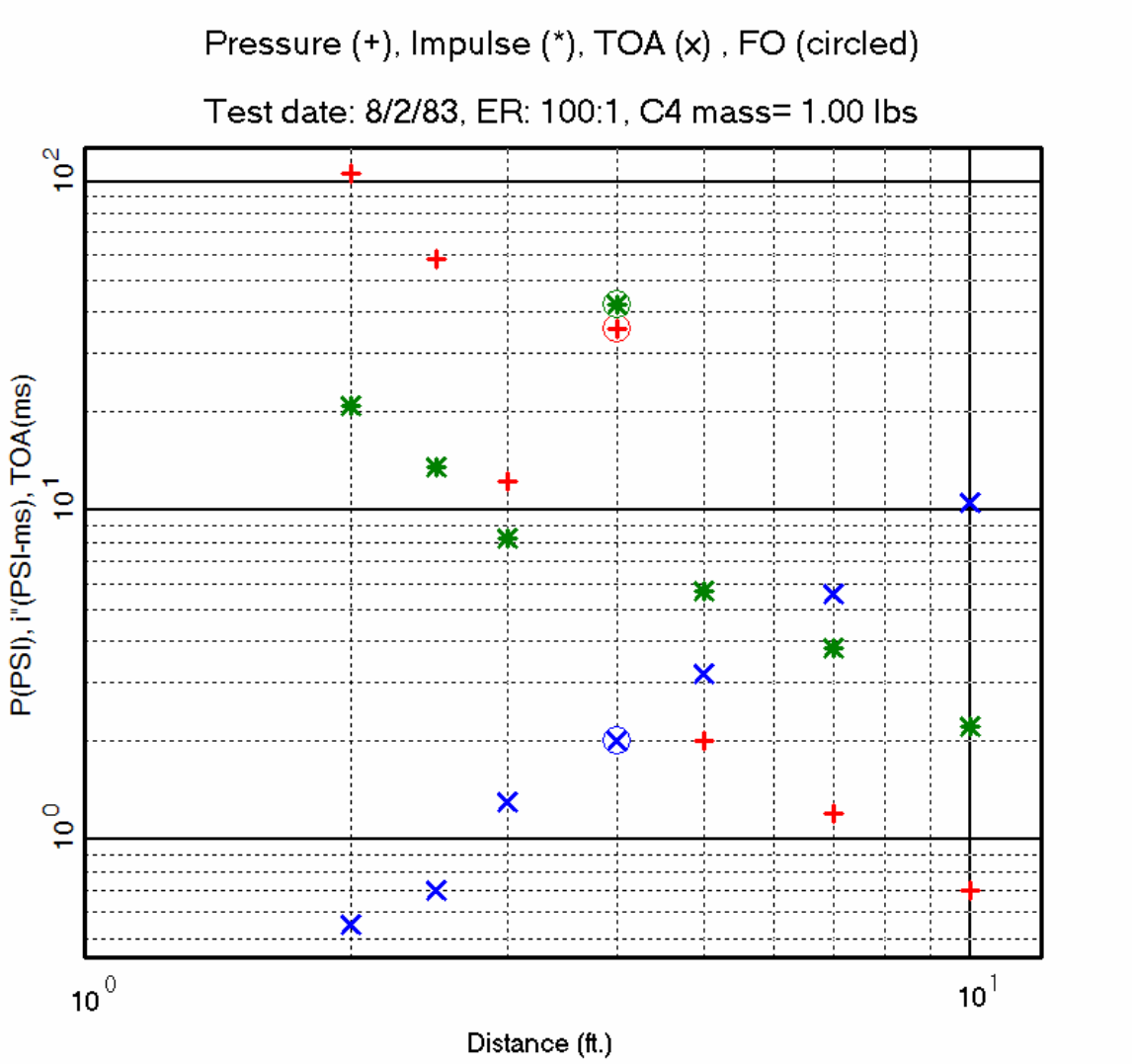

Figure 17: Plot of overpressure, impulse, and time of arrival data for 100:1 foam, 8/2/83.

The second extended range test (March 1984 Test [13]) achieved the desired foam density of 60:1. The results are summarized in Table 11, Table 12, Figure 17 and Figure 18. The data quality was very good in this test with the exception of a zero shift in the gauge at 5 feet which precluded measuring breakaway time and getting a good impulse reading.

[13] Memo, W. F. Hartman, "Test Report for 60:1 Foam Experiment Conducted March 8, 1984", SNL, March 19, 1984

Table 12: Results of extended range 60:1 foam test

Distance (ft)	Pressure (psi)	Impulse (psi-ms)	Time of Arrival (ms)
2	39	20.5	1.2
2.5	15	15.3	1.6
4	1.75	9.2	3.8
5	0.9	3.9 to 6.0	
7.0 A	0.58	3.3	10.2
10.0A	0.19	1.25	15.7
10.0A	0.18	1.21	15.9

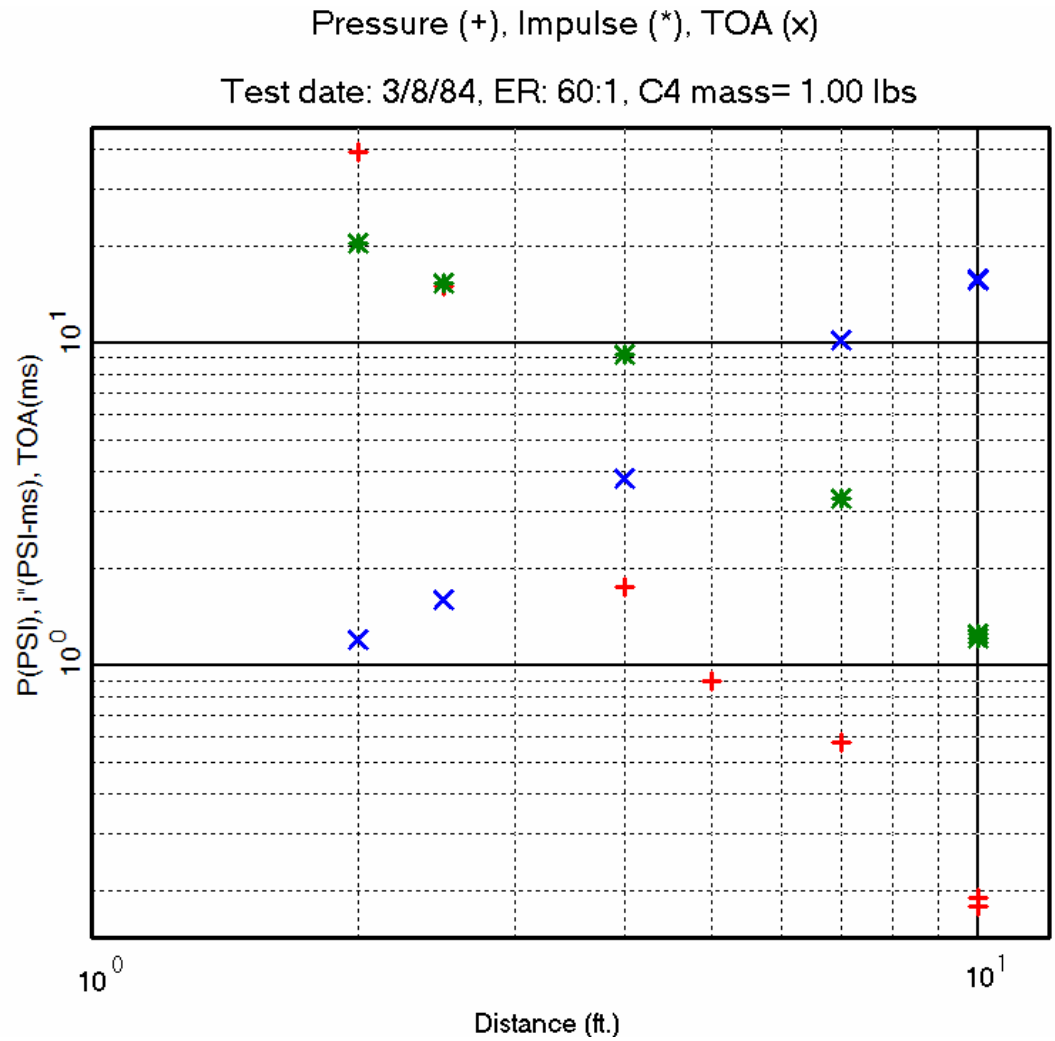

Figure 18: Plot of overpressure, impulse, and time of arrival data for 60:1 foam, 3/8/84.

3.8 20:1 Foam Experiment [14]

For this experiment the intent was to mitigate with 20:1 foam but the measured density at test time was 27:1. In both this test and the 10:1 experiment described below, nearly one-half of the instrumentation involved recording of the piezoelectric gauges (Celesco) on the FM magnetic tape system. As previously mentioned, the input capacitance of this recording system proved to be very difficult to characterize. As a consequence, this data was never judged to be completely reliable and is not reported here. The remaining results are summarized in Table 13 and Figure 19.

Table 13: Results of 20:1 foam experiment

Distance (ft)	Pressure (psi)	Impulse (psi-ms)	Time of Arrival (ms)
1.5	99	42	0.63
2	45	30.5	1.4
2.0 C, S	51		1.33
2.5	31	32	2.06
4	4.3	21.5	8.46

[14] Memo, L. A. Fjelseth, "Pressure Data from 20:1 Foam Test on July 19, 1982," September 19, 1982.

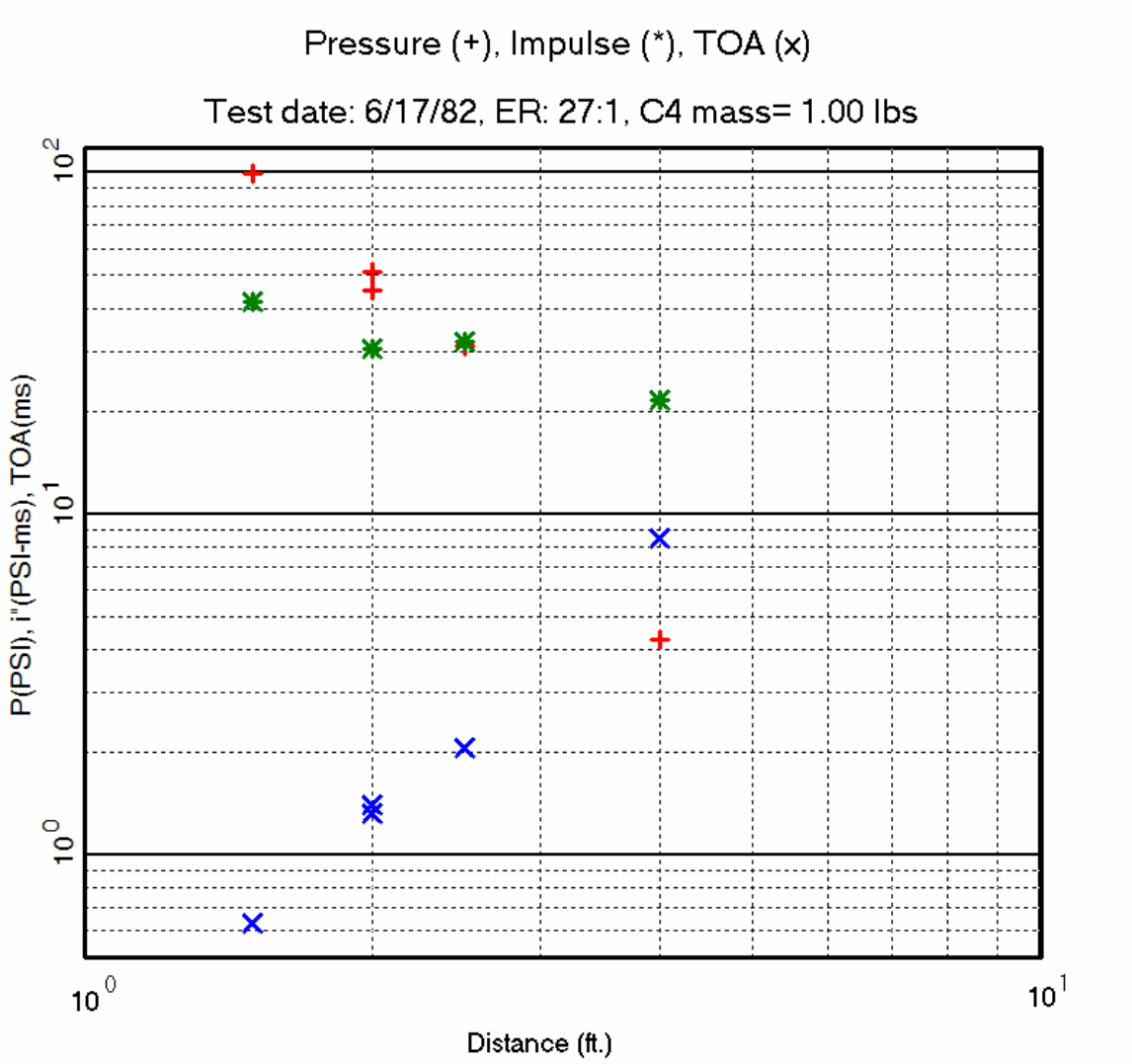

Figure 19: Plot of overpressure, impulse, and time of arrival data for 20:1 foam, 6/17/82.

3.9 10:1 Foam Experiment [15]

This was the most dense foam that was tested. As can be seen by the data (Table 14 and Figure 20), the attenuation was not nearly as rapid as it was with the lighter foams. In a practical sense, even if this foam had proven to be equivalently (or more effective) than the 60:1 or 100:1 foams, it would be extremely difficult to use foams this heavy in a large containment system.

[15] Memo, L. A. Fjelseth, "Digitized Data From 10:1 Foam Test," October 11, 1982.

Table 14: Results of 10:1 foam experiment

Distance (ft)	Pressure (psi)	Impulse (psi-ms)	Time of Arrival (ms)
1.5	139	115	1.29
2	78	62	2.82
2 CS	75		2.5
2.5	33	45	4.08
4	12.3	50	13.54

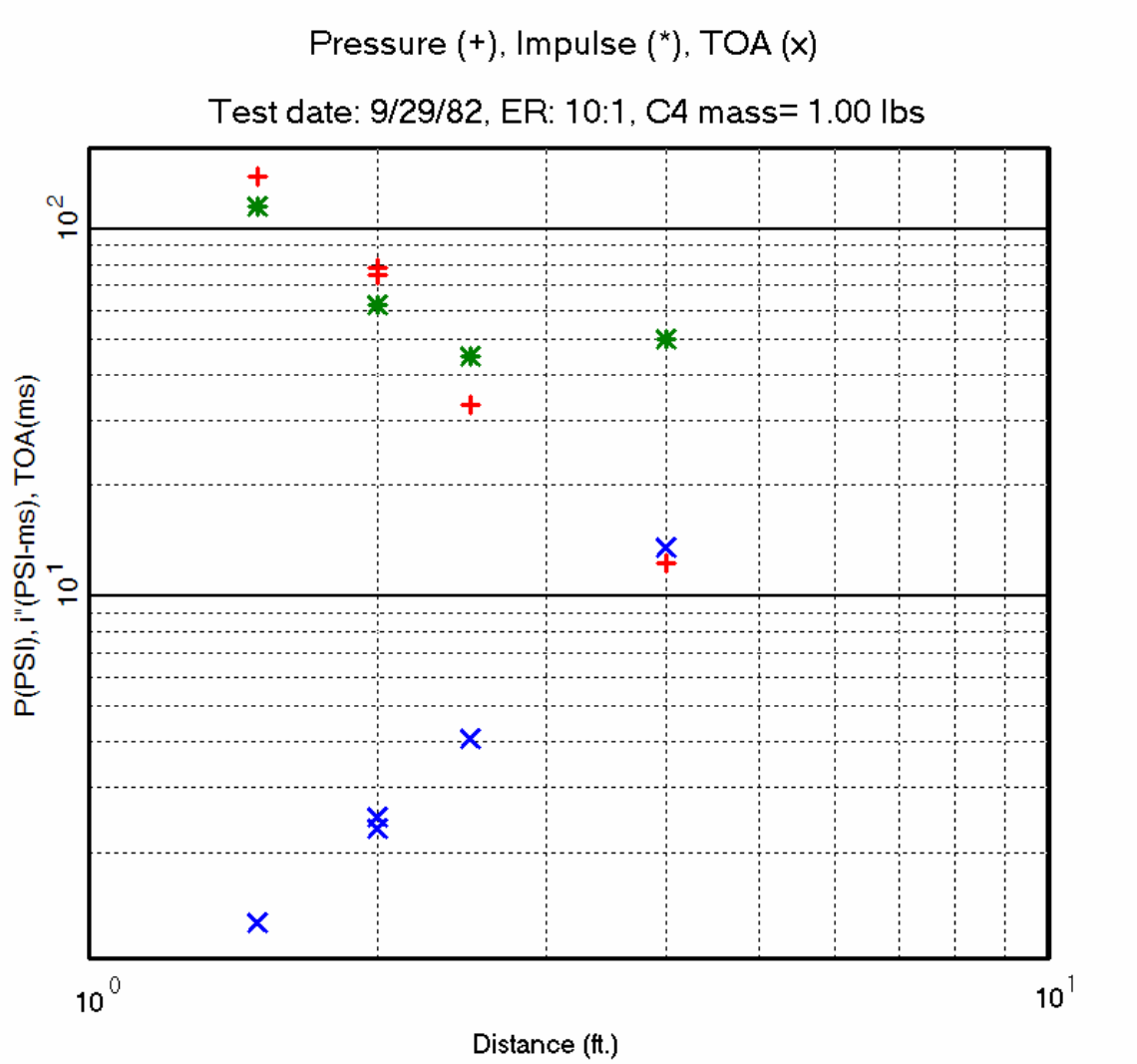

Figure 20: Plot of overpressure, impulse, and time of arrival data for 10:1 foam, 9/29/82.

4 Discussion and Implications of Experimental Data

4.1 Consistency of Results

The baseline test conducted in air, the three 60:1 and the four 100:1 experiments and those foam experiments in which two or more measurements were made at the same distance from the HE charge permit a judgment of the validity of the data to be made.

The graphical comparison of the baseline test and the TM5-1300 data for a one-pound surface detonation in air (Figure 5) show reasonable agreement. While the point at the 2 ft. (3.76 ft/lb$^{1/3}$ scaled) is somewhat disturbing, the other two points show excellent peak pressure measurement agreement. The specific impulse agreement is less satisfying with errors on the order 30%. For the small charge, the lack of precise knowledge of charge coupling to the supporting surface relative to the "standard," in addition to measuring error, may readily account for the discrepancy. The small charge size exacerbates errors due to instrument placement (because small errors in physical distance translate to larger scaled placement error for the small charge).

The peak pressures, scaled specific impulses, and scaled TOAs for all 100:1 and 60:1 foam experiment results are plotted in Figures 21-23. As before, for foam results, the distance, specific impulse, and TOA are scaled by the cube root of explosive mass.

The peak pressure plot (Figure 21) generally shows the 100:1 experiments and 60:1 experiments to be self consistent. For 60:1 foam (circled symbols) the 2.5 psi point at a scaled distance of 4.89 (4/28/83); and for 100:1 the 63 psi (11/15/82) and 58 psi (8/2/83) points at scaled distance 2.5 range are significant outliers.

The plot of scaled specific impulse (Figure 22) is too noisy to allow many detailed conclusions to be drawn. It appears that in the range of about 2-5 scaled distance that specific impulse is greater for 60:1 foam than that for 100:1 foam and that beyond that it is lower for the denser foam. Interestingly, as with air, the scaled specific impulse in the 2-5 scaled range is relatively constant with distance.

The plot of scaled time of arrival (Figure 23) shows generally self-consistent results, with the tests with 60:1 foam clearly and consistently indicating later times of arrival than those with 100:1 foam. In the earlier discussion, Figure 16, it appeared that TOA did not scale well. However, in this figure any discrepancy associated with scaling appears to be small compared to the consistent difference due to foam density variation.

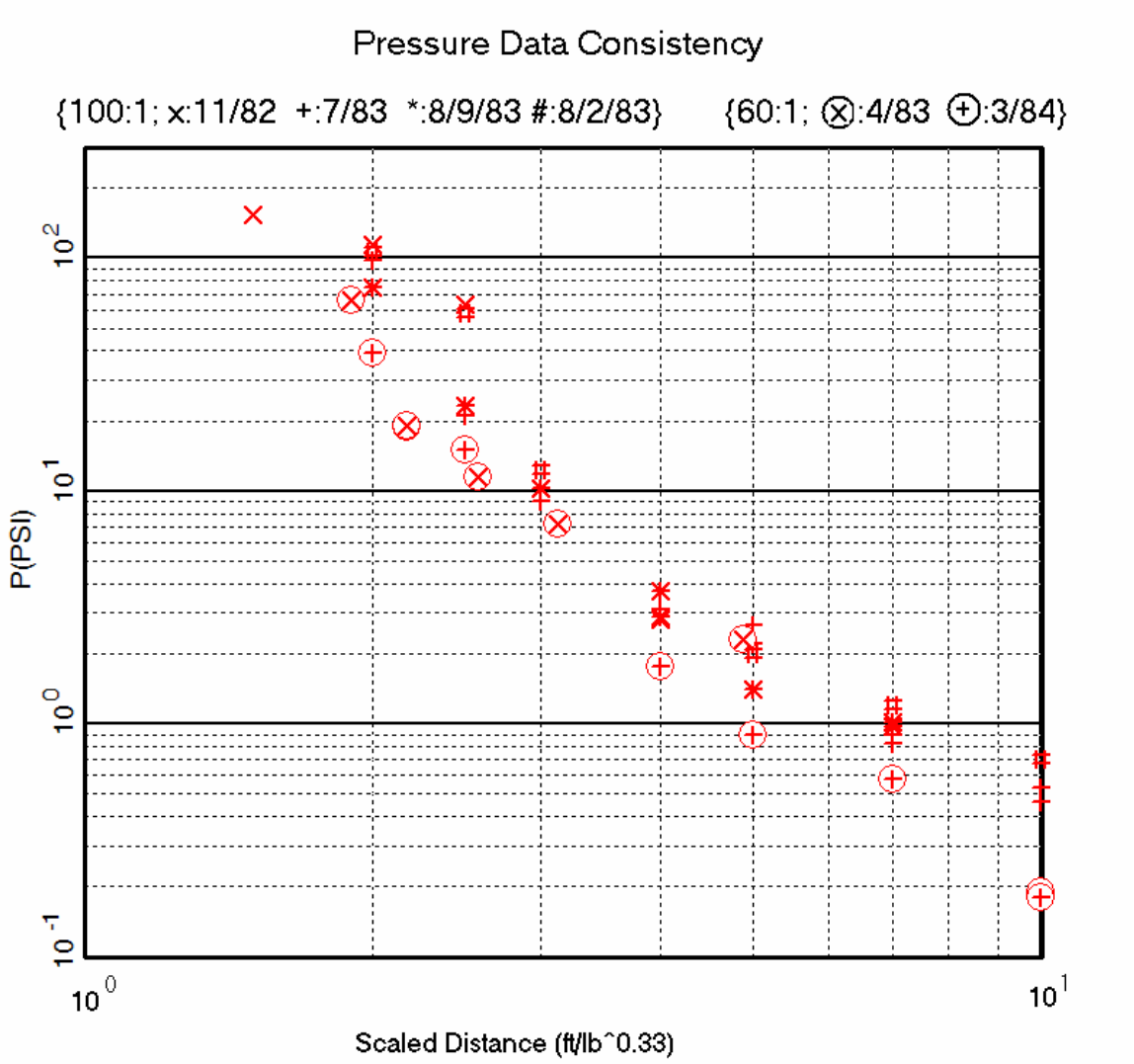

Figure 21: Plot of pressures for tests with 60:1 and 100:1 foams.

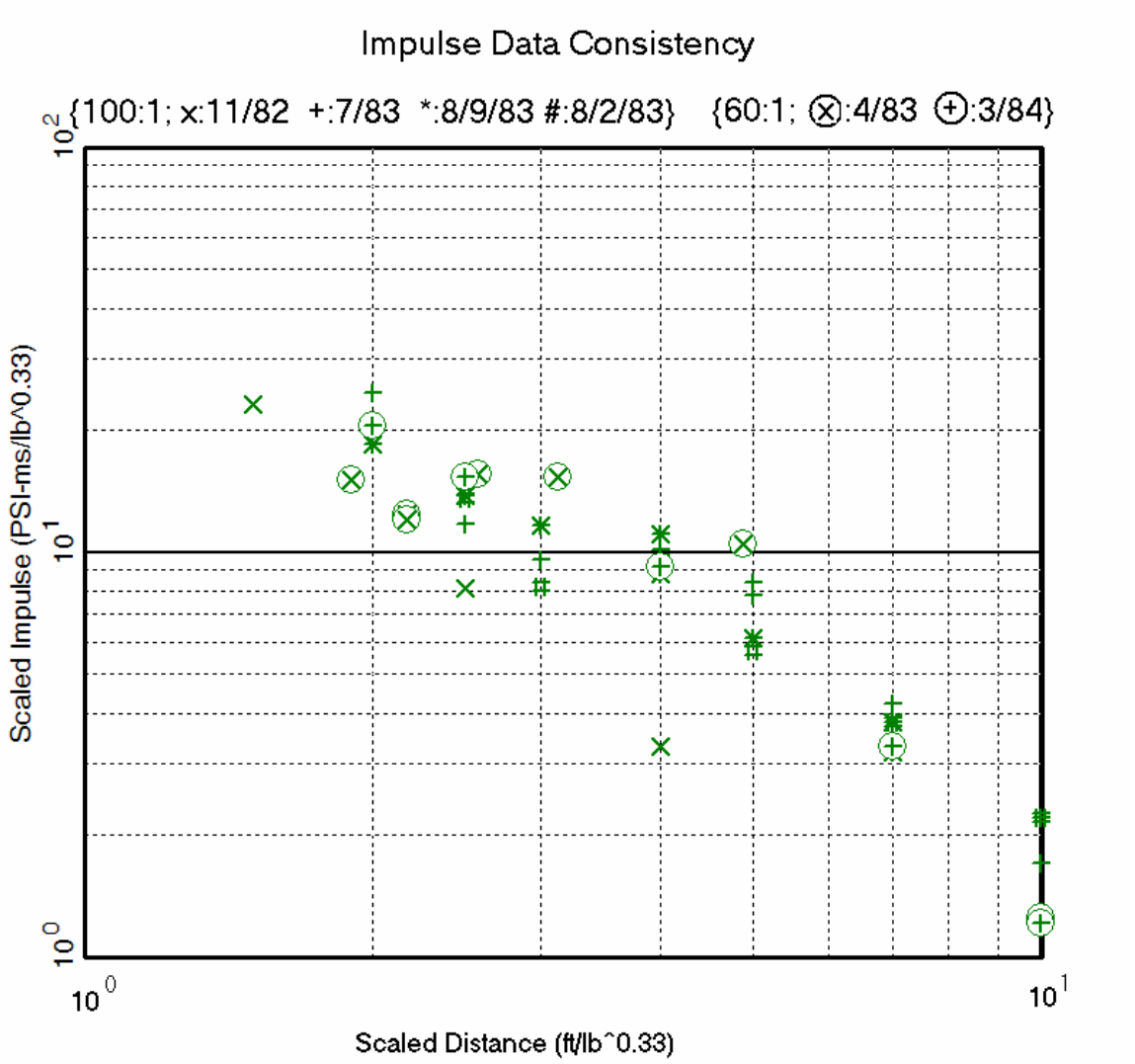

Figure 22: Plot of scaled impulse for tests with 60:1 and 100:1 foams.

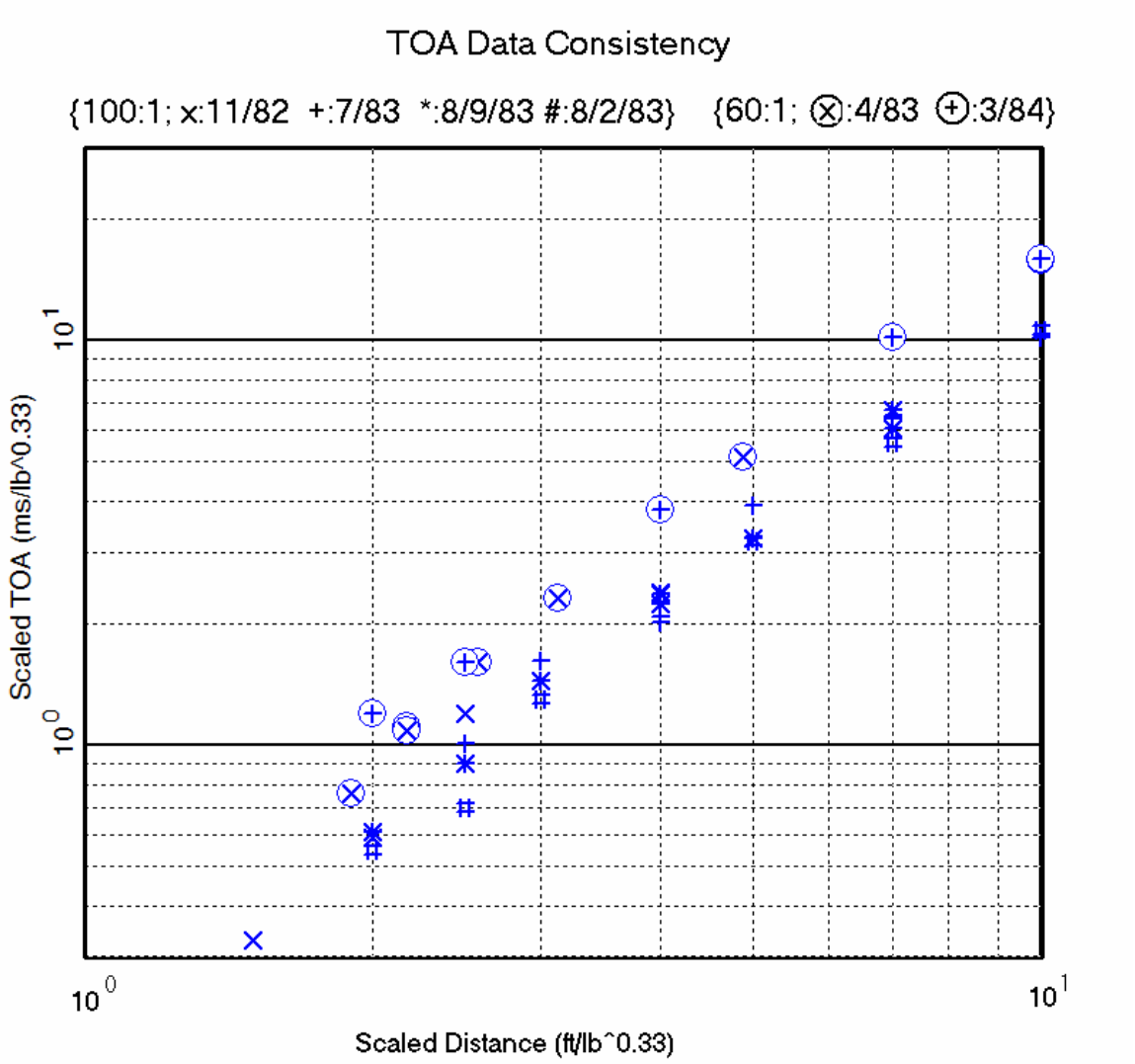

Figure 23: Plot of scaled TOA for tests with 60:1 and 100:1 foams.

As several experiments included redundant gauging, this provides an additional way to assess the credibility of the measurements. This data, extracted from that previously reported, is compiled in Table 15.

Table 15: Results of redundant measurements in foam attenuation experiments

Expansion Ratio	Distance (ft)	Pressures (psi)
1000:1	4FO	59.3, 55.8
	5.5	5.6, 5.4
375:1	4	9.6, 7.8
200:1	4	3.6, 1.1, 5.1
100:1 (6/83)	4	3.1, 3.1
	5	2.2, 2.65
	7	0.82, 0.90
	10	0.53, 0.46
100:1 (HV)	4	2.9, 3.7
	7	0.98, 1.01
60:1 (3/84)	10	0.19, 0.18
60:1 (50-lb)	2.17 (scaled)	21.0, 19.0
	4.89 (scaled)	0.38, 0.48
10:01	2	79, 75

In ten of these fourteen measurements, the redundant readings were within 5%. In three others, the deviation was in the ten to twelve percent region with only the 200:1 experiment yielding values which were obviously inconsistent. This reproducibility of individual measurements, coupled with the ability to reproduce "known" data, led to the conclusion that the measurements being made were accurate.

4.2 Pressure Decrease for Different Foam Densities

The comparison of the decay in pressure magnitude with distance for air and all the foam densities tested appears in Figure 24. An empirical fit to the available data is shown. The fitting was performed on a subset of all the data that dismisses conspicuous outlying points. That process and the details of data used for the fits are described in Appendix B. For the moderate densities of 60:1, 100:1, and 200:1, the percentage rms difference in predicted and observed pressure for all of the data points is 39%. The fit shown is:

$$\ln(P) = 3.7757 + 0.5085\times\rho + \ln\left(\frac{x}{W^{1/3}}\right)\times(-0.0372 + 0.0695\times\rho) - 3.2788\times\ln\left(\frac{0.6640\rho^{1/3}x}{W^{1/3}}\right) \quad (4)$$

Interestingly, the overall agreement does not suffer when all of the data (10:1 through 1000:1 densities) are included and the rms error is 38%. (27:1 and 10:1 curve fits are not shown to avoid clutter.)

Note that all of the foams mitigate the pressure much more rapidly than air. Also noteworthy is that the decrease in pressure amplitude reaches a maximum with about 60:1 foam, i.e. the decrease is less for foams of both lower and higher densities. In fact, the 20:1 curve fit of Figure 24 lies nearly on top of that for 60:1, intersecting it near the middle and exhibiting just a bit more negative slope. The curve for 10:1 lies wholly above those for 100:1, 60:1 and 20:1, and intersects that for 200:1. Arbitrarily choosing a pressure of 10 psi, the distances from a one pound surface detonation for the pressure to be reduced to that value are shown in Table 16.

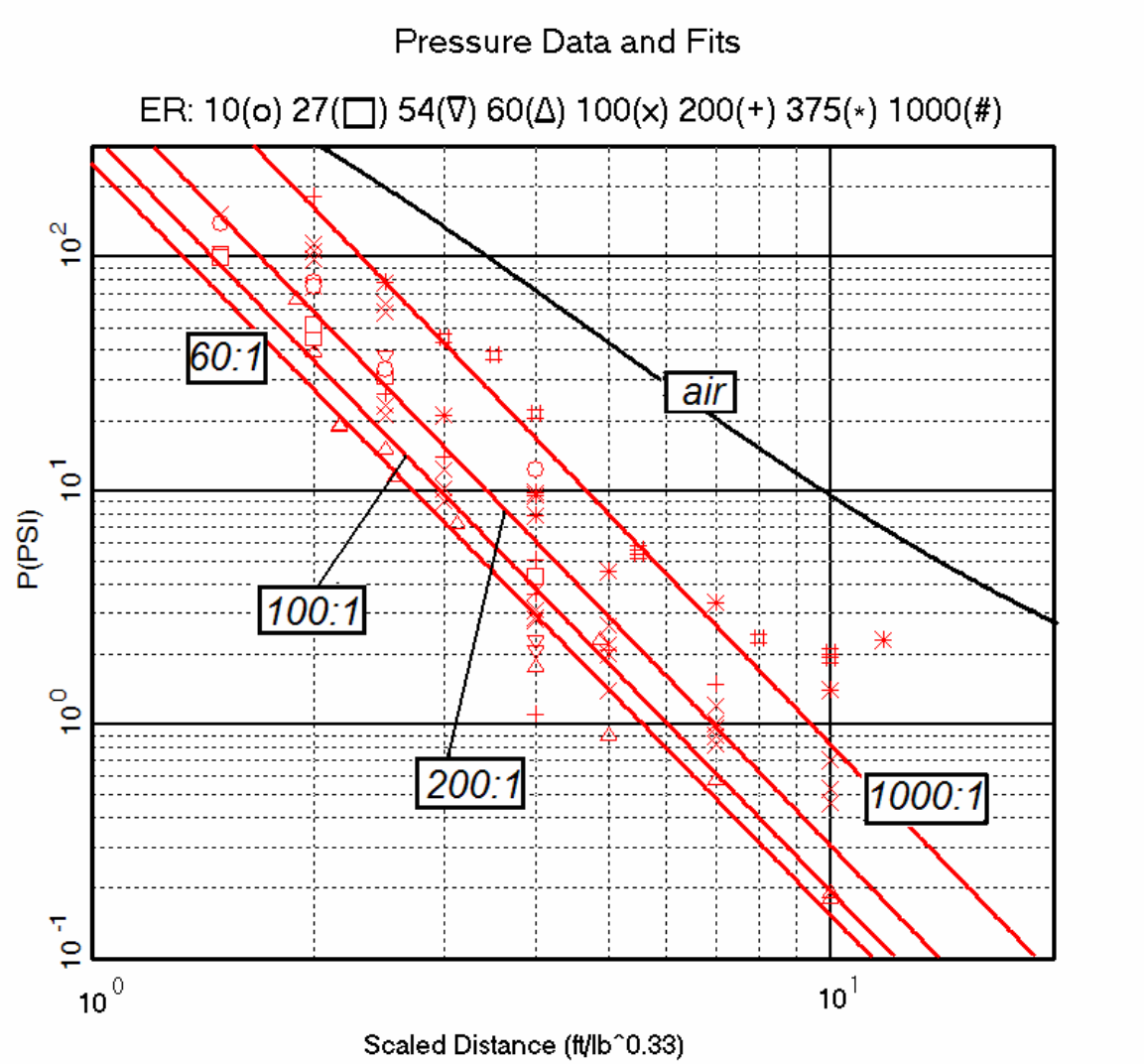

Figure 24: Screened pressure data and empirical fits for all expansion ratios.

Table 16: Distance from a 1-lb C-4 surface burst for the pressure to decrease to 10 psi

Media	Distance (ft)
Air	9.79
l000 to 1	4.68
400 to 1	3.98
200 to 1	3.43
l00 to 1	2.97
60 to 1	2.74
20 to 1	2.77
10 to 1	3.70

Although it is not apparent from this data (because of the inability to make measurements immediately adjacent to the explosive), the higher impedance of the foam relative to air must lead to a crossing of the air and foam and air curves close to the HE surface, i.e. the pressures in foam will be greater than those in air adjacent to the explosive (see analytical results presented in Appendix C)

There is one other interesting aspect of this data. Even for the furthest out measurements, (where the pressures had decreased to fractions of a psi), the attenuation was still greater than the 1/R acoustic approximation, suggesting that dissipation and pulse-spreading processes are still present even at these low pressures.

4.3 Impulse Reduction as a Function of Foam Density

Before discussing the impulse measurements in detail, it needs to be reiterated that these values were determined by integration of the pressure pulses. They are therefore susceptible to the baseline shifts that occasionally occurred in 1980s vintage data recording systems and also to the extraneous noise pulses which seem to be inherent from time to time when working in these sorts of environments. Nevertheless, the internal consistency of this body of data speaks well for its validity and it is presented in Figure 25. As with air, the scaled impulse for foam in the range of scaled distances measured does not decrease so sharply and consistently as overpressure. Consequently, a weak trend is hard to pick out of the noise and no single empirical fit was found that represented the data well.

There are several observations that result from this data. Look first at the air curve from TM 5-1300 (scaled per Eq. 2 for Albuquerque's altitude) which shows a plateau in the scaled range from about 1 out to 3 feet/$lb^{1/3}$. This region of constant impulse indicates that the pulse in air is broadening proportionately to the nearly one order of magnitude

drop in pressure which is occurring over this distance. The pulse continues to spread but at a much slower rate over the next order of magnitude pressure drop, from a scaled range of about 3 ft/lb$^{1/3}$ to about 10 ft/lb$^{1/3}$.

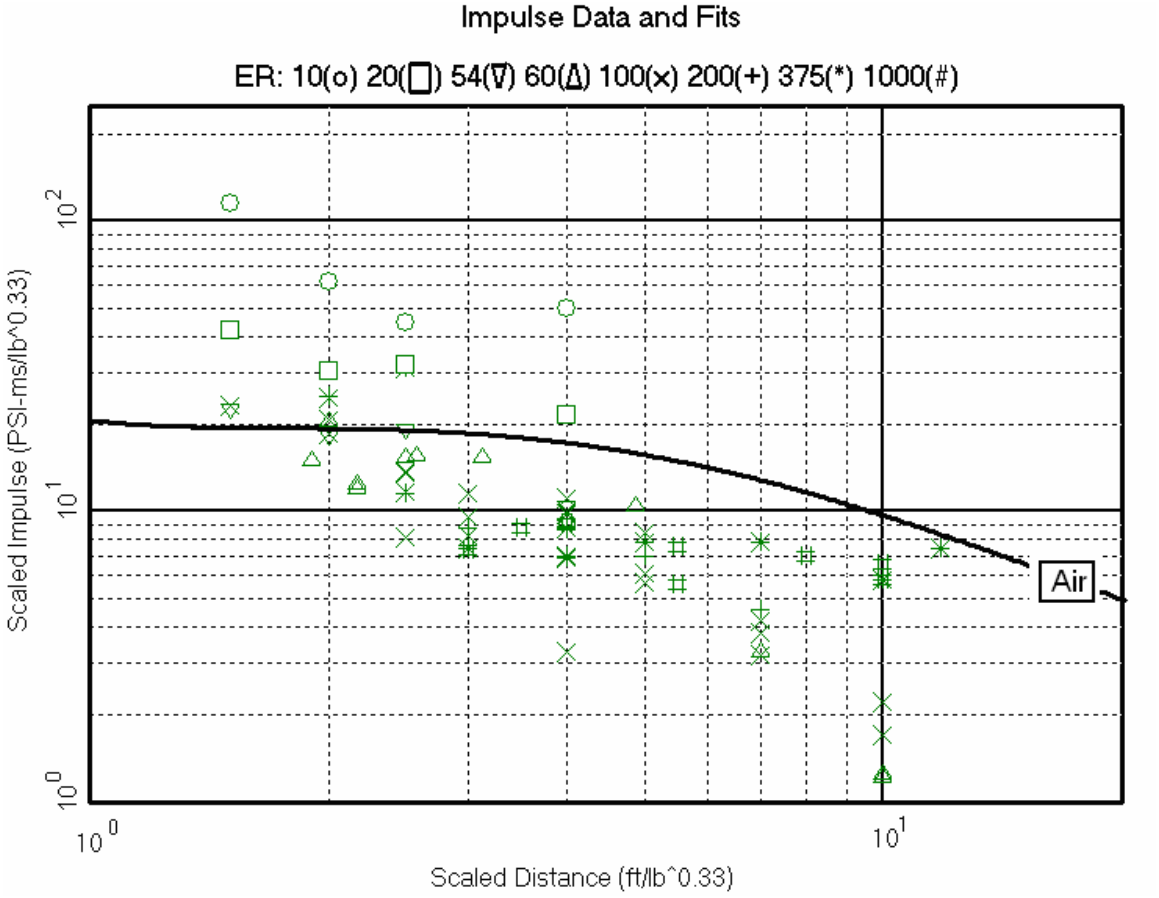

Figure 25: Scaled specific impulse data for all expansion ratios.

The densest foam that was tested (10:1) shows far less impulse attenuation that does air itself. Unfortunately, data for this test does not extend out past about four feet so it cannot be determined if the 10:1 impulse curve will drop precipitously in the far field or not. The 20:1 curve falls nearly on top of the segment of the air baseline test close to the explosive, falling very slightly below this curve when the pressures have decreased to about 10 psi.

Surprisingly, all of the lighter foams, up to and including 60:1, exhibit nearly identical behavior out to about 5 feet/lb$^{1/3}$ - here all of the pressures are down to a few psi. There is a very rapid decrease in impulse down to about 10 psi-ms. (at about 3 feet/lb$^{1/3}$), followed by the same plateauing as is observed in free air. Beyond five feet/lb$^{1/3}$, the heavier foams parallel the free air curve with the impulse decreasing at an accelerated rate. The 400:1 and 1000:1 foams show very little decrease and may even be asymptotically approaching the curve for air.

One conclusion from this impulse data is that foams with expansion ratios of 60:1 to 200:1 are the most effective in impulse mitigation and that they decrease the distance required to reduce the impulse to 10 psi-ms by a factor of three relative to a free air burst.

4.4 Time of Arrival Data

While the impulse data just presented has implications with respect to survivability of structures, the greatest value of the time of arrival data is with respect to understanding the foams' response to blast wave loading. If the pulse were very steep (preferably a discontinuity) in the pressure-time plane, then the shock velocity, in conjunction with the corresponding pressure, could be used to determine an equation of state for the material. Here, such a discontinuity does not exist because of the dispersive nature as the disturbance transits the foam. The time of arrival value recorded here is not that of the peak pressure but rather the time that the low pressure leading edge of the pulse reaches the gauge location. As with the pressure, an empirical fit was developed to estimate scaled TOA as a function of scaled distance and density (expansion ratio). The results are presented in Figure 26. That process and the details of data used for the fits are described in Appendix B. Applying the fit to all of the data (10:1 through 1000:1) the rms error is 11.3%.

The curve fits shown in Figure 26 are as follows:

$$\frac{TOA}{W^{1/3}} = \frac{x}{A(\rho)W^{1/3}} - \frac{\sqrt{B(\rho)}}{(A(\rho))^{3/2}} \tan^{-1}\left\{\sqrt{\frac{A(\rho)}{B(\rho)}}\left(\frac{x}{W^{1/3}}\right)\right\} \tag{5}$$

where,

$$A(\rho) = \begin{cases} 0.5216 \times \rho^{-1.0521} & \text{for } \rho > 0.9914 \\ -0.2381 \times \rho + 0.9063 & \text{otherwise} \end{cases} \tag{6}$$

$$B(\rho) = 2.3431 \times \rho^{-0.6121} \tag{7}$$

Both $A(\rho)$ and $\frac{dA(\rho)}{d\rho}$ are continuous at $\rho = 0.9914$ so that the $TOA\left(\rho, \frac{x}{W^{1/3}}\right)$ surface is smooth everywhere. The corresponding speed is:

$$V(x,\rho) = \left\{A(\rho) + \frac{B(\rho)}{\left(x/W^{1/3}\right)^2}\right\} W^{1/3} \tag{8}$$

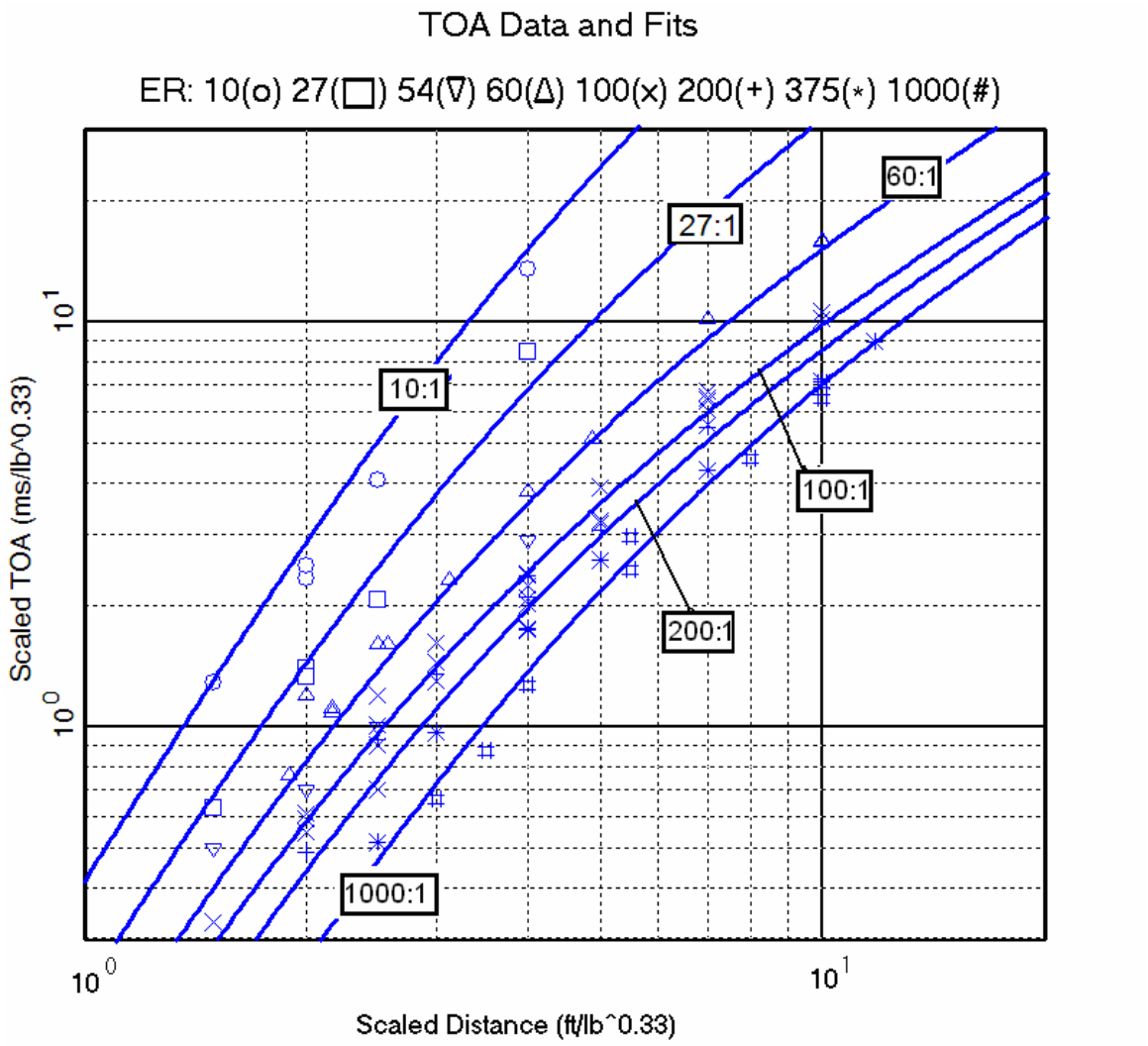

Figure 26: Time of arrival data and empirical fits for all expansion ratios.

The data of Figure 26 are both very consistent and surprisingly interesting. As the foam density increases, the time required for the pulse to reach a given distance increases, i. e. the wave velocity decreases. Close in, the wave velocity for the foams with an expansion ratio of 100 or greater have a wave velocity (and at these distances, the pulse has a relatively steep leading edge) of about 3600 ft/s; the corresponding velocity for the heavier foams (less than 60:1) is about 2000 ft/s.

Figure 27 shows the implied wave speed versus scaled range according to Equation (8). At scaled distances in the range of 5-10 ft/lb$^{1/3}$ (depending upon density), the curves approach nearly constant velocity which might be considered an "acoustic" velocity for that particular foam. These values are shown in Table 17. In each case, the velocity shown in the second column is that consistent with Eq. (8) and the TOA-surface fit evaluated at the scaled distance of 10 feet. The last column of Table 17 is constructed as the ideal acoustic velocity for a pure substance (the simple equation of state used is described later). The difference between the two velocities is greatest for the lightest foam.

The required thermodynamic properties in the ideal acoustic velocity are evaluated as for a pure substance, admitting a single temperature and pressure for negligibly disturbed material (the disturbance is a small reversible compression). It is plausible that these conditions are more nearly met in the denser foam at the 10-foot range. The experimental velocity exceeding the ideal acoustic velocity is consistent with the wave leaving liquid water in its wake that is not in equilibrium with the gas phase. If the liquid phase lags the gaseous phase in temperature and velocity there is more energy in the gas phase disturbance so it "wants" to exhibit more strength than it could if it were brought into equilibrium with the liquid.

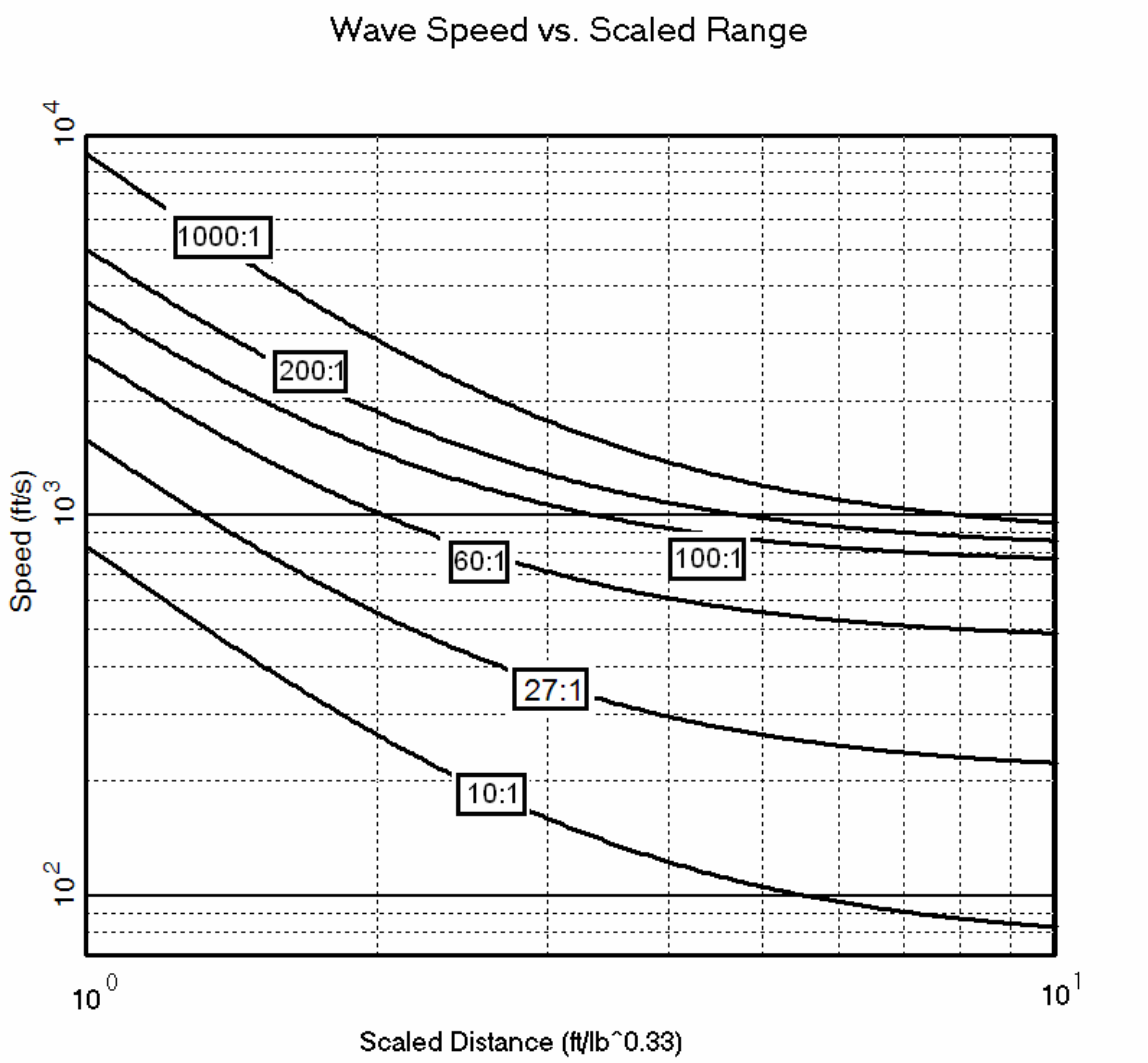

Figure 27: Shock speed versus range for various ER as derived from TOA fit.

Table 17: Velocity of leading edge of wave at low pressures

Foam Expansion Ratio	Wave Velocity (ft/s)	$\sqrt{\left.\frac{\partial P}{\partial \rho}\right\|_s}$ (ft/s)
Air	1100	
1000:1	1050	715
400:1	990	526
200:1	890	396
100:1	720	290
60:1	505	229
20:1	190	136
10:1	99	99

4.5 Reflected Pressures

In the use of pressure data to calculate the response of structures, loading histories are usually constructed that depend upon the reflected rather than the side-on pressure. In several of the foam attenuation experiments, measurements were made of these reflected (or face-on) pressures and this data has been listed along with the side-on measurements in the experiments that have been previously discussed. In addition, two experiments were conducted[16] [17] for the purpose of investigating the pressure and impulse amplification which occurs when the pulse impacts on an orthogonal rigid surface.

Both of these experiments used a four-pound explosive charge but the data which is reported below has been scaled to the standard one-pound charge to permit easy comparison with the other results. In both tests the foam containment was a 10'x12' rectangular plywood enclosure. Eight face-on pressure measuring gauges (in redundant pairs) were flush-mounted in the four enclosure walls. The charge was positioned so that horizontal distances of 4, 5, 6, and 7 feet from charge-center to wall position were realized.

The first of these experiments employed 130:1 foam and the side-on measurements appear in Table 18.

[16] Memo, W. F. Hartman, "Results of Test to Determine Ratio of Reflected-to-Incident Pressures and Impulses", SNL, March 16,1984. Although not stated in the title, the foam density in this test was 130:1.

[17] Memo, W. F. Hartman, "Results of Test to Determine Reflected-to-Incident Pressure and Impulse Ratios in 60:1 Foam (Ratio Test 3), SNL, May 14, 1984

Table 18: Side-on measurements in 130:1 ratio test

Scaled Distance ($ft/lb^{1/3}$)	Pressure (psi)	Scaled specific impulse ($psi\text{-}ms/lb^{1/3}$)	Scaled TOA ($ms/lb^{1/3}$)
4	41.8	13.2	1.1
4.5	1.1	8.2	1.4
5	8	9.4	1.6

All three sets of data, pressure, specific impulse, and pulse time of arrival are consistent with the earlier results. The data from the face-on gauges in this experiment appear in Table 19. The intent was to make duplicate measurements at all four locations; one of the gauges at the scaled distance of 4.6 $ft/lb^{1/3}$ was extremely noisy, unusable and is not reported. Also, one of the gauges at a scaled distance of 3.4 $ft/lb^{1/3}$ had a large spike late in time which precluded interpreting a good impulse value.

Table 19: Face-on data for 130:1 ratio test

Scaled Distance ($ft/lb^{1/3}$)	Pressure (psi)	Scaled specific impulse ($psi\text{-}ms/lb^{1/3}$)	Scaled TOA ($ms/lb^{1/3}$)
2.9	59.5	35	1.4
2.9	48	33	1.3
3.4	19.7	30	1.8
3.4	28	-	1.9
4	7.5	26	2.4
4	6	21	2.4
4.6	3.7	15	3.1

There is about 15% difference in pressure from the mean between the redundant gauges. This is somewhat greater than the variations observed in the side-on measurements. The impulse and time-of-arrival data are in much better agreement.

The second experiment designed specifically to measure the ratio between the incident and reflected pressures used 60:1 foam. The test set up was similar, again using side-on gauges to provide validation for the experiment and a set of four duplicate measurements of the face-on pressures and impulses. In this case, the gauges were positioned somewhat closer to the four-pound charge than in the 130:1 test to provide information at higher values of pressure and impulse. As measurements of these same quantities for 60:1 foam had already been made, these values are also shown for comparative purposes.

Table 20: Side-on data for 60:1 foam experiment

Scaled Distance ($ft/lb^{1/3}$)	Pressure (psi)		Scaled specific impulse ($psi\text{-}ms/lb^{1/3}$)		Scaled TOA ($ms/lb^{1/3}$)	
	Predicted	Measured	Predicted	Measured	Predicted	Measured
1.9	29	>23	26	24	0.8	0.85
2.2	19	23	18	18	1.15	1.13
2.5	13	15	13	14	1.5	1.51

The pressure pulse measurement at 1.9 feet was clipped by the recording system; however, the width of this clipped spike was so narrow that it did not appear to significantly affect the impulse measurement. The conclusion from this set of measurements was that the foam behavior was consistent with that observed in previous 60:1 tests. The data from the face-on gauges in this experiment are shown in Table 21.

Table 21: Data from face-on gauges in 60:1 ratio test

Scaled Distance ($ft/lb^{1/3}$)	Pressure (psi)	Scaled specific impulse ($psi\text{-}ms/lb^{1/3}$)	Scaled TOA ($ms/lb^{1/3}$)
2.1	~250	53-84	1
2.1	270-350	82-91	0.9
2.3	125-160	62-65	1.2
2.3	112	79	1.2
3	14	40	2
3	17	41	2
3.3	10	43	2.3
3.4	8	36	2.4

The uncertainty and ranges shown on some of the closer-in values resulted both from clipping of the pulses and from noise on the trailing edge of the pressure pulse which influenced the impulse determination.

All of the reflecting surfaces data of the foregoing four tables is summarized in Figure 28 which provides a visual representation of the important behaviors. The 60:1 foam (smaller symbols), as compared to 130:1, exhibits delayed arrival, *higher or as high* incident pressures at these ranges, and comparable scaled impulse. The face-on measurements, as compared to side-on; exhibit higher pressures, higher impulses, and consistent arrival times.

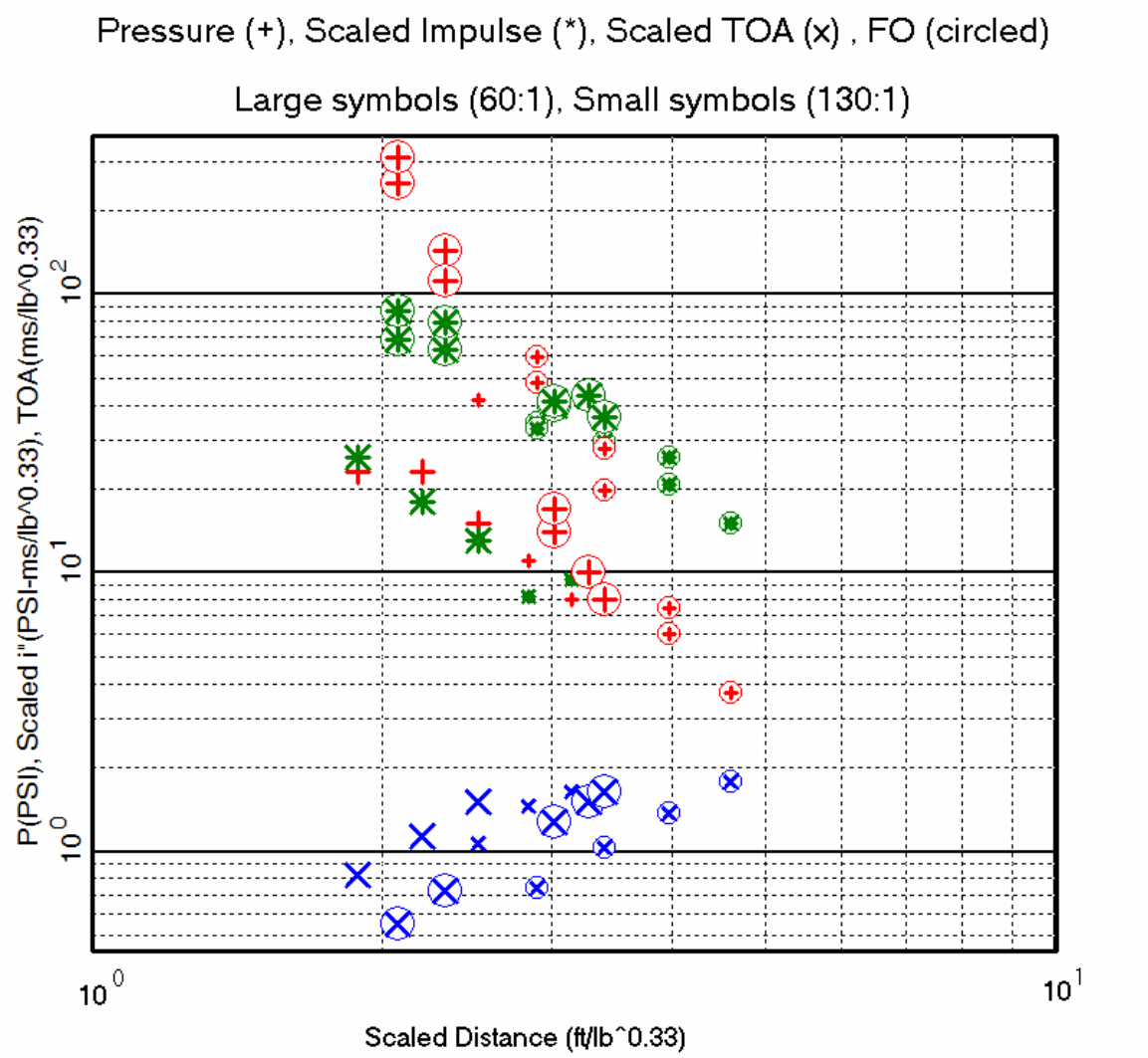

Figure 28: Face-on and side-on data comparisons.

Figure 30 includes the face-on data from the two tests just described and other solitary measurements of face-on pressure from other tests. For comparison, side-on pressures as predicted by the fit described earlier are also plotted for each expansion ratio represented by experimental data. The data is reasonably consistent. In the range of about 3-4 ft/lb$^{1/3}$ it is clear that the 130:1 experiments exhibit higher peak pressures than the 60:1. The face-on data from lighter foams are higher as expected.

For air the ratio of reflected to side-on pressure is two at sufficient ranges so that the shock is weak. Figure 29 shows the ratio of the observed face-on peak pressure measurements to the expected side-on values at the same locations where the expected side-on pressure is calculated using Equation 4. It appears that in foam the limiting ratio is less than 2. It is also clear that the pressure ratio increases much more rapidly in foam than it does in air, reaching a value in excess of ten at pressures of 20 psi or greater. At 20 psi the ratio for air is approximately 5.

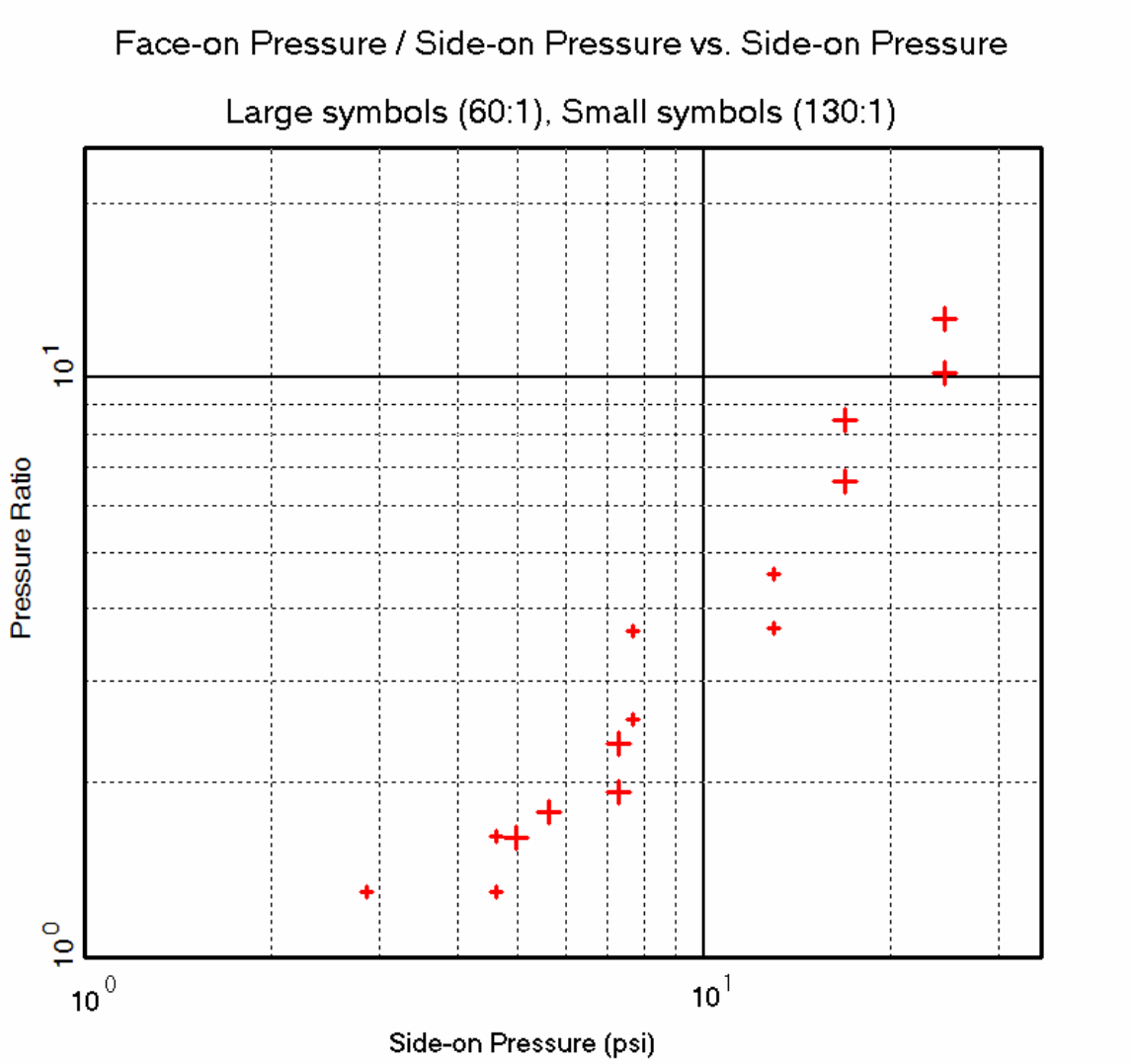

Figure 29: Ratio of observed face-on peak overpressure to predicted (Eq. 4) peak side-on pressure vs. predicted side-on pressure at the range of the observation.

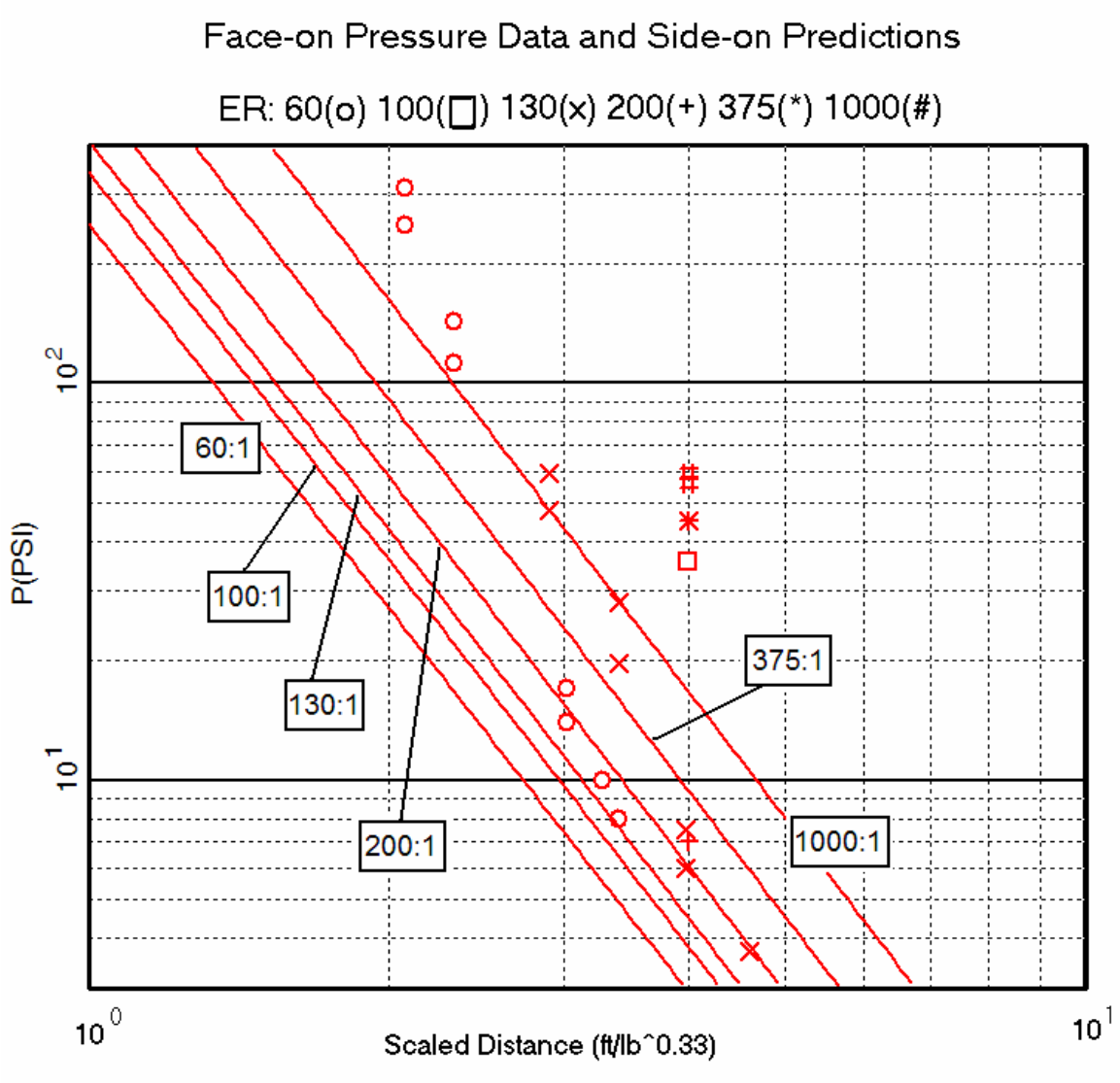

Figure 30: Peak face-on measurements (symbols) and side-on pressure estimates for various foam densities.

The purpose of these experiments was to determine the ratio of the reflected to the incident pressure and impulse as a function of pressure and foam density (or expansion ratio). This data is shown in Table 22 using the side-on pressure data from the 130:1 test interpolated between the 100:1 and 200:1 curves for the130:1 calculation (this was required because of the very narrow range of the measurements shown in Table 18) and the actual 60:1 side-on measurements as shown in Figure 24. In those cases where the value of a measurement was estimated as a range, the midpoint of that range was used for this determination. The ranges in the value for the pressure and impulse ratios result from the redundant measurements which were made.

Table 22: Ratio of reflected to incident pressures and impulses in aqueous foams

130:1 Foam			60:1 Foam		
Incident Pressure (psi)	$\frac{P_r}{P_{so}}$	$\frac{i_{r"}}{i_{so"}}$	Incident Pressure (psi)	$\frac{P_r}{P_{so}}$	$\frac{i_{r"}}{i_{so"}}$
10	4.8-6.0	3.7- 3.9	23	10.9-13.5	3.7-4.3
5.2	3.8-5.4	3.5	15.8	7.1-9.0	4.0-5.4
2.8	2.1-2.7	2.6-3.2	7	2.0-2.4	4.5-4.7
1.9	1.9	2	4	2.0-2.5	4.1-4.9

The impulse amplification is somewhat of a different story (Figure 31). Looking first at the 60:1 data, the magnification ratio is essentially constant at about 4.5. This is probably not surprising as the data corresponds to a radial distance from the charge of 2.1 to 3.3 feet, a distance where the side-on impulse itself changes very little with distance (See Figure 22 or Figure 25). The 130:1 data was taken slightly further out (2.9 to 4.6 feet), a region where the pressures are lower and there is more slope to the side-on impulse curve. What this data suggests is that there may not be much discernible difference between the reflected amplification factor of the two foams at the higher pressures and that for foams of these densities and at pressures of 4 to 20 psi, the ratio of the reflected impulse to the incident impulse is 4 ± 1.

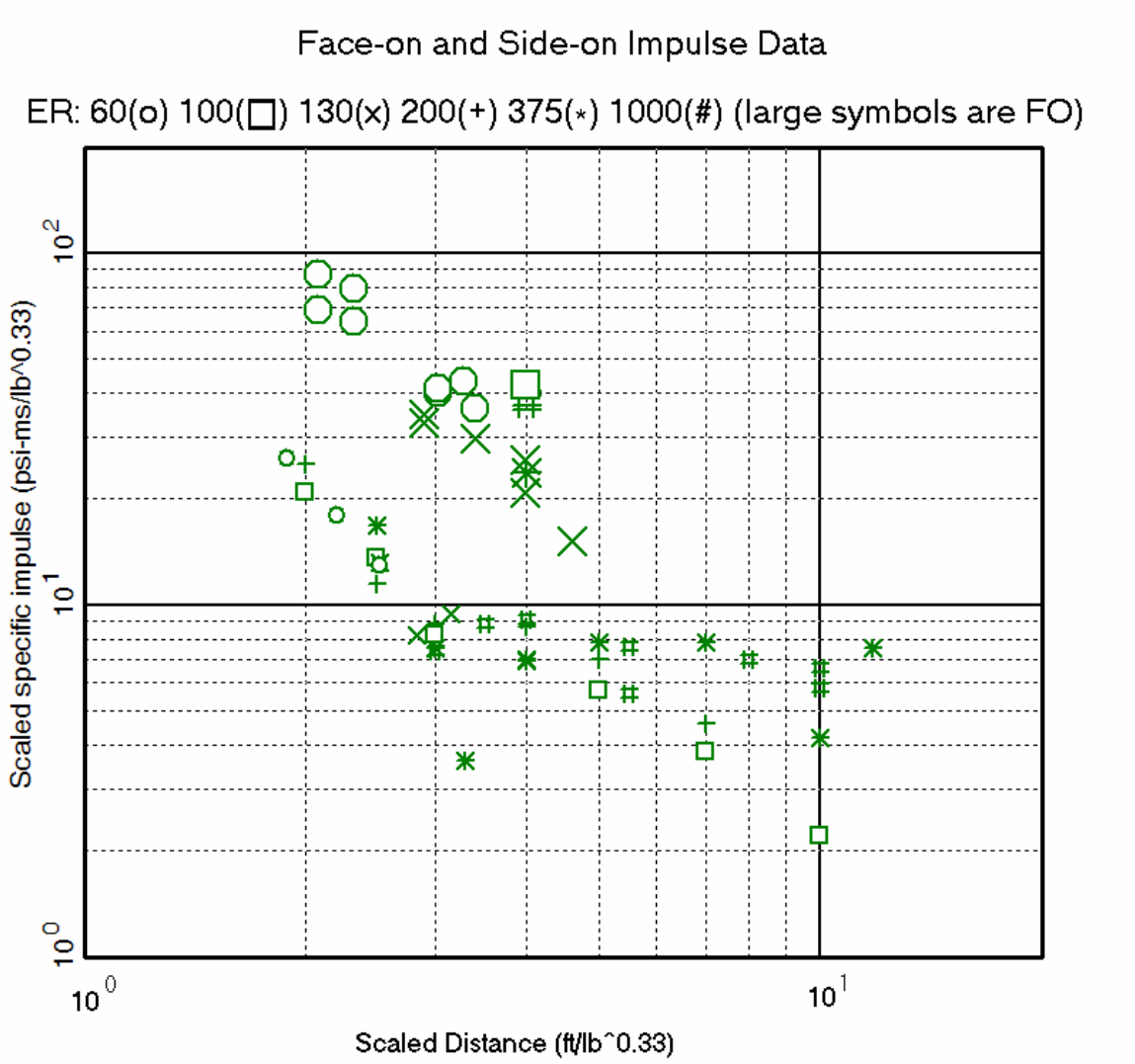

Figure 31: Face-on and side-on specific impulse measurement comparisons.

4.6 Pressure Decrease Across an Interface

In many situations, the interest will not be what pressures exist within the foam itself but rather the existing pressures at some location outside of the foamed volume. Attempts to measure this pressure drop were made in four of the experiments previously discussed; these data are repeated in Table 23. For the data presented here, the pressure observations are outside of the foam containment and separated from the foam by a plywood boundary.

Table 23: Experimental results from measurements to determine interface decrease

Expansion Ratio	Distance Air/Foam (ft)	Measured Pressure (psi)
200:1	2.2/1.1	1.96
100:1	2.2/1.1	2.6
54:1	2.2/1.1	1.7
60:1 (50-lb shot)	4.34/0.54 (scaled)	0.43

To determine the pressure drop across the interface, it is necessary to a) estimate the pressure in the foam prior to reflection and b) estimate the pressure in the air just beyond the interface. The first of these is achieved by the use of the foam attenuation curves in Figure 24. The second is estimated by assuming that at these low pressures, the pressure wave in the air is acting acoustically and the only reduction in magnitude results from the $1/R$ divergence. Ignoring the plywood and applying these estimates the data are shown in Table 24.

Table 24: Interface pressures and reduction across foam/air interface

Expansion Ratio	Pressure in Foam prior to interface (psi)	Corrected Air Pressure Outside of Interface (psi)	Pressure Reduction Ratio	Predicted Ratio (see ¶ 5.6)
200:1	41.3	2.94	14	2.5
100:1	26.2	3.9	6.7	3.0
54:1	19.5	2.55	7.6	3.6
60:1 (50-lb shot)	2.44	0.48	4.6	1.8

The acoustic velocity in 60:1 foam is, from the lowest pressure measurements, about 500 ft/s. Using this value, the densities of this foam (1.1 lb/ft^3) and of air (0.062 lb/ft^3, Albuquerque) and the acoustic velocity of air yields a predicted ratio of acoustic impedances $(\rho C)_{foam} \big/ (\rho C)_{air}$ of about 8. At higher pressures, the wave velocity in foam is considerably higher, about 1000 ft/s for 60:1 foam above 20 psi and up to 1800 ft/s in foams of 100:1 or lighter at pressures above 30-40 psi (Figure 24 and Figure 27).

The last column of Table 24 shows an alternate theoretical prediction (presented in Section 5.6) of pressure drop passing from the edge of the foam to air based on calculated, pure-phase foam Hugoniots. That theory predicts lower pressure ratios than are reported in Table 24.

4.7 Effects of Foam on Shaped Charges and Flyer Plates

Some of the potential applications of foam could require the firing of shaped charges or small, explosively-driven flyer plates through the foam. While not directly related to the purpose of this report, a series of experiments was conducted to determine the effect of foam on shaped charges and the velocity decrease of flyer plates resulting from the drag of the foam.[18] As these experiments have not been formally documented elsewhere, they have been included here.

The shaped charges (JRCY-1041) which were employed in the first series of tests contained only about 11 grams of RDX. A 2" standoff between the charge and the first of the ¼" mild steel witness plates was employed. The 2" between the shaped charge and the witness plates was filled with 60:1 foam. In the first of the two tests tabulated below, foam was also allowed to penetrate into the cone of the shaped charge; it was excluded from this volume in tests 3 and 4. The final entry in the table records the depth of penetration of these jets in the absence of foam based upon an extensive series of tests which had been previously conducted.

Table 25: Effects of foam on shaped charge penetration

Test Number	Foam Configuration	Penetration Depth (in.)
1	2" of 60:1 with foam in shaped charge cavity	4.25 to 4.5
2	2" of 60:1 with foam in shaped charge cavity	4.25 to 4.5
3	2" of 60:1 foam; none in shaped charge cavity	4.25 to 4.5
4	2" of 60:1 foam; none in shaped charge cavity	4.25 to 4.5
-	none	4.25 to 5.25

Comparing the results of the shots with foam with the free air behavior, it is concluded that, if any effect is present, it falls within the repeatability of shaped charge performance. It is also concluded that, because of the small amount of explosive in these shaped charges and the dense foam that was used, this result will hold in general. It should be noted that there is no discernible change in penetration resulting from the presence of foam in the cone of the shaped charge.

The flyer plate devices used in this series of tests consisted of a 3/16" inch thick, 1.25" diameter steel disc propelled by a 13/16" thick, 1.25" diameter slab of explosive. The flyer plate velocity was determined by the time between the explosive firing and contact with a foil switch attached to the front of the initial witness plate. The penetration depth was again determined by a series of mild steel witness plates, each of 1/8" thickness.

---

[18] Memo, P. W. Cooper and William F. Hartman, "Effects of Foam on Device Performance", Sandia National Laboratories, Aug. 3, 1983

A total of five experiments of three basic types were conducted. In all of the tests, the first witness plate was located six feet from the initial position of the flyer plate. In test 1, there was no obstruction between the flyer and the witness plates. In tests 2 and 3, the flyer had to pass through both walls of a corrugated box which was to hold the foam in tests 4 and 5 but no foam was present in these two events. In the final two tests, the box was filled with 60:1 foam. The results of these tests are shown in Table 28.

Table 26: Results of test to assess effects of foam on flyer plate performance

Test	Configuration	Total Separation (ft)	Foam Thickness (ft)	Elapsed Time (ms)	Velocity (mm/μs)	Penetration Depth (in)
1	No mitigation	6	0	1.52	1.2	0.5
2	Cardboard Box Only	6	0	1.71	1.07	0.25 to 0.38
3	Cardboard Box Only	6	0	1.71	1.07	0.25 to 0.38
4	Cardboard Box Filled with foam	6	4	2.07	0.88	0.13 to 0.25
5	Cardboard Filled with foam	6	4	2.07	0.88	0.13 to 0.25

Two things about the data are significant. The first is the repeatability and consistency of the data; for both repeated shots, the measured flight times were within three microseconds of each other. The second observation is that the measured penetrations are entirely consistent with those expected based upon the flyer plate velocity.

From these experiments, it is obvious that anything placed in the trajectory of these small flyer plates significantly degrades its velocity. For 60:1 foam, at these velocities, the loss is about 0.08 mm/μs - these reductions will drastically reduce the penetration capability of the flyer. Conversely, these drag-induced velocity reductions can be very beneficial in reducing the velocity of light shrapnel (low mass to cross sectional area ratio) from explosive devices if the devices are surrounded by a layer of heavy foam.

5 Analyses

5.1 Introduction

For the most part, the preceding section presented data results without much theoretical conjecture. As stated in Section 1.3, the primary interest in foam containment became particle capture. Nonetheless, an occasional theoretical analysis was completed in years following the conduct of the tests.

Presented in the following sections are the results of simple attempts to model the blast wave in foam with a classical one-dimensional formulation of conservation of mass, momentum and energy while treating the media as a homogenous mixture. The lack of temperature and velocity equilibrium between the liquid and gas phases of the mixture is understood to severely limit the usefulness of these analyses to varying degrees depending upon the local conditions considered. Nonetheless, the following sections present these analyses along with comparisons to the available data.

5.2 Summary of the Conservation Equations

The simple system under study is shown in Figure 32. The shock wave moves with velocity, U, into quiescent media (designated by the $_0$ subscript) and behind the shock conditions are disturbed (designated by the $_1$ subscript). The principal variables; e, u, ρ, and P are respectively the internal energy, velocity, density, and pressure of the medium.

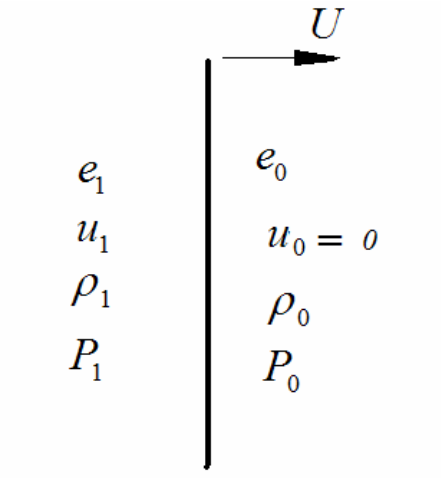

Figure 32: Shock wave system.

Affixing a frame of reference to the shock, conservation laws are:

mass: $\rho_0 U = \rho_1 (U - u_1)$ (9)

momentum: $P_0 + \rho_0 U^2 = P_1 + \rho_1 (U - u_1)^2$ (10)

energy: $$\frac{P_0}{\rho_0}+\frac{U^2}{2}+e_0=\frac{P_1}{\rho_1}+\frac{(U-u_1)^2}{2}+e_1 \qquad (11)$$

The pressure behind the shock may be arbitrarily high depending upon the local shock strength. The foregoing conservation equations and an equation of state, that relates internal energy to pressure and density, are sufficient to fix all of the remaining variables when one condition is specified. That is, if we have one observation such as shock speed or pressure behind the shock, the other variables are all fixed if they are to obey the conservation equations and an equation of state. The collection of shocked states consistent with the equation of state, the conservation laws, and the undisturbed state is the Hugoniot of the material.

5.3 Equations of State

Results will be presented for two investigations using different equations of state. Appendix C incorporates Ref [7] in its entirety. The theoretical part of that analysis focused on the conditions near and at the surface of the detonation of TNT and C-4 in aqueous foam. For that region, supercritical to water, a two parameter equation of state (Redlich-Kwong) was found to be appropriate.

Subsequent investigations utilized a simple mixing rule for which water vapor and air mixed as an ideal gas. The mass fraction of air is constant and set by the initial state of the foam. The fraction of water existing as vapor varies with local conditions. Where water exists in both phases the partial pressure of the water vapor in the gas phase is taken to be the saturation pressure of the water at the local temperature. These assumptions lead to a unique $T(P,\rho)$ which in turn provides the needed $e(T(P,\rho),\rho)$ when combined with: $e=xe_{\text{air}}+(1-x)e_{\text{water}}$, where x is the air mass fraction. The subcritical water properties were found using the relations documented in Reference [8].

5.4 Computed Hugoniots Comparison

The Hugoniots resulting from the two equations of state are plotted in Figure 33 and, as expected, they coincide near water's critical pressure (22 MPa). The results at higher pressures (dashed lines) are from the analysis described in Appendix C. Neither mixing model should be expected to be very accurate at pressures and temperatures near water's critical point.

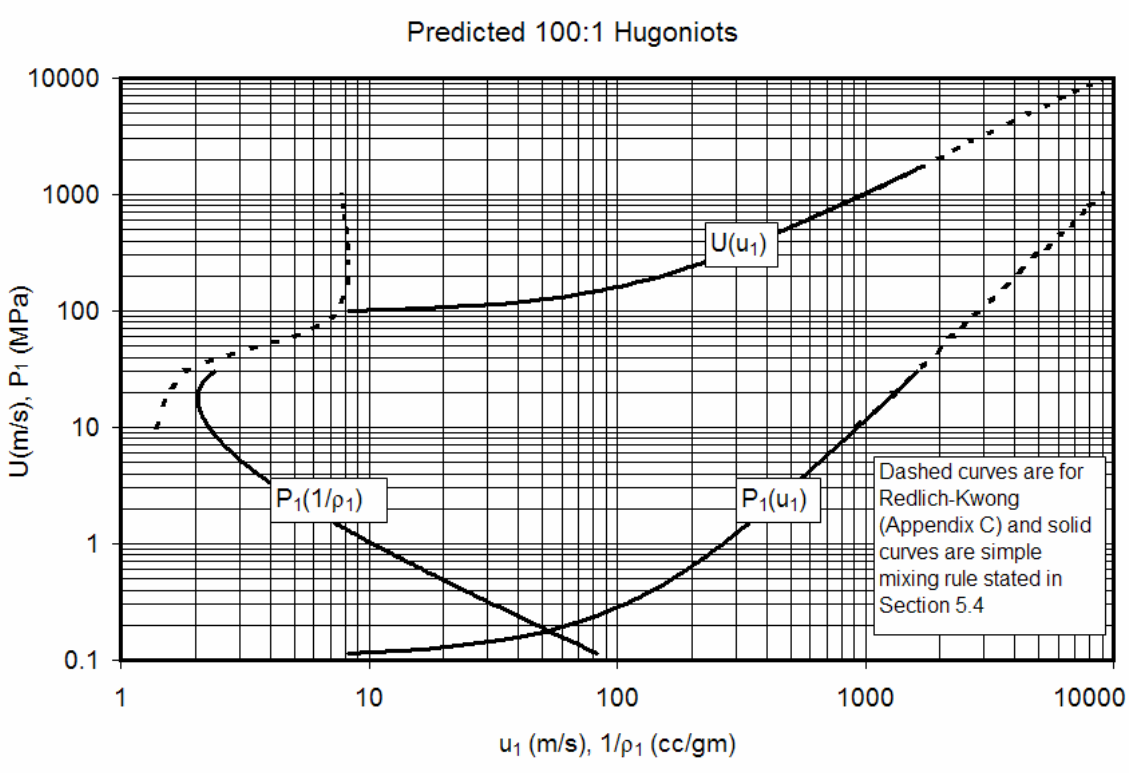

Figure 33: Predicted Hugoniots for two equations of state.

In addition to limited equation of state accuracy, the nonhomogeneity of the foam gives rise to the real behavior of shocked foam departing from the Hugoniots just outlined. In Equations 9-11, there is only one density and one particle velocity behind the shock. In fact, it is likely that in mixed phase regions liquid water and vapor are generally accelerated to different velocities. In moderately strong shock regions it is also likely that the liquid phase and vapor phase are not in thermal equilibrium immediately behind the shock. Where the shock is very strong both momentum and thermal transport between the phases should be very rapid due to the expected small droplet size. At pressures that are high relative to ambient pressure but lower than the critical pressure of water there is very little vaporization immediately behind the shock. The model predicts a substantial jump in temperature across the shock, but the elevated pressure prevents evaporation in the immediate wake of the shock. As the shocked material expands back to atmospheric pressure additional vaporization is predicted.

5.5 Comparison of Computed Hugoniot with Experimental Data

All of the experimental pressure measurements described earlier in the report are at ranges for which the pressure is well below the critical pressure of water. Figure 34 shows computed and measured Hugoniots in the unconventional *P*-*U* plane. The figure demonstrates conclusively the inadequacy of the simple model attempted. The fact that the observed wave velocity is considerably greater than that computed reflects the lack of equilibration between the phases of the foam.

The analysis presented in Ref. [9] applied a two-dimensional hydrodynamic code calculation to the problem of HE detonation in foam and made comparisons to data included in this report. That study varied assumptions regarding the degree of velocity and temperature equilibrium between the liquid and gas phases. Assuming equilibrium, their calculations also demonstrated much later TOAs at ranges of modest pressure, consistent with the current findings.

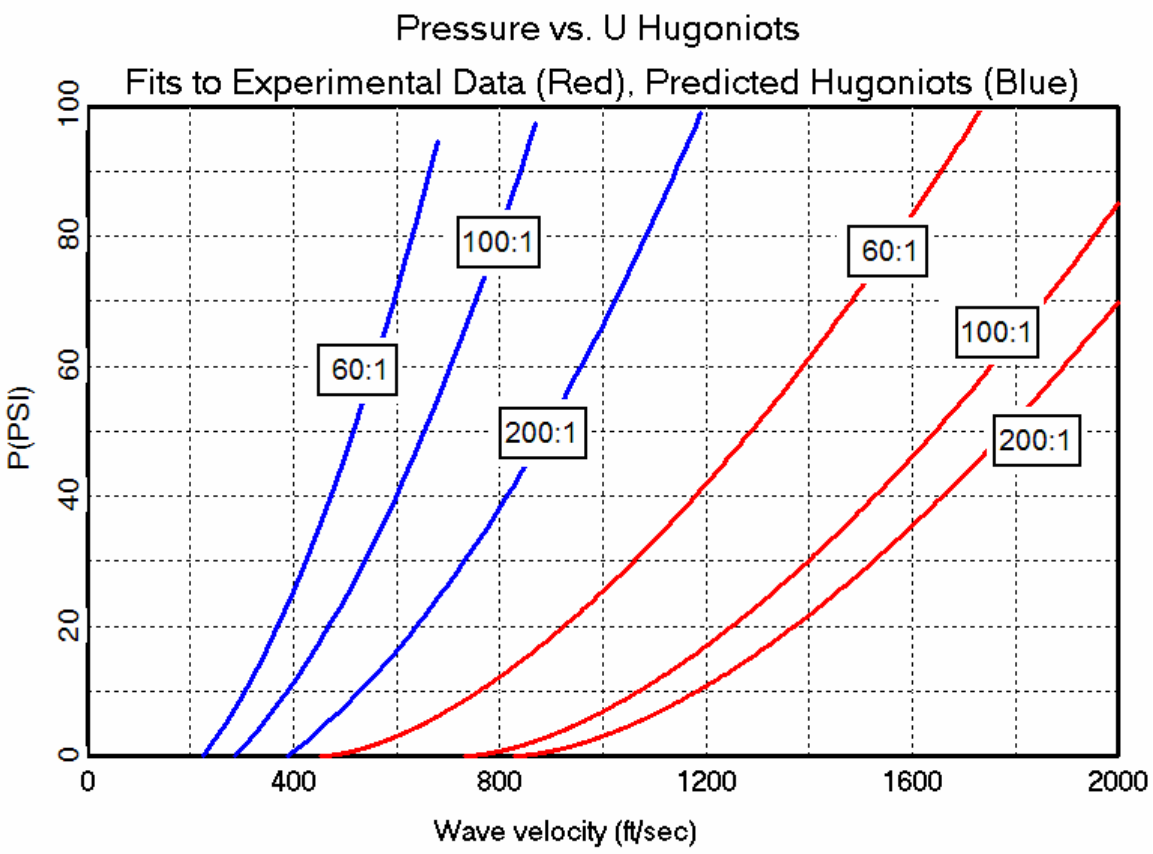

Figure 34: P-U "Hugoniots" as measured and calculated from simple model.

5.6 Impedance Mismatch Calculations

Figure 35 shows the results of the foregoing theory applied to the foam interface data described earlier in Table 24. Shown in the *P-u* plane are the predicted Hugoniots for the foam densities listed in Table 24 and for air. On each of the foam Hugoniots the circular symbol corresponds to the pressure listed in Table 24 at the edge of the foam. The release isentropes through those points intersect the air Hugoniot at the theoretical pressure prediction for the wave moving into the air. The release isentrope is constructed by conserving mass, momentum, and entropy (dismissing the energy equation).

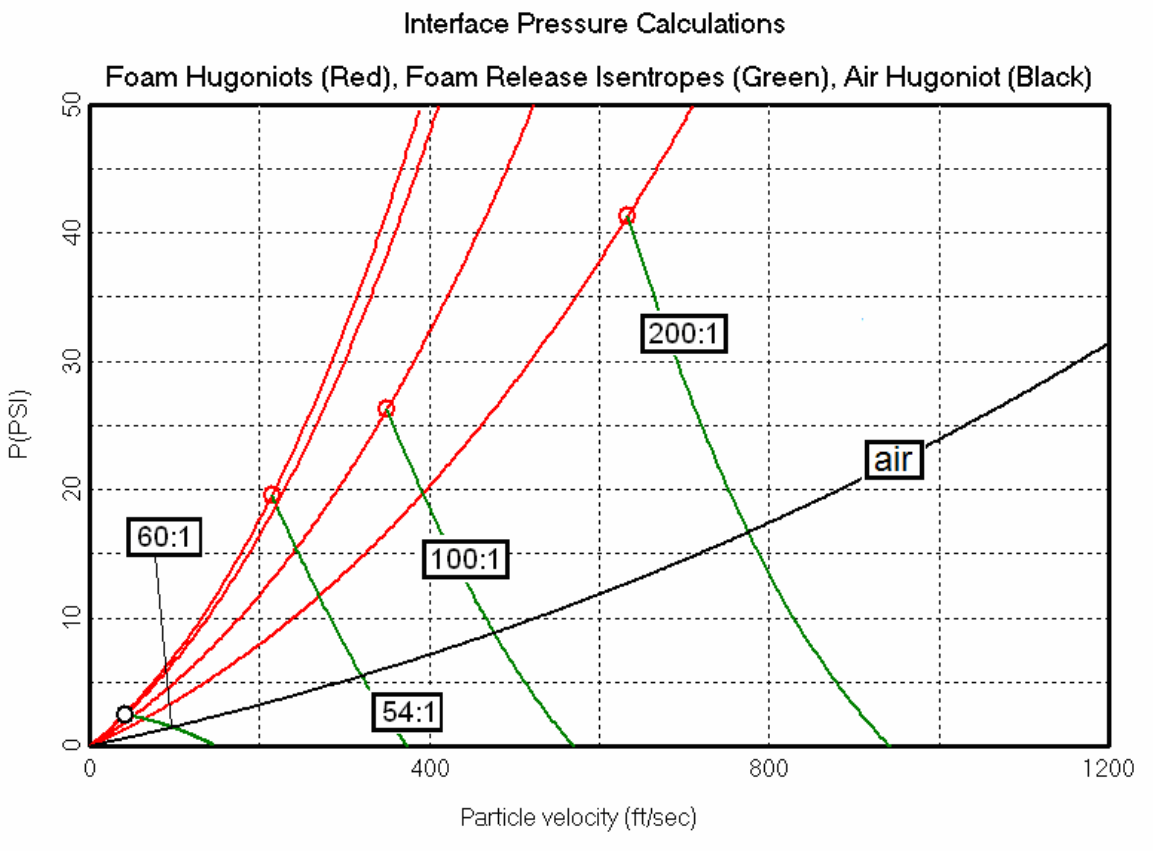

Figure 35: Impedance mismatch calculation for conditions of Table 24.

6 Conclusions

Among the conclusions which resulted from this series of experiments and the interpretation of the data are:

1. Foam is extremely effective in mitigating both the pressures and impulses which result from HE detonations. Empirical relations were developed for pressure and TOA as functions of expansion ratio and scaled distance. No such relation is promoted in this report for scaled impulse because a satisfactory correlation was not found.
2. The reduction in the pressure is greater than it is for the impulse.
3. Of the foam densities considered, an expansion ratio of 60:1 provides both the greatest pressure and the greatest impulse reduction. Foams both heavier than 60:1 and foams much lighter than this are decidedly less effective; the differences between 60:1 and 100:1 behavior are slight and probably within experimental uncertainty.
4. Firing shaped charges within a foamed environment should have little effect upon the shaped charges' performance. On the other hand, the velocity of small flyer plates fired through foam can be seriously degraded.

5. The spreading of the pressure pulse as it traverses through foam suggests that internal reflections at the air-liquid interfaces play an important role in the pressure reduction. Other factors that are believed to prominently figure in this process are the energy lost in a) the breakup of the foam bubbles and b) the heating of the liquid component of the foam.
6. Though most of the experiments discussed were performed at a charge weight of 1 pound, the experiments performed at other weights appear to confirm the validity of $W^{1/3}$ scaling of distance.

7 References

1) F. H. Winfield and D. A. Hill, *Preliminary Results on the Physical Properties of Aqueous Foams and Their Blast Attenuating Characteristics*, Suffield Technical Notes, Defense Research Establishment, Suffield, Ralston, Alberta
2) J. S. de Krsinski and A. Kholsa, *Shock Wave Propagation and Attenuation in Foams*, Fifth Australian Conference on Hydraulics and Fluid Mechanics, Dec. 9, 1974
3) Department of the Army Technical Manual TM 5-1300, (also Department of the Navy Publication NAVFAC P-397 and Department of the Air Force Manual AFM 88-22) Structures to Resist the Effects of Accidental Explosions, Departments of the Army, the Navy, and the Air Force, June, 1969.
4) Sachs, R.G., *The Dependence of Blast on Ambient Pressure and Temperature*, BRL Report No. 466, Aberdeen Proving Ground, Maryland, 1944.
5) Baker, W.E., *Explosions in Air*, Wilford Baker Engineering, San Antonio, 1983.
6) Larsen, M.E., *NEST Containment Calculator,* Sandia Report SAND94-2030, Unclassified Controlled Nuclear Information.
7) Boughton, B.A., *Shock Propagation in Aqueous Foam*, Sandia Internal Memo, March, 1988.
8) Reynolds, W. C., Thermodynamic Properties in SI, Department of Mechanical Engineering, Stanford University (1979).
9) Crepeau, J., Needham, C., Caipen, T., Grady, D. and Harper, F., *First Principles Calculations of the Interaction of Blast Waves with Aqueous Foams*. Sandia Report 99-1587C, July, 1999.

Appendix A: Transient signals from the 6/18/83 Test

The data taken on 6/18/83 was deemed the cleanest test of the series. This appendix incorporates the recorded wave forms for pressure and impulse for that test. The intent of including this data is to preserve the entire waveforms of a group of measurements deemed of good quality. The character of the transient behavior may be of interest for comparison in future modeling efforts.

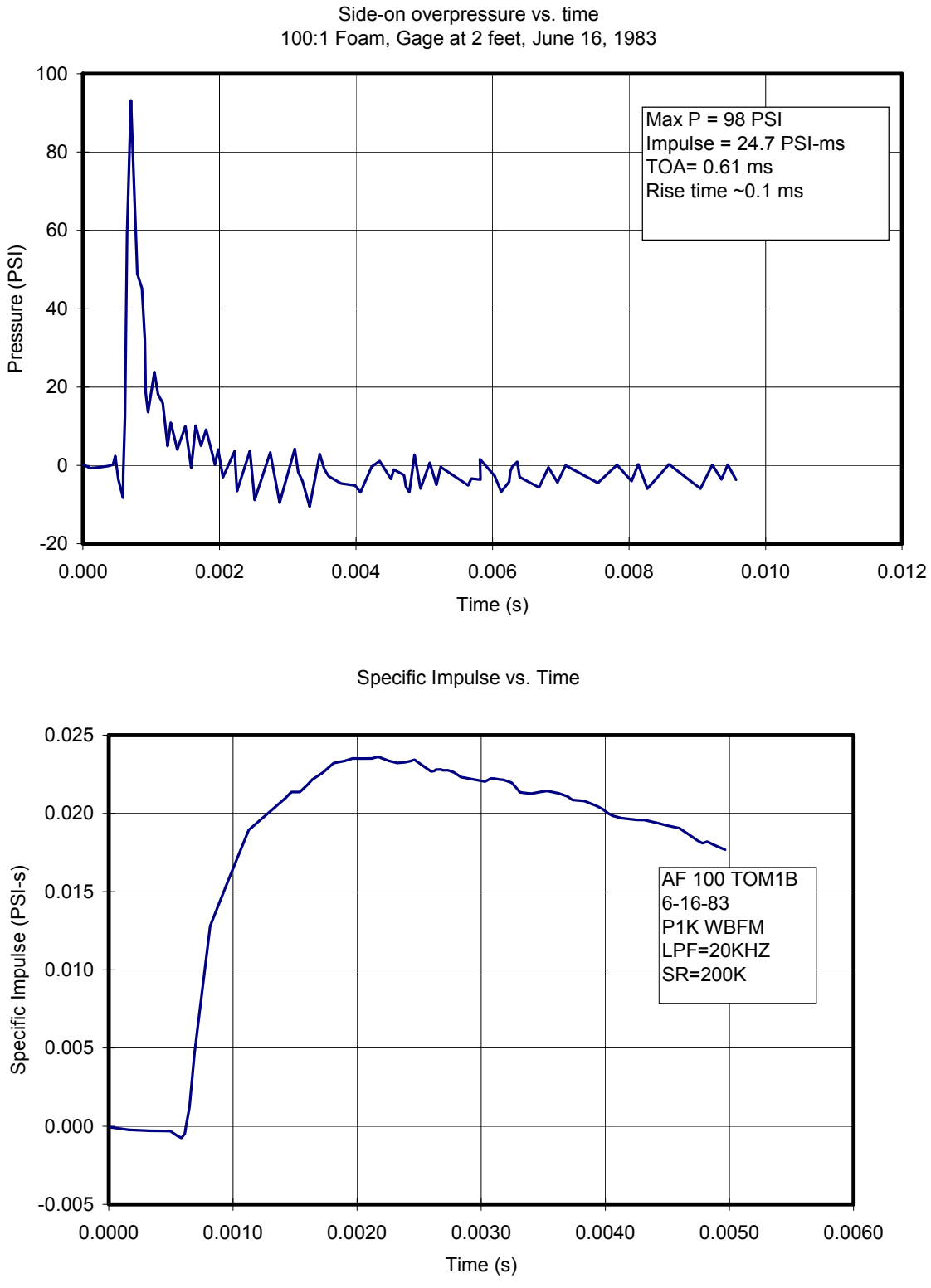

Figure 36: Transient pressure and specific impulse at 2 feet, 100:1 foam, 6/16/83.

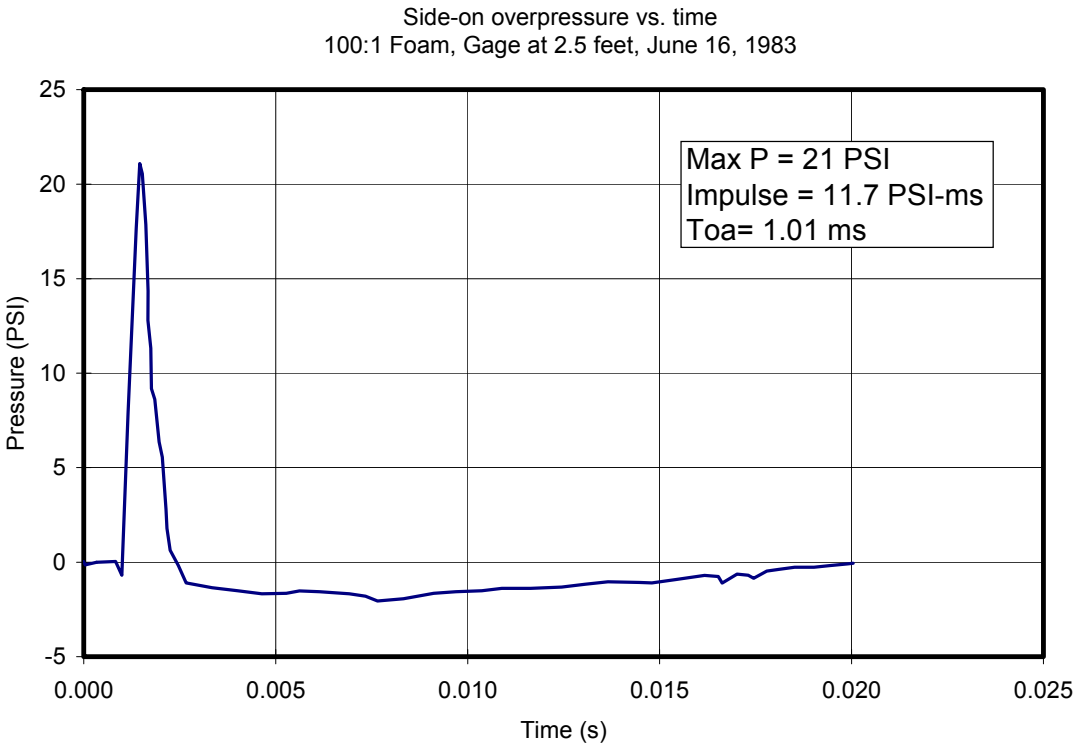

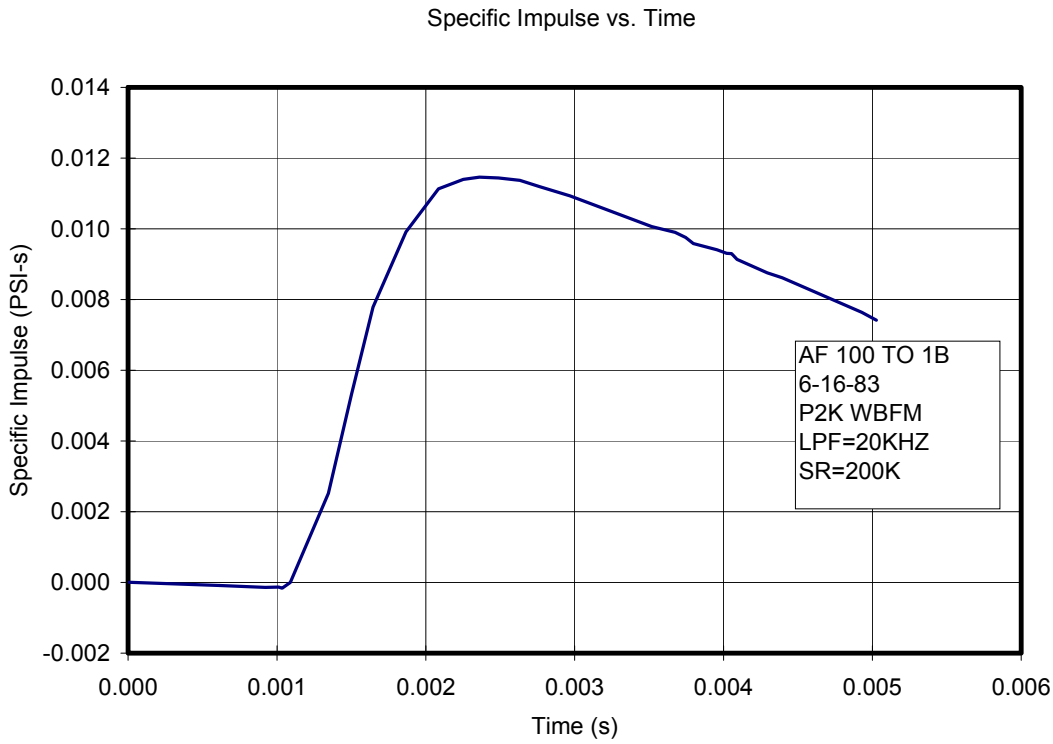

Figure 37: Transient pressure and specific impulse at 2.5 feet, 100:1 foam, 6/16/83.

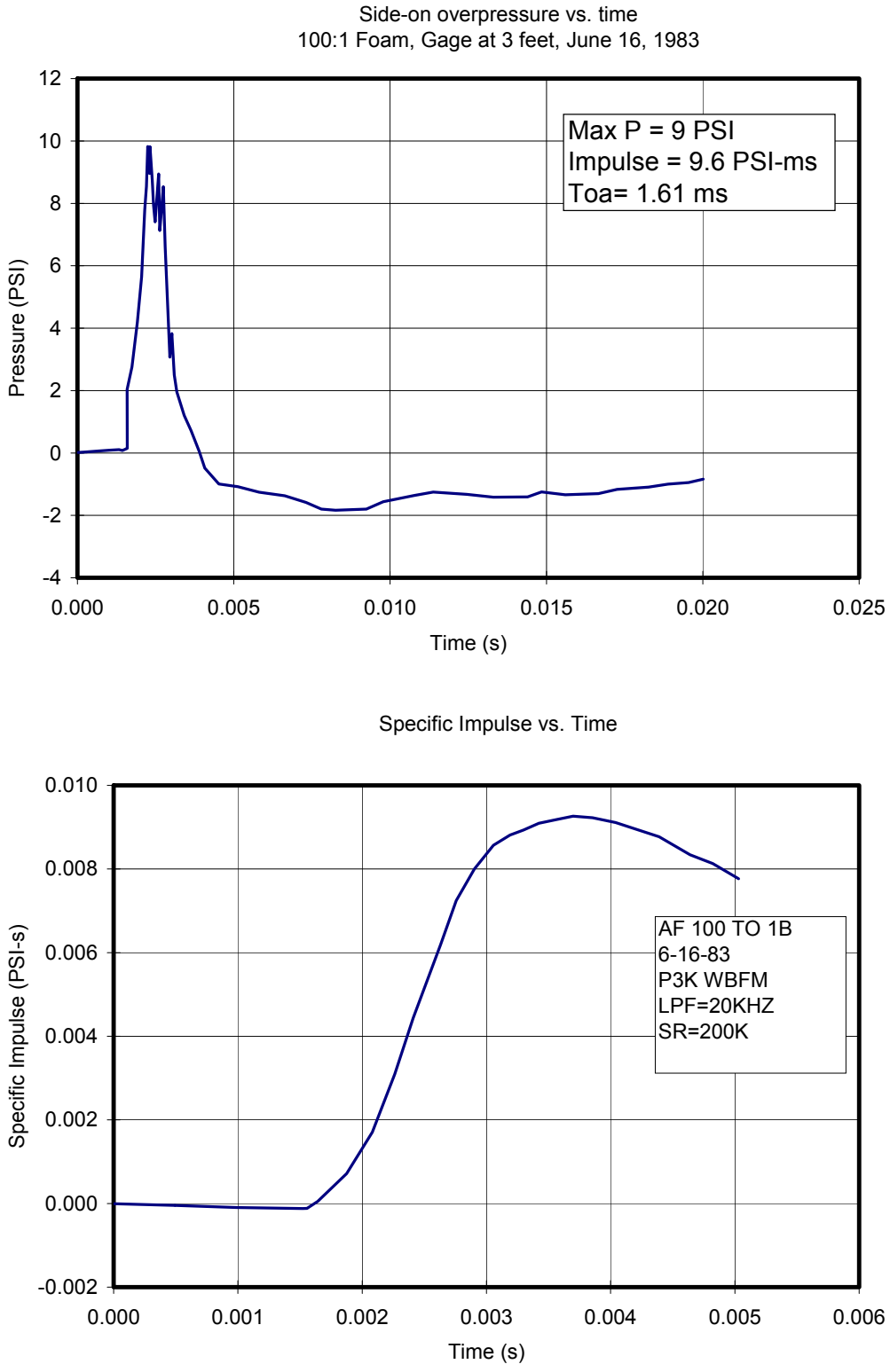

Figure 38: Transient pressure and specific impulse at 3 feet, 100:1 foam, 6/16/83.

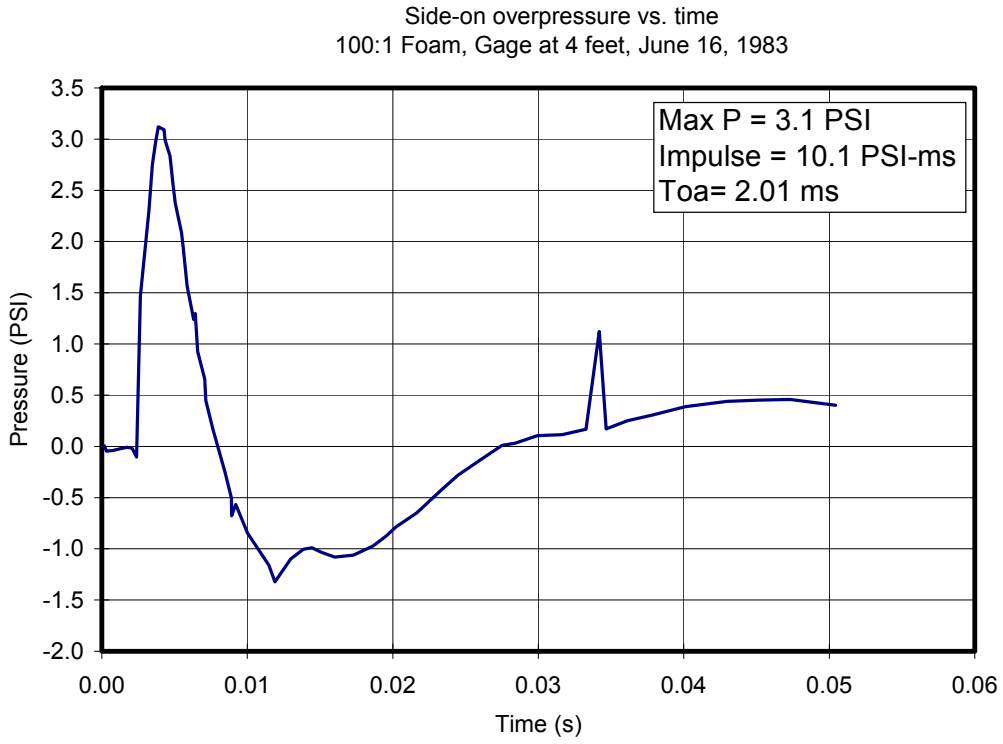

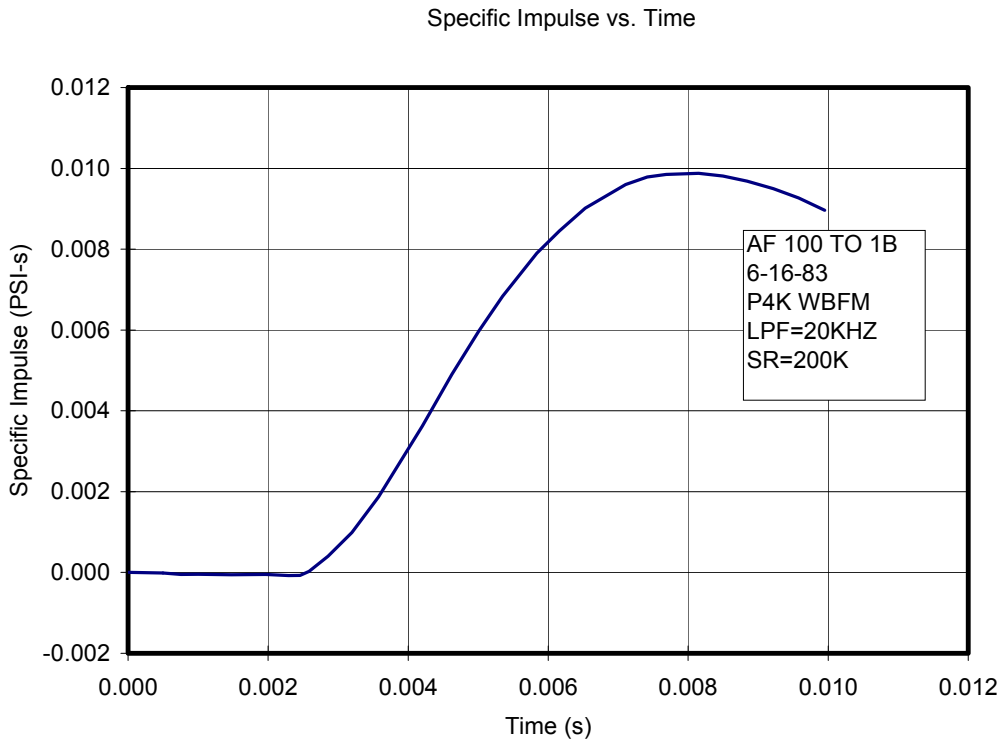

Figure 39: Transient pressure and specific impulse at 4 feet, 100:1 foam, 6/16/83.

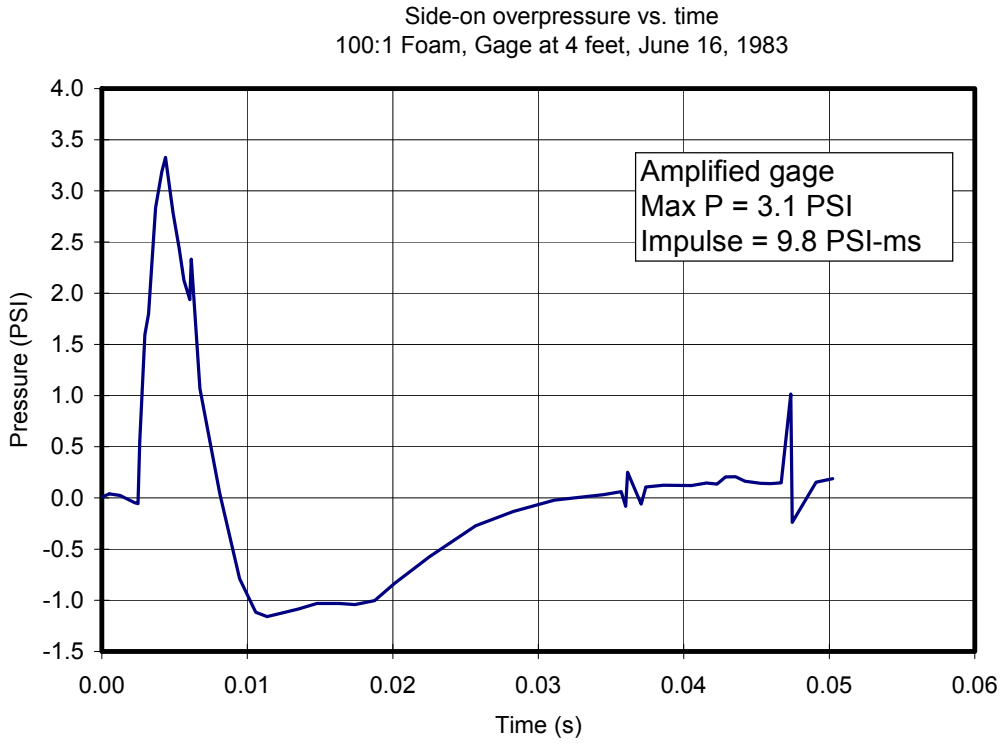

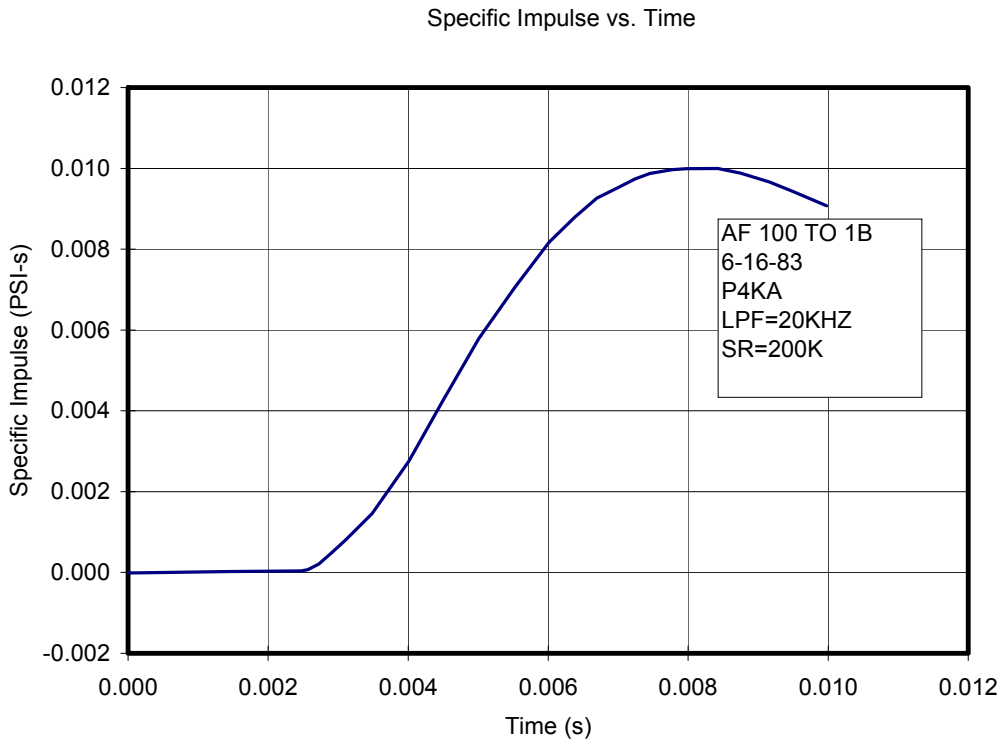

Figure 40: Transient pressure and specific impulse at 4 feet, 100:1 foam, 6/16/83 (amplified gauge).

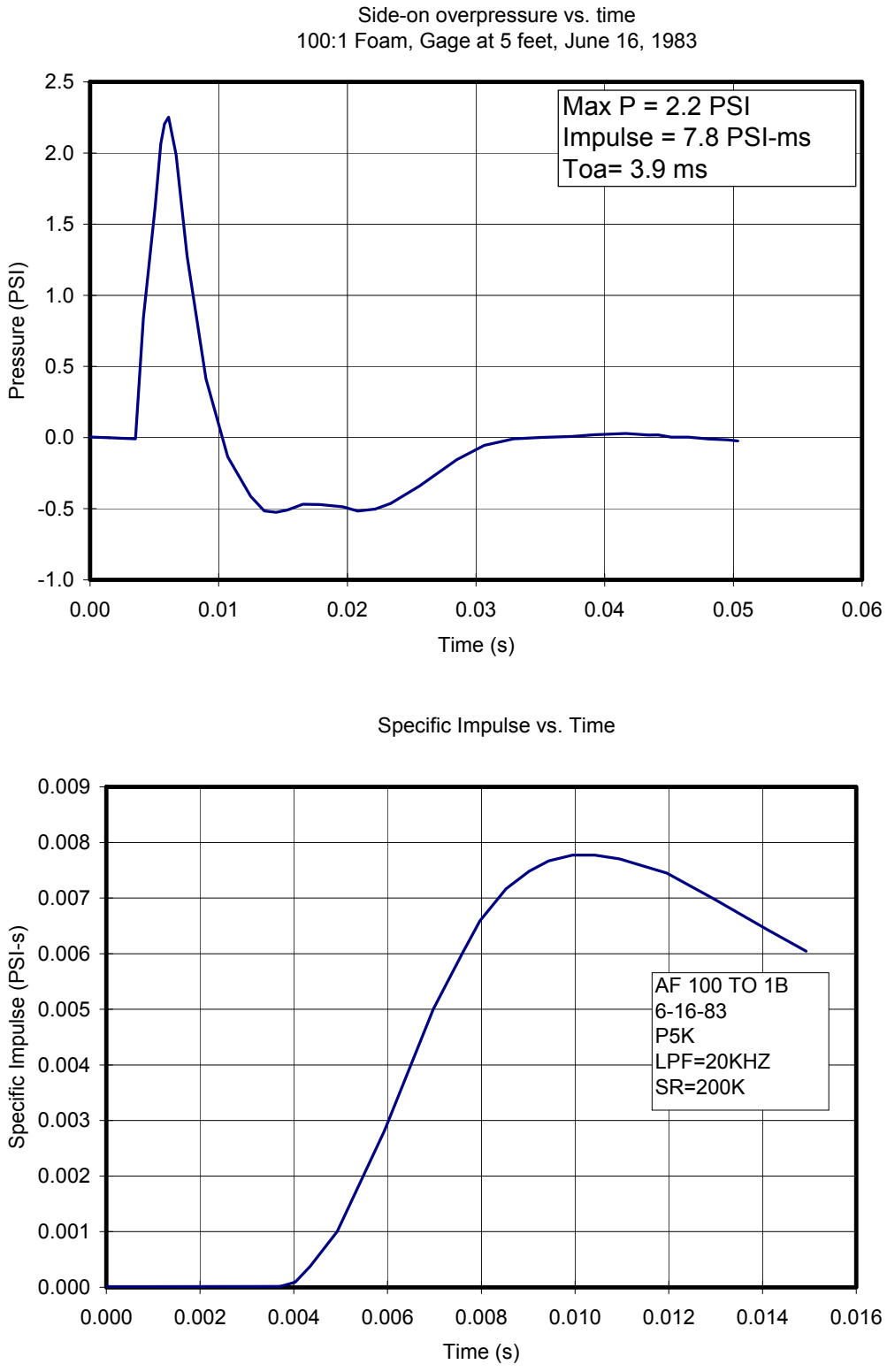

Figure 41: Transient pressure and specific impulse at 5 feet, 100:1 foam, 6/16/83.

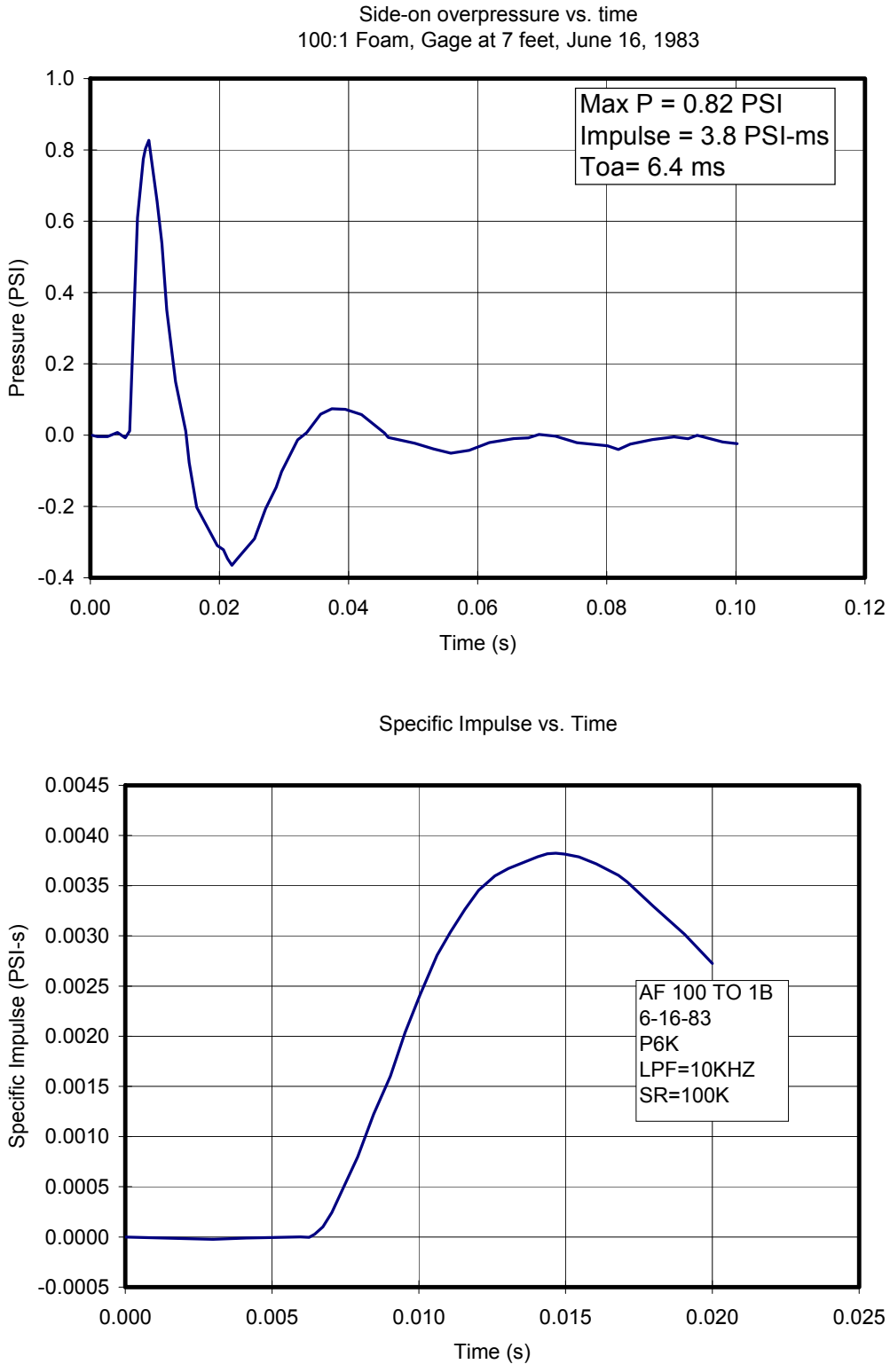

Figure 42: Transient pressure and specific impulse at 7 feet, 100:1 foam, 6/16/83.

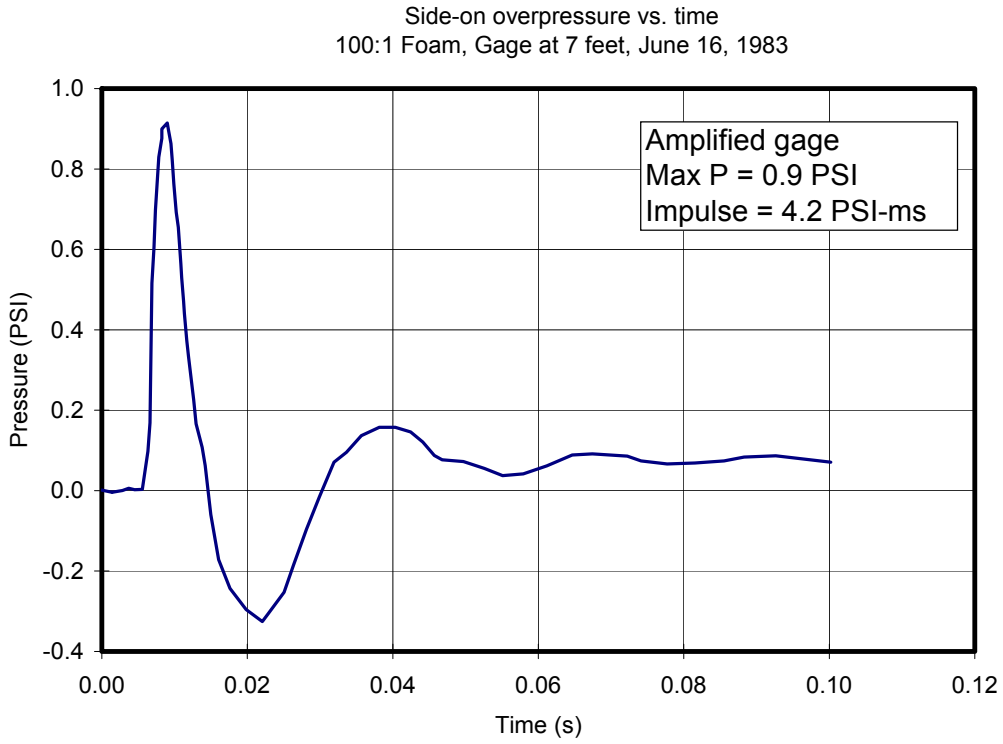

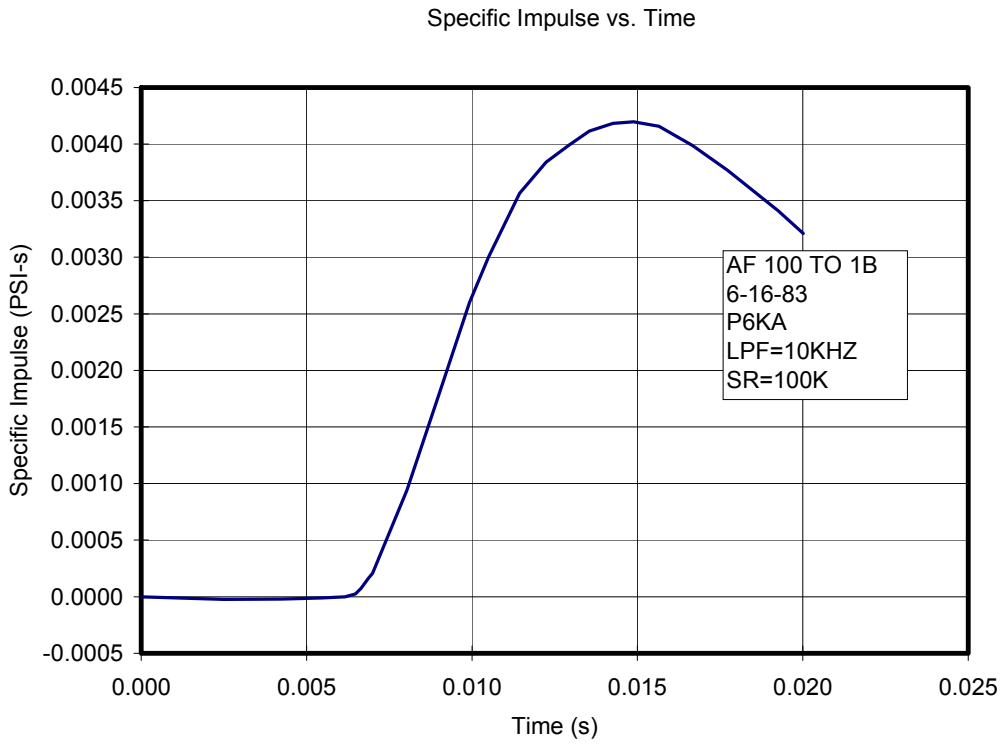

Figure 43: Transient pressure and specific impulse at 7 feet, 100:1 foam, 6/16/83 (amplified gauge).

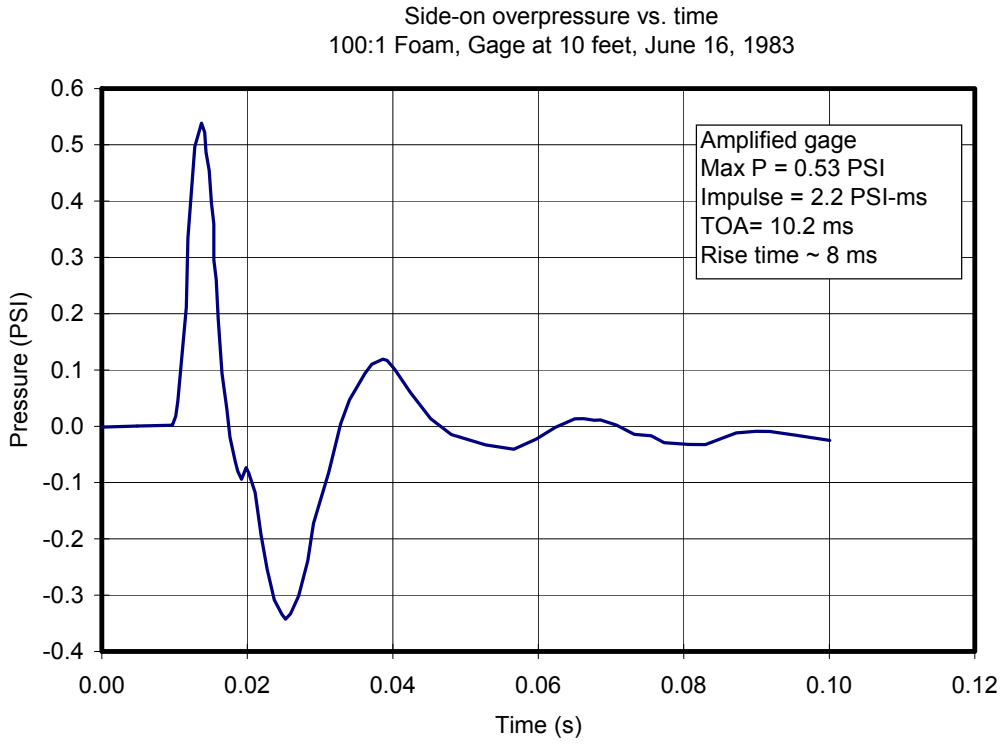

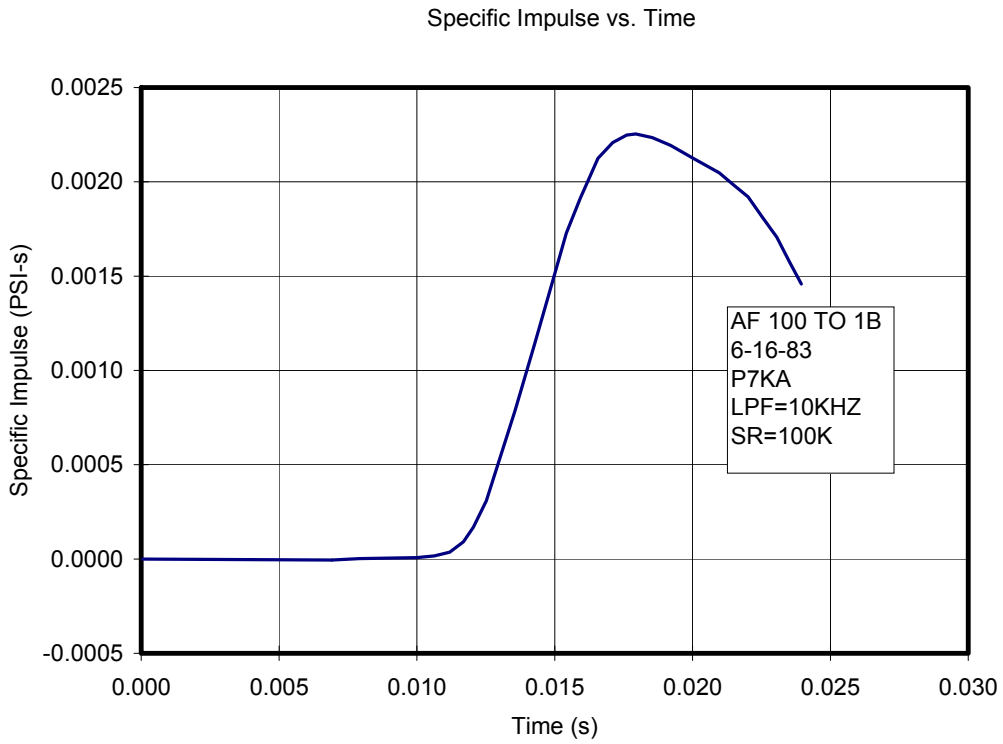

Figure 44: Transient pressure and specific impulse at 10 feet, 100:1 foam, 6/16/83 (amplified gauge).

Appendix B: Curve fits for pressure and time of arrival

A Fitting Introduction

This appendix summarizes the data and techniques used for the curve fits presented earlier. Table 27 lists the data from all of the experiments that include pressure data or TOA data used in the fits presented in the report. The last two columns of the table indicate whether that data line was used in developing the fit for Eqs. 4 and/or 5. Mostly, the data were culled if the earlier discussion indicated problems with the data point. A face-on measurement is appropriate for TOA fitting but not for side-on overpressure. However, additional points were dismissed when they appeared to be exceptional outliers. Not shown in the table are the point by point differences between the empirical fits and individual data points. These were visible during the fitting process and were the basis for dismissing some outlying points.

Fits were sought for pressure, impulse, and time of arrival. For each of these a somewhat arduous effort was expended iterating through a proposed functional form, optimizing the fit of that form, and evaluating its behavior over the space of data considered. It was desirable to find a functional form so that the dependent variable would be a function continuous in both scaled distance and foam density. Note that the current discussion is limited to foam (not air-only) so that density is only a very weak function of atmospheric pressure; hence atmospheric pressure is not a parameter in these fits.

As noted previously, the "noise" in the impulse data was comparatively large. Also, over the distance range covering most of the impulse data, the impulse varies weakly with range. Consequently, no functional form fits that data well and none is recommended in this report. Reference [6] documents an impulse fit that has been used for estimation purpose, but the current effort demonstrates that it is really a rough indication of impulse and it is purposefully omitted from the current presentation.

On the other hand, empirical fits are offered earlier in the report for side-on pressure and time of arrival. In both of these cases the fits are behaved over the range of densities for which experimental data have been presented. Moreover, in both cases they fit fairly well. Specifically, the functional forms were fit to just the moderate densities (60:1, 100:1, and 200:1) and to the broader range of densities. Widening the range of data considered did not significantly results in departure between the observations and the empirical fits.

Equations 4 and 5 are both of the form $y(\rho, x^*) = f_1[x^*, \rho]$, where ρ is the foam density and x^* the scaled range. For TOA, the form $y(\rho, x^*) = f_2[x^*, A(\rho), B(\rho)]$ was convenient. $A(\rho)$ is a two-piece function with the transition occurring at some ρ^*. The transition density, ρ^*, was made one of the search parameters along with the other coefficients in $A(\rho)$. The coefficients in $A(\rho)$ were constrained to force continuity in both value and slope at ρ^*. This care was important for the TOA function so that its derivative, used to find disturbance velocity, was also a continuous function. The fitting was done using Solver in Excel (TMs of Microsoft). For either TOA or pressure the objective function was:

$$H = \sqrt{\frac{1}{N}\sum\left(1 - P_i / O_i\right)^2}$$

where P_i is the predicted value, O_i the observed, and N the number of points used in the fit.

Table 27: Summary of data used in fits of Equations 4 and 5.

date	Table	Config	W (lb)	x (ft)	P (psi)	i'' (psi-ms)	TOA (ms)	ER	Eq. (4)	Eq. (5)
9/6/1983	2		1	3	45.1	7.4	0.66	1000	X	X
9/6/1983	2		1	3.5	37.8	8.8	0.87	1000	X	X
9/6/1983	2		1	4	21.2	9.1	1.26	1000	X	X
9/6/1983	2	FO	1	4	59.3	38.5	1.37	1000		X
9/6/1983	2	FO	1	4	55.8	37.5	1.37	1000		X
9/6/1983	2		1	5.5	5.6	7.6	2.43	1000	X	X
9/6/1983	2		1	5.5	5.4	5.6	2.95	1000	X	X
9/6/1983	2		1	8	2.34	7	4.61	1000	X	X
9/6/1983	2		1	10	1.92	6.6	6.43	1000		X
9/6/1983	2		1	10	2.04	5.82	7.05	1000		X
3/28/1983	3		1	2.5	77.6	11.8	0.52	375	X	X
3/28/1983	3		1	3	21	7.5	0.97	375	X	X
3/28/1983	3		1	4	9.8	7	1.73	375	X	X
3/28/1983	3		1	4	9.6	6.9	1.75	375	X	X
3/28/1983	3		1	4	-1	-1	-1	375		
3/28/1983	3		1	4	7.8	-1	-1	375	X	
3/28/1983	3		1	5	4.5	7.8	2.59	375	X	X
3/28/1983	3		1	7	3.3	7.8	4.3	375	X	X
3/28/1983	3		1	10	1.4	4.2	7.11	375		X
3/28/1983	3		1	10	-1	-1	-1	375		
3/28/1983	3	foam/air	1	3.3	3.8	3.6	1.36	375		
3/28/1983	3	FO	1	4	45	23.7	1.47	375		X
3/28/1983	3		1	11.8	2.3	7.5	8.9	375		
4/13/1983	4		1	2	181	25	0.49	200	X	X
4/13/1983	4		1	2.5	26	11.5	0.93	200	X	X
4/13/1983	4		1	3	13.9	8.8	1.35	200	X	X
4/13/1983	4		1	4	3.6	8.7	2.36	200	X	X
4/13/1983	4		1	4	1.1		2.36	200		X
4/13/1983	4		1	4	5.1		2.09	200	X	X
4/13/1983	4		1	5	2.1	7	3.07	200	X	X
4/13/1983	4		1	7	1.48	4.6	5.47	200	X	X
4/13/1983	4		1	10				200		
4/13/1983	4	foam/air	1	3.3	1.96		1.93	200		
4/13/1983	4	FO	1	4	7		2.09	200		X
11/15/1982	5		1	1.5	154	23.2	0.33	100	X	X
11/15/1982	5		1	2	115		0.59	100	X	X
11/15/1982	5		1	2.5	63	8.1	1.2	100		X
11/15/1982	5		1	4	2.8	3.3	2.39	100	X	

11/15/1982	5	foam/air	1	3.3	2.6		1.75	100		
7/6/1983	6		1	2	98	24.7	0.61	100	X	X
7/6/1983	6		1	2.5	21	11.7	1.01	100	X	X
7/6/1983	6		1	3	9	9.6	1.61	100	X	X
7/6/1983	6		1	4	3.1	10.1	2.01	100	X	X
7/6/1983	6		1	4	3.1	9.8	2.07	100	X	X
7/6/1983	6		1	5	2.2	7.8	3.9	100	X	X
7/6/1983	6		1	5	2.65	8.4		100	X	
7/6/1983	6		1	7	0.82	3.8	6.4	100		X
7/6/1983	6		1	7	0.9	4.2	6.5	100		X
7/6/1983	6		1	10	0.53	2.2	10.2	100		X
7/6/1983	6		1	10	0.46	1.7		100		
8/9/1983	7		1	2	74.5	18.5	0.61	100	X	X
8/9/1983	7		1	2.5	23.2	13.8	0.9	100	X	X
8/9/1983	7		1	3	10.2	11.6	1.44	100	X	X
8/9/1983	7		1	4	2.9	8.8	2.36	100	X	X
8/9/1983	7		1	4	3.7	11.1	2.24	100	X	X
8/9/1983	7		1	5	1.4	6.1	3.24	100	X	X
8/9/1983	7		1	7	0.98	3.2	6.7	100		X
8/9/1983	7		1	7	1.01	3.8	6.05	100		X
11/23/1982	8		1	1.5	107	22.5	0.5	54	X	X
11/23/1982	8		1	2	44	18.3	0.7	54	X	X
11/23/1982	8		1	2.5	38	19.3	1	54	X	
11/23/1982	8		1	4	2.3	10.5	2.9	54	X	X
11/23/1982	8		1	4	2.1			54	X	
11/23/1982	8	foam/air	1	3.3	1.7	2.8	2.2	54		
4/28/1983	9		50	7	66	55.5	2.8	60	X	X
4/28/1983	9		50	8	18.8	45.8	4.1	60	X	X
4/28/1983	9		50	8	19	44.3	4	60	X	X
4/28/1983	9		50	9.5	11.4	57.5	5.9	60	X	X
4/28/1983	9		50	11.5	7.2	56.5	8.5	60	X	
4/28/1983	9		50	18	2.3	38.4	18.9	60		X
4/28/1983	9	foam/air	50	18	0.38	8.9	18	60		
4/28/1983	9	foam/air	50	18	0.48	8.7	19	60		
8/2/1983	10		1	2	106	20.8	0.55	100	X	X
8/2/1983	10		1	2.5	58	13.5	0.7	100		
8/2/1983	10		1	3	12.3	8.2	1.3	100	X	X
8/2/1983	10	FO	1	4	35.5	42.1	2	100		X
8/2/1983	10		1	5	2	5.7	3.2	100	X	X
8/2/1983	10		1	7	1.2	3.8	5.6	100		X
8/2/1983	10		1	10	0.7	2.2	10.6	100		X
3/8/1984	11		1	2	39	20.5	1.2	60	X	
3/8/1984	11		1	2.5	15	15.3	1.6	60	X	
3/8/1984	11		1	4	1.75	9.2	3.8	60	X	
3/8/1984	11		1	5	0.9			60	X	
3/8/1984	11		1	7	0.58	3.3	10.2	60		X
3/8/1984	11		1	10	0.19	1.25	15.7	60		X
3/8/1984	11		1	10	0.18	1.21	15.9	60		X
6/17/1982	12		1	1.5	99	42	0.63	27	X	X
6/17/1982	12		1	2	45	30.5	1.4	27	X	X

6/17/1982	12	1	2	51		1.33	27	X	X
6/17/1982	12	1	2.5	31	32	2.06	27	X	
6/17/1982	12	1	4	4.3	21.5	8.46	27	X	X
9/29/1982	13	1	1.5	139	115	1.29	10	1.5	139
9/29/1982	13	1	2	78	62	2.82	10	2	78
9/29/1982	13	1	2	75	-1	2.5	10	2	75
9/29/1982	13	1	2.5	33	45	4.08	10	2.5	33
9/29/1982	13	1	4	12.3	50	13.5	10	4	12.3

Appendix C: B.A. Boughton Memo of 3/3/88

Sandia National Laboratories
Albuquerque, New Mexico 87185

date: March 3, 1988

to: W. F. Hartman, 5214

from: B. A. Boughton, 5214

subject: Shock Propagation in Aqueous Foam

A reasonably complete description of the shock parameters as a function of distance from the explosive is an important component in development of a particle capture model. This information is also necessary to improve the method used to calculate the plume's initial conditions for cases with aqueous foam mitigation. Overpresssure plays a key role in determining the radius over which the liquid in the foam will be vaporized. Particle velocity governs acceleration-induced fragmentation and, therefore, determines the size of the water droplets remaining after passage of the shock. The diameter and number density of these liquid drops control the cooling of the hot gases which make up the thermal plume and also determine the efficiency of particle removal. This memo describes an approach which makes use of experimental data to determine the properties of the shocked state without requiring specification of an equation of state in the two-phase region.

Measurements of time of arrival and overpressure at distances greater than about 9 charge radii from spherical C-4 charges detonated on the ground were made in a series of experiments conducted as part of the NEST R & D program between 1982 and 1984. Aqueous foams with expansion ratios ranging from 10:1 to 1000:1 were investigated. In this work, only 60:1 and 100:1 expansion ratio foams will be considered since these densities appear to be optimal from both the shock attenuation and particle capture points of view. The pertinent experimental data are summarized in the Appendix. A description of the shocked conditions is obtained using these measurements together with the Hugoniot relations. Flow parameters at locations closer to the explosive are computed by supplementing the experimental data with values of overpressure and shock velocity at the charge surface as determined from an analysis of the explosion products/foam interface.

In the following section, the analysis used to calculate the interface conditions is described including the equation of state employed in this superheated region. Next, the measurements of overpressure and arrival time are presented along with the derived quantities — shock velocity and particle velocity. Finally, our results are compared with data obtained by Vakhnenko et al. (1984).

Analysis of the Explosion Products/Foam Contact Discontinuity

The available experimental data can be extrapolated back to the surface of the charge by calculating the flow properties at the interface between the explosion products

and foam. These properties are determined by imposing continuity of pressure, p, and particle velocity, u, across the contact surface. This is equivalent to finding the point in p–u space where the foam Hugoniot crosses the release isentrope of the explosive.

An equation of state for the foam at the high pressures and temperatures that exist at the interface must be specified before the Hugoniot can be constructed. Under these conditions, the water present in the foam will be highly superheated and, in fact, will be in a state above the critical point. An equation of state capable of treating the two-component (air and water vapor) superheated mix will suffice since we are interested only in predicting the interface conditions and are not concerned with lower pressures where vapor and liquid water will coexist. From a calculational standpoint, it is desirable to choose the simplest formulation that will produce acceptable results over the pressure and temperature range of concern. For this reason, we have considered equations of state with two free parameters.

Bjerre and Bak (1969), in an extensive review of two-constant equations of state, chose a form first derived by Redlich and Kwong (1949) as the most accurate. For a pure substance, the Redlich-Kwong equation can be expressed in terms of pressure, temperature and specific volume as

$$p = \frac{RT}{\vartheta - b} - \frac{a}{T^{0.5}\vartheta(\vartheta + b)} \tag{1a}$$

or as a cubic in compressibility $Z = p\vartheta/RT$

$$Z^3 - Z^2 + (A^* - B^* - B^{*2})Z - A^*B^* = 0, \tag{1b}$$

where R is the gas constant, $A^* = ap/R^2T^{2.5}$ and $B^* = bp/RT$.

The constants a and b are determined by imposing the thermodynamic stability criteria at the critical point

$$\left.\frac{dp}{d\vartheta}\right|_{T_c} = 0 \qquad \text{and} \qquad \left.\frac{d^2p}{d\vartheta^2}\right|_{T_c} = 0,$$

where the subscript c denotes a critical property. If these constraints are made on Equation (1a), it is readily shown that

$$a = \frac{\Omega_a R^2 T_c^{2.5}}{p_c} \qquad \text{and} \qquad b = \frac{\Omega_b R T_c}{p_c}, \tag{2}$$

where $\Omega_a = [9(2^{1/3} - 1)]^{-1}$ and $\Omega_b = (2^{1/3} - 1)/3$. Thus, with values of the critical temperature and pressure for a material, a and b are easily computed.

Equation (1b) is plotted in Figure 1 as a function of reduced pressure $p_r = p/p_c$ for various values of the reduced temperature $T_r = T/T_c$. These results agree with the compressibility function obtained from experimental p-ϑ-T data by Nelson and Obert (1954) and the high pressure-temperature chart of Breedveld and Prausnitz (1973) to within about 5%. Notice that Z is close to unity if both p_r and T_r are large and that the

greatest departures from ideal gas behavior ($Z = 1$) occur at high pressures with temperatures close to the critical value.

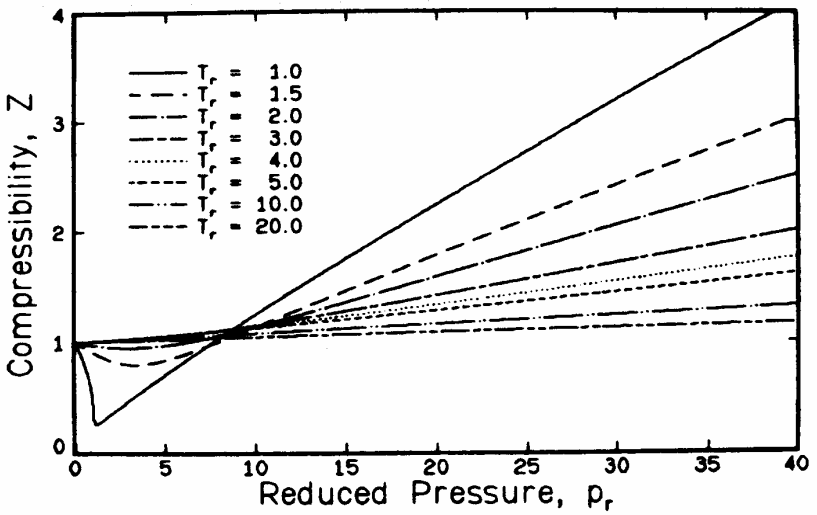

Figure 1. Compressibility derived from the Redlich-Kwong equation of state.

The Redlich-Kwong equation of state as given in Equation (1) is a method to predict the volumetric behavior of a pure, real gas as a function of pressure and temperature. The additional variable of composition must be included to extend this method to mixtures. This is accomplished by making the equation of state constants a function of composition. Experience has shown that the expressions given in Equation (2) can be used directly if a pseudocritical temperature and pressure of the mixture are defined as

$$T_{c_m} = \left\{ \frac{\left[\sum_i y_i (T_{c_i}^{2.5}/p_{c_i})^{0.5}\right]^2}{\sum_i y_i (T_{c_i}/p_{c_i})} \right\}^{2/3} \tag{3a}$$

and

$$p_{c_m} = \frac{T_{c_m}}{\sum_i y_i (T_{c_i}/p_{c_i})}. \tag{3b}$$

Here, the summations are over all the mixture components and y_i is the mole fraction of component i. Although having some basis in statistical thermodynamics, this rule is largely empirical and has resulted after many trials and comparisons of calculated mixture properties with experimental data.

The specific enthalpy of a mixture of fixed composition at some pressure and temperature (p, T) may be written

$$h(p, T) = \Delta h(p, T) + h^0(T). \tag{4}$$

In Equation (4), $h^0(T)$ is the mixture enthalpy at temperature T but in an ideal-gas state, i.e., as $p \to 0$, and can be expressed as an integral of the ideal gas heat capacity $c_p^0(T)$. The departure function $\Delta h(p, T)$ relates the enthalpy of the mixture at (p, T)

to the ideal gas reference state at the same temperature. Applying Maxwell's relations for a constant temperature process we find

$$\Delta h(p,T) = \frac{bRT}{\vartheta - b} - \frac{a}{T^{0.5}(\vartheta + b)} - \frac{3a}{2bT^{0.5}} \ln \frac{\vartheta + b}{\vartheta} \tag{5}$$

for a pure material or mixture that obeys the Redlich-Kwong equation of state.

Using the Redlich-Kwong equation of state with the mixture enthalpy given by Equations (4) and (5), we can solve the conservation of mass, momentum and energy relations across the shock front and construct Hugoniot curves. These results are presented in Figure 2 for 60:1 and 100:1 ER foam. The Hugoniot characterizes all pairs of values of (p,u) for the state on the disturbed side of the shock that are compatible with the three conservation relations when values of (p_0,u_0) on the undisturbed side are specified. For the results presented here, we have assumed $p_0 = 1$ atm and $u_0 = 0$. Also shown are the release isentropes from the Chapman-Jouguet state for C-4 and TNT. The point at which the Hugoniot crosses the release isentrope defines the conditions at the contact surface between the detonation products and the foam.

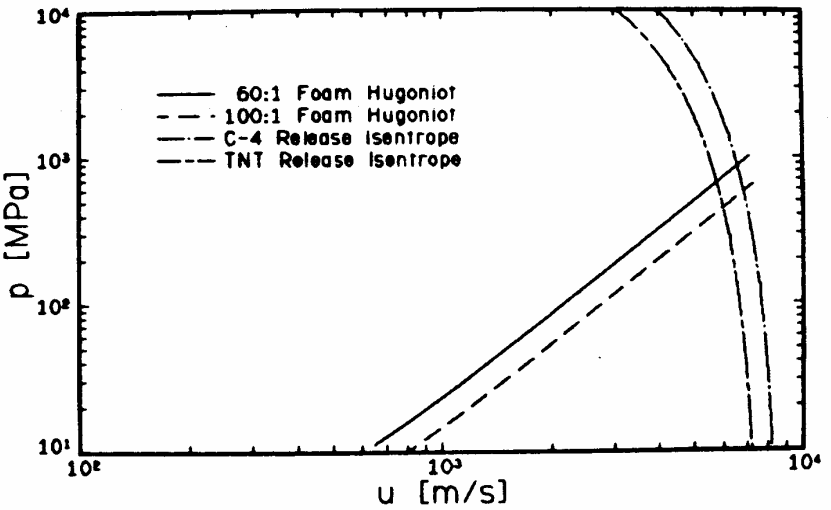

Figure 2. Hugoniot curves for foam and release isentropes for two high explosives.

Table 1. Properties at the Contact Surface

	C-4			TNT		
	p, MPa	U, m/s	u, m/s	p, MPa	U, m/s	u, m/s
60:1	860	7350	6590	660	6450	5770
100:1	580	7560	6850	440	6650	6000

The properties at the contact surface are summarized in Table 1. The values for TNT can be compared with similar calculations made by Vakhnenko et al. (1984).

For foams with an average expansion ratio of 80:1, they found $p \simeq 500$ MPa and $U \simeq 6000$ m/s. These values are not only consistent with our analysis, but are within 10% of our predictions for 80:1 ER foam.

Experimental Data and Derived Quantities

The measured values of overpressure and time of arrival are shown in Figures 3 and 4. Here we have used the nondimensionalization $p^* = p/p_0 - 1$, $t_a^* = t_a a_0/(E/p_0)^{1/3}$ and $r^* = r/(E/p_0)^{1/3}$, where $a_0 = 340.29$ m/s is the speed of sound in air under standard atmospheric conditions and E is the total explosive energy. Also included are the property values at the surface of the explosive derived in the preceding section. Immediately noticeable is the relatively small difference in shock attenuation between 60:1 and 100:1 ER foam. This supports our decision to use 100:1 ER foam in full-scale containments. The small penalty paid in using 100:1 ER foam is more than offset by the additional logistical requirements and the inability to rapidly generate large quantities of 60:1 ER foam. This conclusion continues to hold if particle capture and cloud buoyancy are factored in.

Analytical expressions which represent the variation in flow properties with distance from the explosive are convenient when developing computer-based simulations. To facilitate numerical evaluation, the overpressure and arrival time data have been fit with functions of the form

$$\ln Y = b_0 + b_1 \ln r^* + b_2(\ln r^*)^2 + b_3(\ln r^*)^3, \tag{6}$$

where Y is p^* or t_a^*. The least squares fits are the solid lines in Figures 3 and 4. The b_i are given in Table 2.

Table 2. Coefficients of Least Squares Fits for Overpressure, Arrival Time and Shock Velocity where $\ln\{p^*, t_a^*, U^*\} = b_0 + b_1 \ln r^* + b_2(\ln r^*)^2 + b_3(\ln r^*)^3$

	b_0	b_1	b_2	b_3
60:1 ER				
p^*	-4.585273	-3.500705	-7.184958×10^{-2}	-
t_a^*	5.709352×10^{-1}	1.375820	-2.439057×10^{-1}	-
U^*	-8.834586×10^{-1}	3.432597×10^{-2}	3.835160×10^{-1}	3.709878×10^{-2}
100:1 ER				
p^*	-3.866971	-3.326363	-9.182947×10^{-2}	-
t_a^*	1.571933×10^{-1}	1.396603	-2.143066×10^{-1}	-
U^*	-4.844042×10^{-1}	-3.131901×10^{-2}	3.437589×10^{-1}	3.616579×10^{-2}

Breakup of the water drops that are suspended in the foam is a result of their sudden exposure to the high velocity flow that exists behind the shock front. Therefore, before the breakup process can be modeled, the particle velocity $u^* = u/a_0$ following the shock must be characterized. An estimate of u^* can be obtained using the Hugoniot conditions together with the curve fits for overpressure and time of arrival.

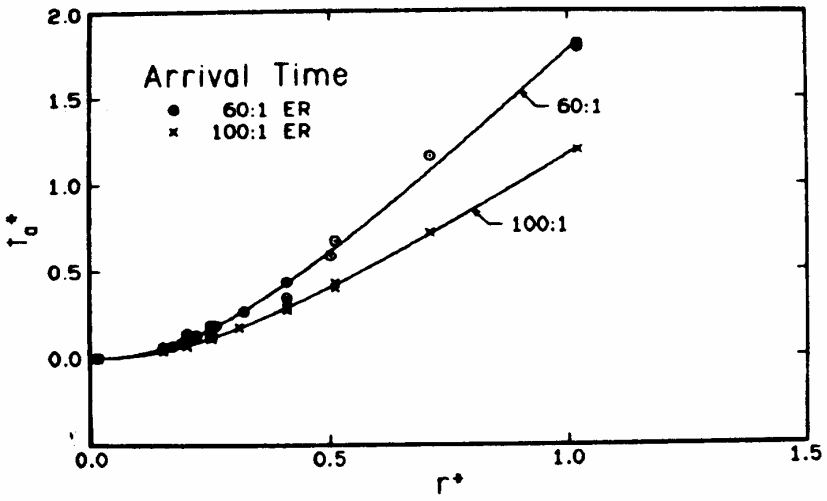

Figure 3. Time of arrival as a function of distance.

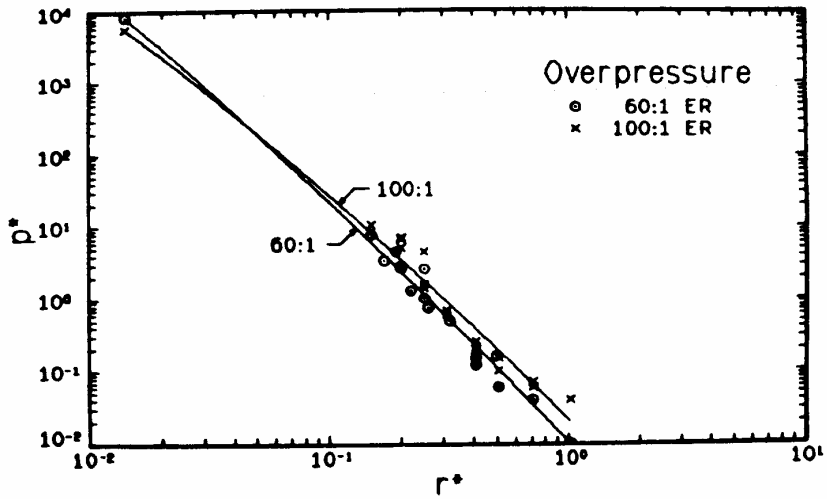

Figure 4. Overpressure as a function of distance.

First, the dimensionless shock velocity is calculated from the relationship

$$U^* = U/a_0 = (dt_a^*/dr^*)^{-1}.$$

Rather than differentiating the least squares fit of t_a^* over the entire range of r^*, we have used the derivative directly only over those values of r^* where measurements were made. Extrapolation back to the charge surface was achieved by forcing U^* to match the value shown in Table 1 from the analysis of the contact surface discontinuity. A reasonable

approximation to the shock velocity is then obtained in the form of Equation (6) with the constants given in Table 2. Determining the shock velocity in this way, i.e., by differentiation, is clearly not the most desirable procedure because of the sensitivity of the derivative to uncertainties in the curve fit to the t_a^* measurements. For example, small changes in the concavity of the arrival time curve can noticeably alter the shock velocity prediction. Unfortunately, there is no alternative method to calculate U^* with the existing data. Figure 5 shows the shock velocity for 60:1 and 100:1 ER foam. As expected, U^* is higher in the lower density medium. However, the results for the two foam densities differ by no more than $\sim 30\%$.

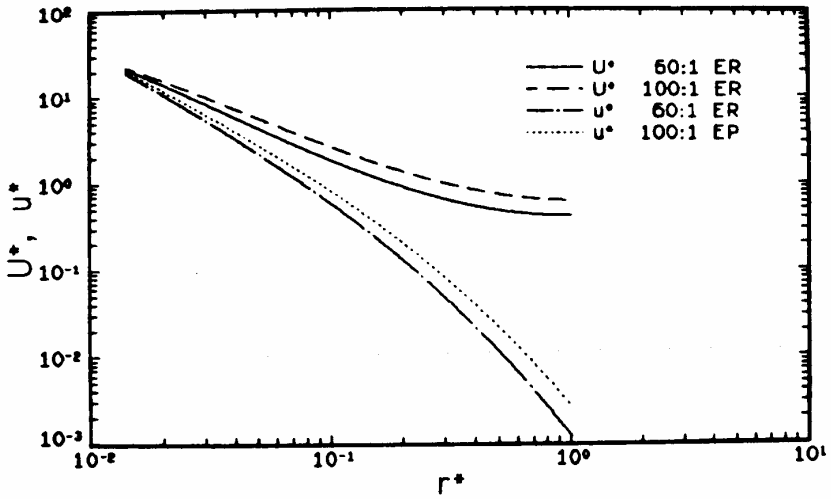

Figure 5. Shock and particle velocities in foam.

The particle velocity can now be determined using

$$u^* = \left(\frac{p_0 \vartheta_0}{a_0^2}\right) \frac{p^*}{U_*},$$

where ϑ_0 is the specific volume of the undisturbed foam. These results are also shown in Figure 5. The particle velocity is larger in 100:1 ER foam. This implies that compared to 60:1 ER foam, the water drops will be broken up over an extended range of distances in 100:1 ER foam. The maximum difference in particle velocity between 60:1 and 100:1 ER foam is roughly 50%. Considering that the measurement errors in overpressure and arrival time are 20-30% and about 5%, respectively, this difference remains on the order of the uncertainty in the experimental data. Again, we can conclude that 60:1 and 100:1 expansion ratio foam are essentially equivalent.

Comparison with Russian Data

In this section, our results are compared with measurements made by Vakhnenko et al. (1984) (hereafter, VKP). The VKP data were obtained from experiments conducted with spherical explosive charges having a mass of 0.5 to 2.8 kg. The heat of

detonation was 5.4 MJ/kg. Aqueous foams with expansion ratios from 67:1 to 100:1 were used. VKP make no distinction between these foams, which is a reasonable assumption as Figures 3 through 5 illustrate.

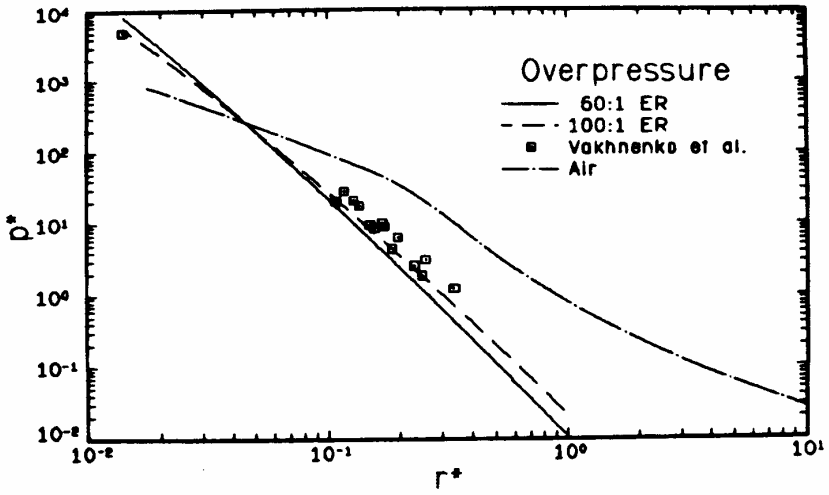

Figure 6. Comparison of VKP overpressure data and curve fits.

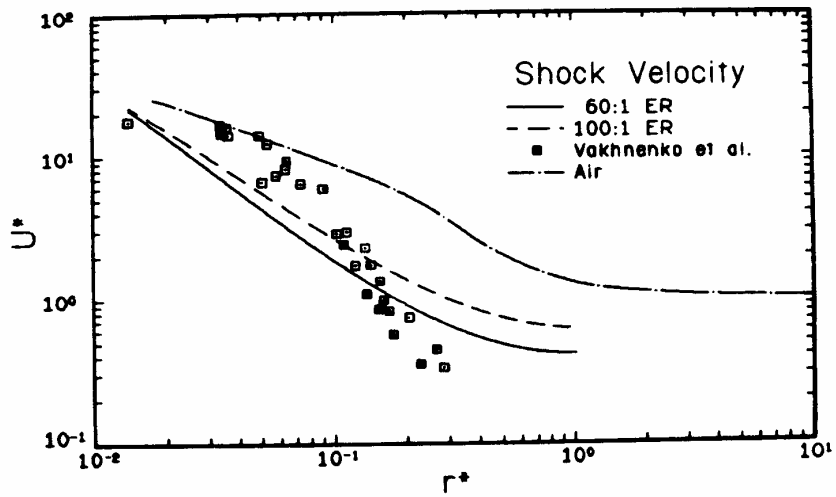

Figure 7. Comparison of VKP shock velocity data and curve fits.

Figure 6 compares our curve fits with the VKP overpressure data. Here there is close agreement. The small discrepancy may be caused by uncertainties in the foam expansion ratio as mentioned by Kuznetsov et al. (1986). Also shown is the overpressure as a function of r^* for a ground burst in air. At locations close to the source ($r^* < 0.05$), p^* is higher in foam than in air because of the foam's large density. However, the shock

is very rapidly attenuated in foam and by $r_* = 0.2$ the overpressure is an order of magnitude below the corresponding value in air.

Finally, in Figure 7, the VKP measurements of shock velocity are compared with the least squares fits of U^* for 60:1 and 100:1 ER foam. The agreement here is not as good, with the predictions and data differing by up to 100%. This sort of agreement is probably all that can be expected considering the previously mentioned shortcomings in obtaining U^* by differentiation. In addition, the description of the VKP experiments is not complete enough to where a reliable evaluation of the data can be made.

Conclusion

Measurements of overpressure and time of arrival were used together with conditions calculated at the charge surface to develop simple expressions for the flow properties as a function of distance from an explosion mitigated by aqueous foam. Both 60:1 or 100:1 ER foam were considered. These formulas can now be used in analyses of the particle capture process and to develop an improved description of the initial conditions for mitigated detonations.

A weakness in this work was the need to differentiate the arrival time curve to obtain the shock velocity. This was exacerbated by the lack of measurements at locations closer than $r^* \simeq 0.1$ (about 9 charge radii) from the explosive. An improved description of the properties within this region may be required to develop a droplet breakup model with acceptable accuracy. Unfortunately, it appears that small uncertainties in the particle velocity may produce relatively large errors because of the velocity-squared dependence of the Weber number.

References

Bjerre, A. and Bak, T. A. (1969) 'Two parameter equations of state', *Acta Chem. Scand.*, **23**, 1733-1744.

Breedveld, G. J. F. and Prausnitz, J. M. (1973) 'Thermodynamic properties of supercritical fluids and their mixtures at very high pressures', *AIChE J.*, **19**, 783-796.

Kuznetsov, N. M., Timofeev, E. I. and Gubanov, A. V. (1986) 'Analysis of shock wave damping in thermodynamically equilibrium foam', *Combust., Explos. Shock Waves USSR*, **22**, 615-620.

Nelson, L. C. and Obert, E. F. (1954) 'Generalized $pv\vartheta T$ properties of gases', *Trans. ASME*, **76**, 1057-1066.

Redlich, O. and Kwong, J. N. S. (1949) 'On the thermodynamics of solutions', *Chem. Rev.*, **44**, 233-244.

Vakhnenko, V. A., Kudinov, V. M. and Palamarchuk, B. I. (1984) 'Damping of strong shocks in relaxing media', *Combust., Explos. Shock Waves USSR*, **20**, 97-103.

BAB:5214:bab
Copy to:
1421 J.M. DeLaurentis
5214 K.C. Goettsche
5214 E.J. Graeber
5214 P.N. Johnson
5214 M.E. Larsen
5214 H.S. Tessler

Appendix. Overpressure and Time of Arrival Data for 60:1 and 100:1 ER Foam

Data from 1 lb C-4, 60:1 ER test October 28, 1982

Dimensional			Dimensionless		
r, ft	dp, psi	ta, msec	r*	p*	ta*
1.5	114.00	0.50	0.15	7.76	0.057
2.0	42.00	0.90	0.20	2.86	0.102
2.5	38.00	1.10	0.25	2.59	0.125
4.0	2.20	3.00	0.41	0.15	0.341

Data from 50 lb C-4, 60:1 ER test May 10, 1983

Dimensional			Dimensionless		
r, ft	dp, psi	ta, msec	r*	p*	ta*
6.0	50.00	2.10	0.17	3.40	0.065
7.0	66.00	2.80	0.19	4.49	0.086
8.0	19.00	4.10	0.22	1.29	0.126
9.5	11.00	5.90	0.26	0.75	0.182
11.5	7.20	8.50	0.32	0.49	0.262
18.0	2.30	18.90	0.50	0.16	0.583

Data from 1 lb C-4, 60:1 ER test March 8, 1984

Dimensional			Dimensionless		
r, ft	dp, psi	ta, msec	r*	p*	ta*
2.0	39.00	1.20	0.20	2.65	0.136
2.5	15.00	1.60	0.25	1.02	0.182
4.0	1.80	3.80	0.41	0.12	0.432
5.0	0.90	5.90	0.51	0.06	0.670
7.0	0.58	10.20	0.71	0.04	1.159
10.0	0.19	15.70	1.02	0.01	1.784
10.0	0.18	15.90	1.02	0.01	1.807

Appendix (continued)

Data from 1 lb C-4, 100:1 ER test November 18, 1982

Dimensional			Dimensionless		
r, ft	dp, psi	ta, msec	r*	p*	ta*
1.5	155.00	0.33	0.15	10.55	0.038
2.0	105.00	0.59	0.20	7.14	0.067
2.5	66.00	1.02	0.25	4.49	0.116
4.0	2.80	2.39	0.41	0.19	0.272

Data from 1 lb C-4, 100:1 ER test June 16, 1983

Dimensional			Dimensionless		
r, ft	dp, psi	ta, msec	r*	p*	ta*
2.0	98.00	0.63	0.20	6.67	0.072
2.5	21.00	1.06	0.25	1.43	0.120
3.0	9.00	1.54	0.31	0.61	0.175
4.0	3.10	2.56	0.41	0.21	0.291
4.0	3.10	2.56	0.41	0.21	0.291
5.0	2.20	3.72	0.51	0.15	0.423
7.0	0.82	6.30	0.71	0.06	0.716
7.0	0.90	6.30	0.71	0.06	0.716
10.0	0.53	10.50	1.02	0.04	1.193

Data from 1 lb C-4, 100:1 ER test July 28, 1983

Dimensional			Dimensionless		
r, ft	dp, psi	ta, msec	r*	p*	ta*
2.0	75.00	0.64	0.20	5.10	0.073
2.5	23.00	0.94	0.25	1.57	0.107
3.0	10.00	1.50	0.31	0.68	0.170
4.0	2.90	2.40	0.41	0.20	0.273
4.0	3.70	2.40	0.41	0.25	0.273
5.0	1.50	3.50	0.51	0.10	0.398
7.0	0.98	0.00	0.71	0.07	0.000
7.0	1.00	6.30	0.71	0.07	0.716

Distribution

5	MS 0791	06417	Art Shanks
1	MS 0791	06417	Fred Harper
1	MS 0791	06417	John Fulton
1	MS 0791	06417	Lindsay Dvorak
1	MS 0791	06417	Mark Naro
1	MS 0791	06417	Paul Johnson
1	MS 0791	06417	Roger Goode
1	MS 0791	06417	Terry Kraus
1	MS 0791	06417	Tracia Love
1	MS 0791	06417	Weldon Teauge
1	MS 0791	06417	Will Wente
10	MS 0836	9117	Marvin Larsen
1	MS 0836	9117	Richard Griffith
1	MS 1231	08000	Billy Marshall
5	MS 1393	05920	Bruce Boughton
2	MS 9018	8945-1	Central Technical Files
2	MS0899	4536	Technical Library
1	MS 9161	08350	Stewart Griffiths

External:

3 William Hartman
37241 S. Canyon View Dr.
Tucson, AZ 85739